7-2017

Laser-Assisted Metal Organic Chemical Vapor Deposition of Gallium Nitride

Hossein Rabiee Golgir
University of Nebraska-Lincoln, rabiee@huskers.unl.edu

LASER-ASSISTED METAL ORGANIC CHEMICAL VAPOR DEPOSITION OF GALLIUM NITRIDE

by

Hossein Rabiee Golgir

A DISSERTATION

Presented to the Faculty of

The Graduate College at the University of Nebraska

In Partial Fulfillment of Requirements

For the Degree of Doctor of Philosophy

Major: Electrical Engineering

Under the Supervision of Professor Yongfeng Lu

Lincoln, Nebraska

July, 2017

Laser-Assisted Metal Organic Chemical Vapour Deposition of Gallium Nitride

Hossein Rabiee Golgir, Ph.D.
University of Nebraska, 2017
Advisor: Yongfeng Lu

Due to its unique properties, gallium nitride is of great interest in industry applications including optoelectronics (LEDs, diode laser, detector), high power electronics, and RF and wirelss communication devices. The inherent shortcomings of current conventional deposition methods and the ever-increasing demand for gallium nitride urge extended efforts for further enhancement of gallium nitride deposition. The processes of conventional methods for gallium nitride deposition, which rely on thermal heating, are inefficient energy coupling routes to drive gas reactions. A high deposition temperature (1000-1100 °C) is generally required to overcome the energy barriers to precursor adsorption and surface adatom migration. However, there are certain limitations associated with deposition methods that require high temperatures. As an intensive, coherent and monochromatic light, laser is an ideal candidate for exploring alternative energy coupling pathways. The laser techniques, in some instances, may offer processing advantages that are not available with conventional deposition methods.

To address the challenges, the research efforts in this dissertation mainly focused on laser incorporation in metal organic chemical vapor deposition of gallium nitride films, which led to: 1) rapid growth of *m*-plane gallium nitride nanoplates 2) low-temperature growth of gallium nitride films 3) promotion of energy coupling efficiency; 4) enhancement of gallium nitride deposition; 5) fast growth of gallium nitride epilayers;

and 6) realization of high-performance ultraviolet photodetectors based on the as-grown gallium nitride epilayers.

The *m*-plane-oriented gallium nitride nanoplates were successfully grown on silicon substrates at 450 °C, using CO_2 laser-assisted metal organic chemical vapor deposition with perpendicular geometries.

Vibrational excitations of precursor molecules were realized using a kilowatt wavelength-tunable CO_2 laser with a spectrum range from 9.2 to 10.9 μm. The resonant excitation of the NH-wagging mode of ammonia molecules was demonstrated to be more efficient than nonresonant excitations in promoting the deposition rate and improving the gallium nitride quality attributed to a higher energy coupling efficiency.

Low-temperature growth of crystalline gallium nitride films on *c*-plane sapphire substrates was achieved by laser-assisted metalorganic chemical vapor deposition and coupling laser energy into the chemical reactions.

A CO_2 laser-assisted metal organic chemical vapor deposition approach was also successfully developed for the fast growth of high-quality gallium nitride epilayer on the sapphire (0001) substrate. By optimizing the growth parameters, the ~ 4.3 μm thick gallium nitride films showed excellent thickness uniformity and smooth surface with a root mean square.The ultraviolet photodetectors were also realized based on the as-grown laser-assisted metalorganic chemical vapor deposition gallium nitride layers, which exhibited a high responsivity and a fast response time.

ACKNOWLEDGEMENT

Throughout my Ph.D. studies, I have obtained so much from the study in the Department of Electrical and Computer Engineering at the University of Nebraska-Lincoln (UNL). I would like to appreciate UNL and all the people who have provided great help, support and valuable suggestions both in my academic study and personal life.

I would like to thank my supervisor, Professor Yongfeng Lu, who has offered me a very great opportunity to study in his wonderful research group, Laser-Assisted Nano Engineering (LANE) Laboratory. From his great help and advices, I have made great progress in my research and learned to be a responsible and confident people in life. I would like to thank my degree committee members, Profs. Natale J. Ianno and Eva Franke-Schubert from the Department of Electrical and Computer Engineering at UNL, and Prof. Xiaocheng Zeng from the Department of Chemistry at UNL, for serving as my doctoral supervisory committee.

My sincere thanks also go to my colleagues in the LANE laboratory. Dr. Yang Gao gave me detailed training and guidance in specific research projects. Drs. Dawei Li and Yunshen Zhou gave many wise suggestions in research projects. Dr. Masoud Mahjouri-Samani, also gave me lots of help when I first come to US and helped me adapt to the new surroundings quickly. Without their great help and support, I cannot start my study smoothly. Drs. Lisha Fan, and Premkumar Thirugnanam taught me to operate the equipment and provided me technical support in the experiments. I would like to also thank all my previous and current group members including Wei Xiong, Leimin Deng, Xiangnan He, Yao Lu, Chengfei Zhang, Mengmeng Wang, Lei Liu, Xi Houng, Kamran Keramatnejad, Loic Constantin, Wenjia Hou, Ying Liu, Qiming Zhou, Zhe Lin, Shibin

Sun, Clio Azina, and Yutian Lei, as well as all my friends in Lincoln for their great help in my study here. I would like also to thank Dr. You Zhou from the Center for Biotechnology Core Research Facilities (CBCRF) at UNL for teaching me on scanning electron microscopy (SEM) and Dr. Shah Valloppilly from NCMN center at UNL for teaching me on X-Ray Structural Characterization. I would like to thank all the financial support from 1) grants from National Science Foundation; 2) Nebraska Research Initiative grants from the University of Nebraska-Lincoln.

Finally, I would like to thank my lovely wife, Elham Foruzan for her love and unconditional sacrifice in life. She is also a great researcher in field of electrical and power system engineering here at Department of Electrical and Computer Engineering at University of Nebraska Lincoln and I would like to thank my parent and family for their consistent support during the past five years on my PhD program and for their love in life.

TABLE OF CONTENTS

LIST OF FIGURES

LIST OF TABLES

LIST OF ABBREVIATIONS

The following table lists abbreviations and corresponding meanings used throughout the dissertation. The page on which each one is defined or first used is also given.

Abbreviation	Meaning	Page
GaN	Gallium nitride	2
LMOCVD	Laser-assisted metal organic chemical vapor deposition	3
TMGa	Trimethylgallium	22
NH_3	Ammonia	5
α-Al_2O_3	*c*-plane sapphire	15
Si	Silicon	15
CW	Continuous wave	3
CVD	Chemical vapor deposition	2
SEM	Scanning electron microscopy	3
MS	Mass spectrometry	5
OES	Optical emission spectroscopy	5
IR	Infrared	22
CO_2	Carbon dioxide	3
MSM	Metal-semiconductor-metal	25
RF	Radio frequency	14
XRD	x-ray diffraction	3
sccm	Standard cubic centimeters per minute	15
UV	Ultraviolet	3

CHAPTER 1 INTRODUCTION

1.1 Background and motivation

Using of various advanced techniques for thin film and crystal growth has attracted increasing attentions and achieved significant progress. Laser chemical vapor deposition (LCVD) is a potential new method for material synthesis and processing, in which laser energy can be deposited into reactant molecules.[1-6] In this process, the deposition occurred either by direct irradiating laser beam on the substrate, or the gas-phase chemical reactions are induced by laser irradiation in parallel configuration with the substrate. Depending on how the gas-phase reactions are affected by laser energy, the laser irradiation can lead to either pyrolytic or photolytic reaction.[1-6] If the laser thermally heats up and dissociates the reactant precursors, the reaction is pyrolytic. In case that the reactant precursors are vibrationally or electronically excited towards dissociation by absorbing photons without heating, photolytic takes place. The use of lasers for deposition and processing of semiconductor including silicon, gallium arsenide (GaAs), indium phosphide (InP) has been studied by several research groups.[1-6]

Gallium nitride (GaN) has attracted attentions for applications in light-emitting diodes (LEDs), short wavelength optoelectronics, and high-power high-frequency electronics, due to its excellent physical properties, such as wide direct bandgap, high thermal stability, and high electron velocities.[7-9] High quality GaN are routinely grown by metal-organic chemical vapor deposition (MOCVD) and molecular beam epitaxy (MBE).[10-13] These conventional growth techniques generally require a sufficiently high temperature to overcome the activation barriers to precursor chemisorption and adatom surface diffusion, which are inefficient energy coupling routes to drive gas reactions.

Additionally, high substrate temperatures cause sever adverse effects, such as biaxial stress within GaN films, nitrogen loss, and GaN decomposition, which affect the optical performance of the films and degrade the efficiency of GaN-based devices.[14] As an intensive, coherent and monochromatic light, laser is an ideal candidate for selective promotion of GaN growth and exploring alternative energy coupling pathways. The laser techniques offer processing advantages that are not available with conventional deposition methods.[15] For instance, Zhou et al.[16] reported ultraviolet (UV) laser-assisted MOCVD growth of GaN at room temperatures, leading to films with (0002) preferential orientation and a broad x-ray diffraction (XRD) peak. However, the photolysis of the precursors with UV laser resulted in the low density of the reactive radicals, a low GaN growth rate and film quality. On the other hand, carbon dioxide (CO_2) laser-assisted MOCVD has been used successfully to prepare various kinds of thin films at high growth rates.[15,17,18] For example, Iwanaga et al.[17] reported the deposition of large-area silicon films using CO_2 laser CVD with a high growth rate in a relatively low laser power and low substrate temperatures. However, to date, there is no report of a comprehensive study on growth, growth mechanism, structural evolution, and optical/electrical properties of GaN grown by CO_2 laser-assisted MOCVD (LMOCVD).

The research projects in this dissertation address various challenges and goals which mainly focused on the following five tasks: 1) synthesis of semipolar m-plane oriented gallium nitride nanoplates; 2) the investigation of resonant and nonresonant vibrational excitation of ammonia (NH_3) molecules in the growth of gallium nitride; 3) low-temperature growth of crystalline GaN films using vibrational excitation of NH_3

molecules; 4) fast growth of high-quality GaN epilayers; and 5) performance evaluation of UV detectors realized based on as-grown LMOCVD GaN epilayers.

1.2 Dissertation outline

The dissertation focused on controlling the crystallographic orientation of the GaN deposition, exploring alternative efficient energy coupling paths to obtaining low-temperature growth of GaN films and enhancing the GaN growth, optimizing expreimental design for fast growth of high-quality GaN epilayers, and realizing high-performance GaN-based UV detectors. The dissertation is divided into nine chapters. Chapter 1 introduces the motivation and outline of this dissertation. Chapter 2 reviews the background of GaN, technological challenges for GaN growth, laser chemistry control, laser-assisted material synthesis and basic working principles of UV detectors. Chapter 3 describes the experimental methods adopted in the study, including the sample preparation procedure, GaN film characterizations and GaN-based UV detectors device characterization. Chapter 4 demonstrates the growth of m-plane-oriented GaN nanoplates on Si substrates using the LMOCVD method. The high-resolution scanning and transmission electron microscopy images confirmed the formation of m-plane GaN nanoplates. The growth direction of GaN nanoplates was found to be the <10-10> direction. The A_1(TO) mode of Raman further confirmed the m-plane orientation of the GaN nanoplates. Chapter 5 shows that the laser-assisted vibrational excitations of NH_3 molecules promote the GaN deposition rate and improve the GaN film quality on Si (100). The NH-wagging mode (v_2, 1084.63, 968.32, 932.51 cm^{-1}) of NH_3 has a strong infrared activity and the corresponding ro-vibraitional transitions match CO_2 laser emission lines (9.219, 10.350, and 10.719 μm). The resonant vibrational excitation at

9.219, 10.350, and 10.719 μm were more efficient than the nonresonant excitation in dissociating NH_3 molecules and enhancing the GaN deposition rate and the film quality. The optical emission spectroscopy (OES) results showed the resonant excitation of the NH-wagging modes modifies the synthesis process in a way that increases the generation of NH, NH_2, N, N^+, and H intermediate species. This leads to the enhancement in the GaN deposition rates and the improvement in the crystalline quality. The extremely high GaN growth rate of ~84 μm/h with an improved crystalline quality was achieved under the resonant excitation at 9.219 μm. Chapter 6 describes a novel strategy to realize low-temperature growth of crystalline GaN films on *c*-plane sapphire substrates by LMOCVD with laser energy coupled into the chemical reactions. Trimethylgallium and NH_3 were used as precursors for the growth of GaN films. Through the resonant excitation of rotational–vibrational transition (1084.71 cm^{-1}) of the NH-wagging mode (v_2) in NH_3 molecules using a wavelength-tunable CO_2 laser tuned at 9.219 μm, highly *c*-axis oriented GaN films were deposited on sapphire at low substrate temperatures from 250 to 600 °C. The GaN films deposited by LMOCVD showed a higher degree of crystallinity, higher growth rate, and lower defect densities as compared to those synthesized by MOCVD without resonant excitation of NH_3 molecules. Chapter 7 demonstrates a developed CO_2 LMOCVD approach for the fast growth of high-quality gallium nitride (GaN) epilayers on the sapphire (0001) substrate. By employing a two-step growth process, high-quality smooth GaN layers with a fast growth rate of 25.8 μm/h were obtained. The high crystalline quality was confirmed by a combination of different characterization techniques. By optimizing the growth parameters, the ~ 4.3 μm thick GaN films grown for 10 min at 990 °C showed excellent thickness uniformity and

smooth surface with a root mean square surface roughness of ~ 1.9 nm, very narrow XRD peaks, and sharp GaN/sapphire hetero-interfaces. Chapter 8 illustrates high-performance UV detectors have been realized based on as-grown LMOCVD GaN epilayers. The devices exhibit a high responsivity of 0.12 AW^{-1} and a fast response time of 125 ns at 5 V reverse bias, indicating the excellent optical properties of GaN layers. The results demonstrate that LMOCVD technique can produce high-quality GaN epilayers and other nitride related materials with fast growth rates with potential application for next-generation electronics and optoelectronics. Chapter 9 concludes the projects with important results and suggests future research directions.

1.3 References

1. Crim, F. F., Chemical dynamics of vibrationally excited molecules: Controlling reactions in gases and on surfaces. Proceedings of the National Academy of Sciences 2008, 105 (35), 12654-12661.

2. Zare, R. N., Laser control of chemical reactions. science 1998, 279 (5358), 1875-1879.

3. Killelea, D. R.; Utz, A. L., On the origin of mode-and bond-selectivity in vibrationally mediated reactions on surfaces. Physical Chemistry Chemical Physics 2013, 15 (47), 20545-20554.

4. Killelea, D. R.; Campbell, V. L.; Shuman, N. S.; Utz, A. L., Bond-selective control of a heterogeneously catalyzed reaction. Science 2008, 319 (5864), 790-793.

5. Goez, M., Conformation‐Selective Laser Chemistry. Angewandte Chemie International Edition 2003, 42 (21), 2336-2337.

6. Lupo, D. W.; Quack, M., IR-laser photochemistry. Chemical Reviews 1987, 87 (1), 181-216.

7. Akasaki, I.; Amano, H., Breakthroughs in improving crystal quality of GaN and invention of the p–n junction blue-light-emitting diode. Japanese journal of applied physics 2006, 45 (12R), 9001.

8. Asif Khan, M.; Bhattarai, A.; Kuznia, J.; Olson, D., High electron mobility transistor based on a GaN‐Al x Ga1− x N heterojunction. Applied Physics Letters 1993, 63 (9), 1214-1215.

9. Ponce, F.; Bour, D., Nitride-based semiconductors for blue and green light-emitting devices. Nature 1997, 386 (6623), 351.

10. Tarsa, E.; Heying, B.; Wu, X.; Fini, P.; DenBaars, S.; Speck, J., Homoepitaxial growth of GaN under Ga-stable and N-stable conditions by plasma-assisted molecular beam epitaxy. Journal of Applied Physics 1997, 82 (11), 5472-5479.

11. Heying, B.; Averbeck, R.; Chen, L.; Haus, E.; Riechert, H.; Speck, J., Control of GaN surface morphologies using plasma-assisted molecular beam epitaxy. Journal of Applied Physics 2000, 88 (4), 1855-1860.

12. Boyd, A. R.; Degroote, S.; Leys, M.; Schulte, F.; Rockenfeller, O.; Luenenbuerger, M.; Germain, M.; Kaeppeler, J.; Heuken, M., Growth of GaN/AlGaN on 200 mm diameter silicon (111) wafers by MOCVD. physica status solidi (c) 2009, 6 (S2).

13. Nakamura, S.; Harada, Y.; Seno, M., Novel metalorganic chemical vapor deposition system for GaN growth. Applied Physics Letters 1991, 58 (18), 2021-2023.

14. Rabiee Golgir, H.; Gao, Y.; Zhou, Y. S.; Fan, L.; Thirugnanam, P.; Keramatnejad, K.; Jiang, L.; Silvain, J.-F. o.; Lu, Y. F., Low-Temperature Growth of Crystalline Gallium Nitride Films Using Vibrational Excitation of Ammonia Molecules in Laser-Assisted Metalorganic Chemical Vapor Deposition. Crystal Growth & Design 2014, 14 (12), 6248-6253.

15. Herman, I. P., Laser-assisted deposition of thin films from gas-phase and surface-adsorbed molecules. Chemical Reviews 1989, 89 (6), 1323-1357.

16. Zhou, B.; Li, Z.; Tansley, T.; Butcher, K., Growth mechanisms in excimer laser photolytic deposition of gallium nitride at 500° C. Journal of crystal growth 1996, 160 (3-4), 201-206.

17. Iwanaga, T.; Hanabusa, M., CO2 laser CVD of disilane. Japanese Journal of Applied Physics 1984, 23 (7A), L473.

18. Besling, W.; Goossens, A.; Meester, B.; Schoonman, J., Laser-induced chemical vapor deposition of nanostructured silicon carbonitride thin films. Journal of applied physics 1998, 83 (1), 544-553.

CHAPTER 2 BACKGROUND AND REVIEWS

2.1 Introduction to GaN

2.1.1 GaN and properties

Gallium nitride (GaN) is very promising wide band gap semiconductor material for applications including optoelectronics, and high-temperature high power electronics. GaN is one of the most important semiconductor after silicon. The III-V nitride materials and their ternary and quaternary alloys are direct bandgap semiconductors. The energy band gap of these materials contains a wide spectral region from red to deep ultraviolet (1.9 - 6.2 eV).[1-4] Fig. 2.1 illustrates the bandgap and lattice constant of nitride semiconductor materials.

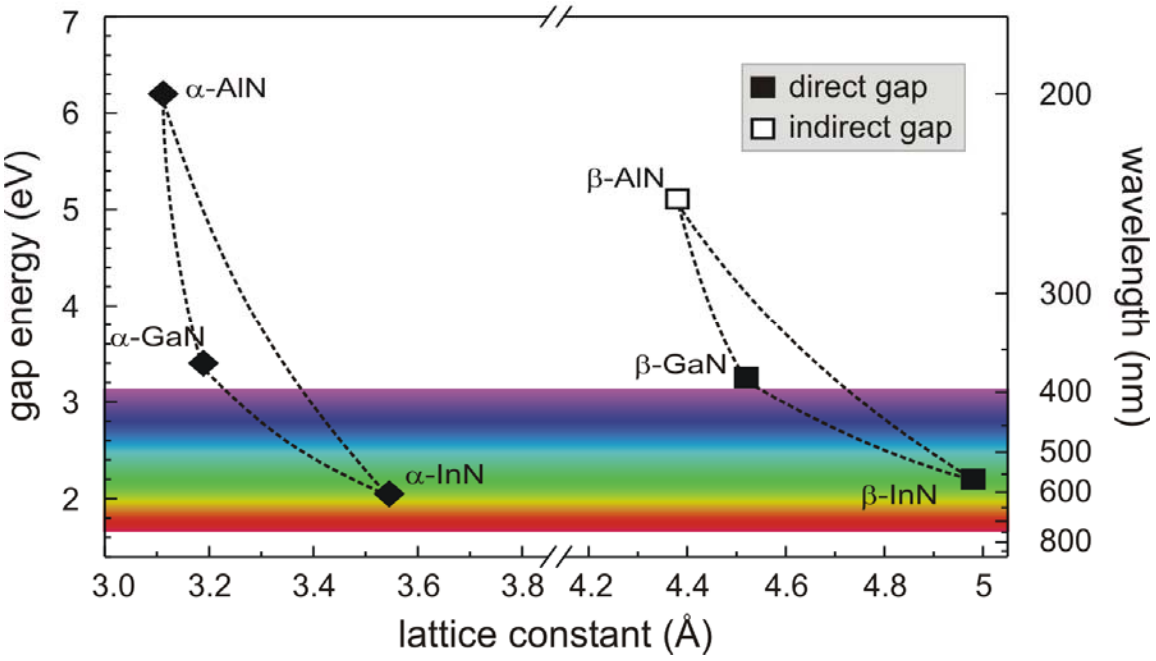

Figure 2.1 Bandgaps of nitride semiconductors with wurtzite and zincblende structure versus their lattice parameter at 300 °K. The right-hand scale gives the light wavelength λ, corresponding to the band gap energy.[5]

Various techniques have been employed for GaN synthesis. The GaN structure has two crystalline phases: wurtzite (WZ) structure with a hexagonal symmetry (the

thermodynamically equilibrium phase), and zincblende (ZB) structure with a cubic symmetry. The schematic image of these two structures is illustrated in Fig. 2.2.[6] In both structures, the Ga and N atoms are tetragonally coordinated with 4 atoms of the opposite type.

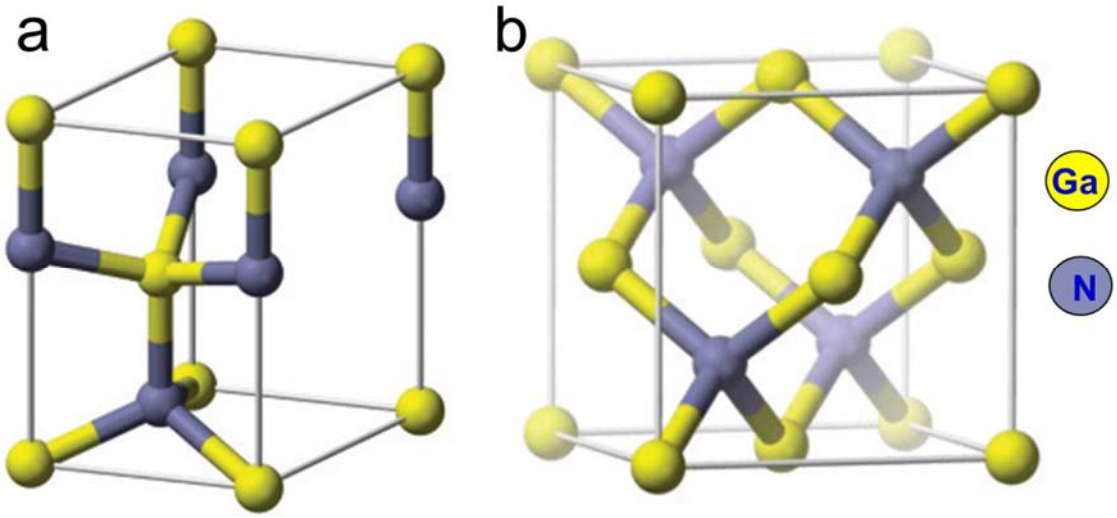

Figure 2.2 (a) Wurtzite lattice structure of GaN and (b) zincblende structure of GaN.[7]

Three important planes of the hexagonal GaN structure are illustrated in Fig. 2.3: the {0001} *c*-plane (green plane) which is basal plane, the {1-100} *m*-plane (orange plane), and {11-20} *a*-plane (blue plane) which is perpendicular to both the m-plane and the *c*-plane.[8-11] Due to the high surface free energy of the *c*-plane, the GaN films prefer to grow along the {0001} direction. Our work focuses on the synthesis of *m*-plane and *c*-plane-oriented films. The non-polar nitride and heterostructures (the layers grown in *a*- and *m*-orientation) do not suffer from the effects of the inbuilt polarization fields, which degrades the recombination efficiency and performance of GaN photonic devices.[8-11] However, the polar nitride films and heterostructures (layers grown in *c*-orientation) suffer from the effects of the inbuilt polarization fields. The inbuilt polarization fields are

not oriented along the heterostructure interface and do not affect its band gap in non-polar nitride films.

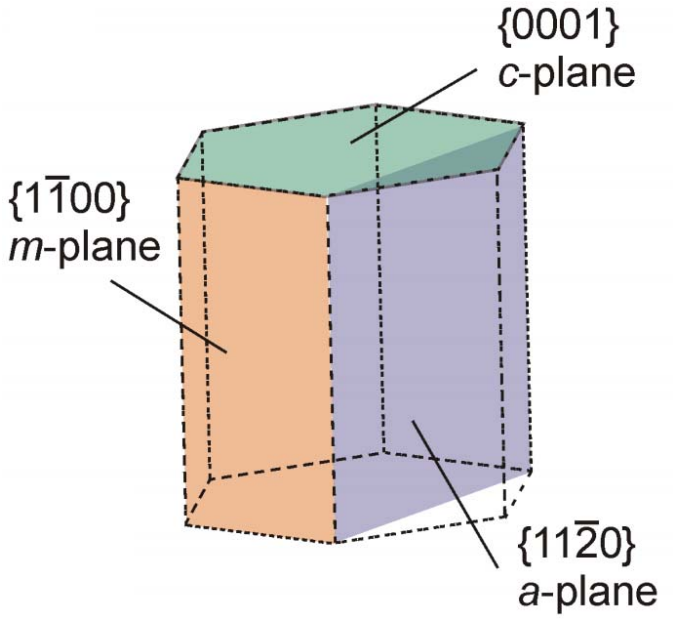

Figure 2.3 Wurtzite lattice structure of GaN with polar and non-polar planes.[5]

GaN semiconductor has unique properties including high thermal, mechanical, and chemical stability compared to other semiconductor materials such as Si and GaAs. These unique properties are mostly because of strong bonding between the gallium and nitrogen atoms. Some reported material properties are as below:[12-13]

- With wide direct band gap, it is useful for photonic devices;
- It is chemically stable at high temperatures;
- It has a good thermal conductivity;
- It has high room-temperature electron mobilities and high breakdown electric field.

Below the important physical properties of the GaN semiconductor have been summarized in Table 2.1.[12-13]

Table 2.1 Physical properties of GaN[12-13]

Properties	Wurtzite	Zinc-blende
Density (g/cm^3)	6.15	-
Band-gap (eV)	3.4	3.2
Bandgap type	direct	direct
Lattice Constants (A)	a = 3.189 c = 5.186	4.52
Effective Electron Mass (m_0)	0.2	0.13
Electron Affinity (eV)	4.1	4.2
Thermal conductivity (W/cm × C)	1.3	1.3
Electron Mobility (cm^2/Vs)	< 1000	< 1000
Hall Mobility (cm^2/Vs)	< 200	< 350
Melting temperature	> 1700 °C	-
Index of refraction (n)	2.67 @ 3.38 eV	2.91 @ 3.2 eV
Piezoelectric constant (C/m^2)	0.375	-

2.1.2 Substrates for GaN heteroepitaxial growth

Current commercial GaN-based devices are fabricated by epitaxy on foreign substrates because the GaN bulk and freestanding substrate technology is still immature.[13-15]The choice of substrate for GaN growth depends on several factors such as the lattice mismatch between the substrate and the GaN (different lattice constants), the difference

in thermal expansion coefficients between the substrate and the GaN, and the substrate cost. The common substrates for GaN heteroepitaxial growth are as follows:[13-15]

2.1.2.1 Silicon

The Si with the price of around $25 per 100 mm wafer is a low-cost substrate. The lattice mismatch between silicon and GaN is approximately 17%, and the thermal expansion coefficient of silicon is 113%. GaN films grown on silicon suffer from tensile stresses as cooling the sample from high growth temperature to room temperature, potentially leading to film cracking. Si has a reactive surface when exposed to ammonia at temperatures above 500 °C during the growth and a thin silicon nitride layer can be formed. From the point of view of integrating GaN devices with Si technology, the Si (100) substrate is preferred because Si (100) is the most widely used in silicon mainstream technology. In contrast to the Si (111), Si (100) does not show a 6-fold symmetry but a 4-fold symmetry which is more suitable for the epitaxial growth of a cubic GaN,[15,16] however, the cubic phase is metastable. The thermodynamically stable hexagonal GaN phase could be also grown on the (100) plane.

2.1.2.2 Silicon carbide (SiC)

SiC substrate with a hexagonal structure is also used for GaN heteroepitaxial growth. With a lattice mismatch of 3.5%, SiC is a very appropriate substrate for growth of high-quality GaN films with low dislocation density. Additionally, this substrate is very resistant to chemical reaction compared to Si. Therefore, a blocking layer is not formed during the GaN growth.[13-16]

The thermal expansion coefficient of SiC is almost twice that of GaN and this substrate is extremely expensive with the cost around $1000 per 100 mm wafer. GaN layers grown on SiC suffer from significant compressive stress during cooling down, which can lead to film cracking.

2.1.2.3 Sapphire

Sapphire (Al_2O_3) as a transparent substrate is the most common substrate for GaN epitaxy growth with a reasonable price (~ $150 per 100 mm wafer) and performance. The lactic mismatch between sapphire and GaN is ~14% and the thermal expansion coefficient of sapphire is 33% larger compared to GaN. As an oxide compound, this dielectric substrate is fully stable to harsh growth environment even at high growth temperatures. Sapphire is resistant to forming an amorphous nitride when exposed to ammonia during GaN growth. Since sapphire is an insulator substrate with a bandgap of 10 eV, the fabrication of specific devices with a backside electrical contact on GaN/sapphire is imposible.[13-16]

2.1.3 - GaN growth techniques

2.1.3.1 HVPE

Hybrid Vapor Phase Epitaxy method (HVPE) is a growth technique for synthesis of III-V compound.[12,17-20] This technique is appropriate for high growth rate deposition (deposition rates ~ 10-200 μm/h and higher). Fig. 2.4 shows the schematic of a hot-walled HVPE system. Hydrochloric acid (HCl) passes over the gallium (Ga) upstream and reacts with Ga at 800 - 900 °C. A volatile gas-phase metal chloride (GaCl) forms as follows:

$$Ga + HCl \rightarrow GaCl + 1/2H_2 \quad (2.1)$$

The volatile metal compound, then, is transported downstream to the substrate and reacts with NH_3:

$$GaCl + NH_3 \rightarrow GaN + HCl + 1/2H_2 \quad (2.2)$$

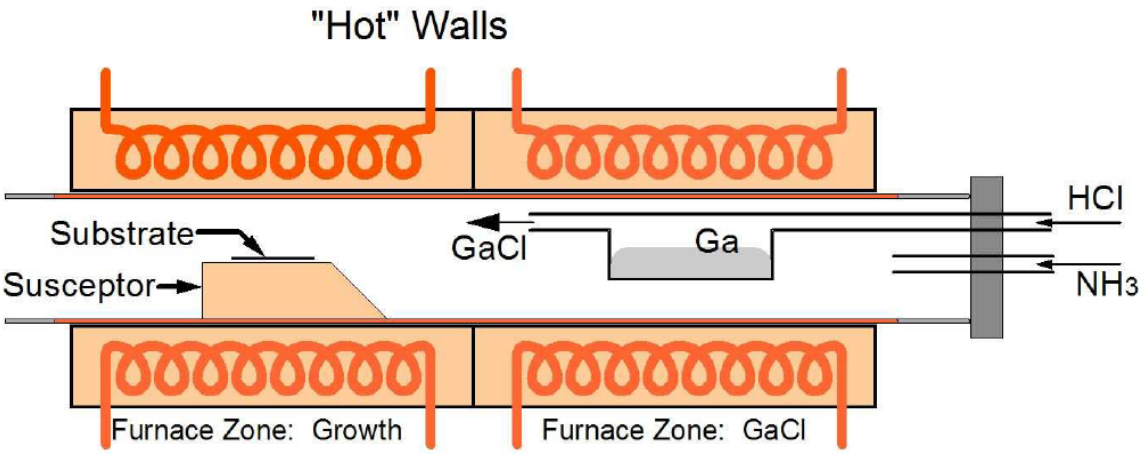

Figure 2.4 A schematic diagram of a hot-walled HVPE reactor (a hot-walled reactor utilizes a tube furnace that heats the entire reactor to a more uniform substrate temperature).[12]

The GaN films grown with HVPE method generally have rough surface morphology with hexagonal shaped hillocks and pyramids. This is because the HCl can chemically attack and etch the films during growth where the etching rate is higher in strained regions, such as the boundaries of coalesced grains.

In HVPE, the GaCl is transported to the substrate only after HCl passes over and reacts with the gallium; which an inherent latency occurs. Therefore, this technique is not appropriate for quick compositional changes during growth and synthesis of thin heterostructures with abrupt interfaces.[17-20]

Because of the presence of reactive HCl and GaCl in the reactor, the choice of substrates for GaN growth using HVPE is more constrained compared to other deposition methods. For example, silicon substrates easily react with HCl and GaCl, forming several by-products including volatile silicon chloride, liquid gallium and H_2.[17-20] The liquid gallium remains on the silicon surface and affects the quality of epitaxial GaN films on substrate.

2.1.3.2 MBE

Molecular beam epitaxy (MBE) is another technique for the epitaxial growth of compound semiconductor films. MBE has a low growth rate of 0.1-1 μm/hr, and performs in a growth temperature of 800-1000 ^oC. These relatively low growth rates limit the applicability of MBE for growth of many GaN-based device structures.[21-23] The basic elements of an MBE growth system are UHV chamber, substrate heater part, individually shuttered and liquid nitrogen shrouded molecular beam effusion cells, and substrate exchange load-lock system, as shown in Fig. 2.5. [21-23]

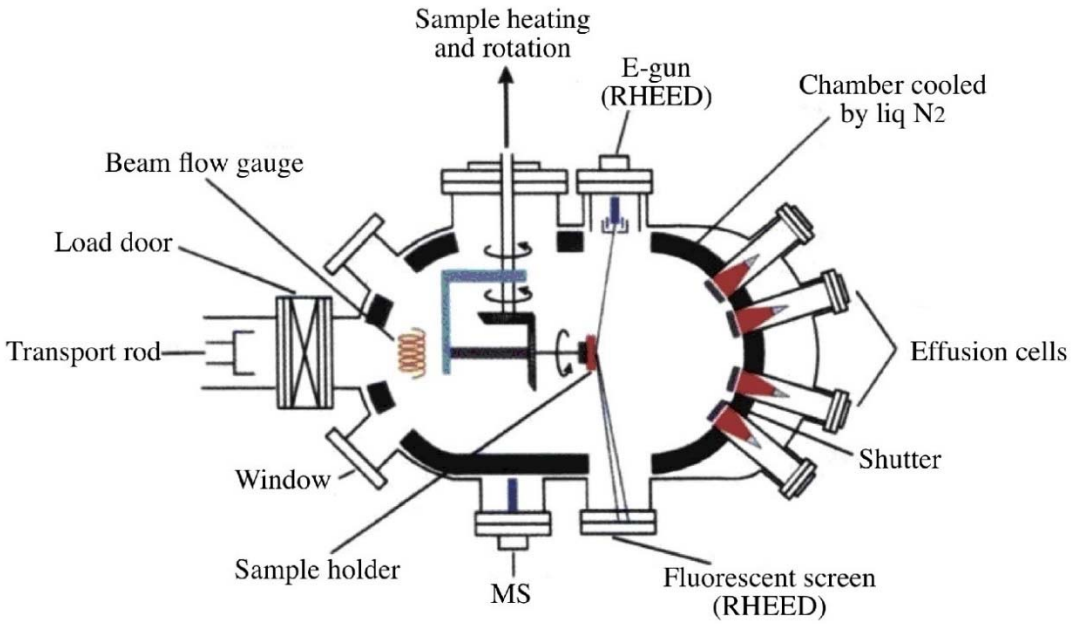

Figure 2.5 A schematic diagram of a typical MBE system. [23]

A base pressure of less than 5×10^{-10} Torr is used in MBE process to obtain films with low impurity levels. The in-situ monitoring of growth conditions and growth rate is done by Fluorescent screen (FRHEED). Atomic layer-by-atomic layer deposition is achieved by using low beam fluxes, which are controlled by temperature variation of the source cells. By rotating substrates during the film deposition, a uniform growth is achieved. GaN growth proceeds according to following steps:[21-23] (1) Atoms impinge on the sample surface, where they are adsorbed, (2) The atoms migrate along the surface towards atomic steps, where they are stabilized by the increased number of atomic bonds, (3) The atoms migrate along the step edges to a kink site, where they are incorporated into the lattice. Deposition involves the lateral motion of step edges or the growth of two-dimensional islands until an atomic layer is completed. [21-23]

2.1.3.3 MOCVD

Metal-organic chemical vapor deposition (MOCVD) is a common technique for growth of high quality epitaxial GaN layers with excellent surface morphology and a precise control over layer thickness and uniformity.[13,24-27] Current commercial GaN devices including lasers, light emitting diodes, photocathodes, heterostructure bipolar transistors, photodetectors, and solar cells are usually synthesized by MOCVD. The MOCVD process involves a series of complex gas phase and surface reactions. The process contains following steps: (a) Evaporation and transport of precursors; (b) Pyrolysis of precursors leading to film deposition; and (c) Removal of the remaining fragments of the decomposition reactions from the reactor. This process often proceeds by the formation of steps on the surface, with the diffusion of adsorbed atoms across the surface and

attachment to a step. The basic growth steps in MOCVD are shown in Fig. 2.6 and are as follows:

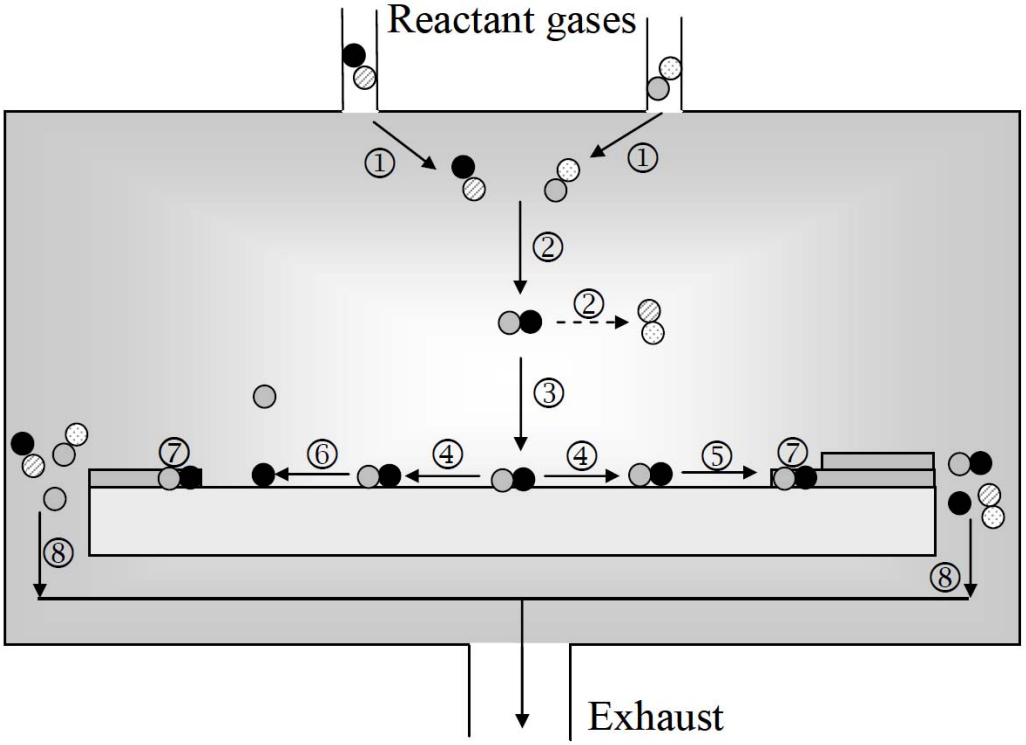

Figure 2.6 Schematic of MOCVD growth mechanisms.[13]

1. The transport of reactant precursors into the reactor.
2. The chemical gas-phase reactions which produce growth species and byproducts.
3. The transport of the growth species to the surface and absorption on the surface.
4. The diffusion of the growth species on the surface.
5. The incorporation of these species at kinks.
6. The desorption or evaporation some of species from the surface.

7. Phase change including vapor-phase condensation and solidification which leads to nucleation and step growth for film formation.

8. The exhaustion of the byproducts of reactions.

The most common chemical reactions in MOCVD process of GaN are driven by pyrolysis. Pyrolysis is the thermal decomposition of reactant species such as NH_3 and metal-organic radicals for material synthesis. Trimethylgallium (TMGa) is the most common gallium precursor for MOCVD growth of GaN. The major product of TMGa pyrolysis with H_2 or N_2 as carrier gases is methane (CH_4). Ammonia NH_3 is used as the most common nitrogen precursor for GaN growth. The growth of high-quality GaN requires very high growth temperatures. While the TMGa is fully pyrolyzed at 550 ºC,[13,24-27] the decomposition of NH_3 occurs at much higher temperatures compared to the metalorganic precursors. It has been reported that the decomposition of NH_3 at atmospheric pressure starts at 600 ºC and a complete decomposition occurs above 800 ºC.[13]

The formation of GaN in MOCVD includes four key steps:[13,28,29] (i) TMGa:NH_3 adduct formation, (ii) amide formation and methane elimination, (iii) trimer formation, and (iv) decomposition reaction and creating N and Ga to form GaN. The general related equations are given by:[13,28,29]

$$(CH_3)_3Ga + NH_3 \rightarrow (CH_3)_3Ga{:}NH_3 \quad (2.3)$$

$$(CH_3)_3Ga{:}NH_3 \rightarrow (CH_3)_2Ga{:}NH_2 + CH_4 \quad (2.4)$$

$$3[(CH_3)_2Ga{:}NH_2] \rightarrow [(CH_3)_2Ga{:}NH_2]_3 \quad (2.5)$$

$[(CH_3)_2Ga:NH_2]_3 \rightarrow 3GaN + 6CH_4$ (2.6)

The MOCVD growth of high-quality GaN is as follows: Substrate cleaning with annealing under H_2 at high temperature. A thin (20-30 nm) low-temperature (~550 ºC) GaN is first grown as nucleation layer and this layer is annealed to be recrystallized. The islands formed during nucleation start to coalesce as the three-dimensional growth continues, converting to a two-dimensional surface. The step-flow growth of final GaN layer is typically performed at a temperature ~ 1020 ºC with a growth rate of ~2-4 μm/h.[13]

The large thermal and lattice mismatch between common substrates including Si, sapphire and SiC with GaN is an issue in MOCVD growth of GaN on these substrates. Intrinsic defects in GaN are typically donor-like defects (nitrogen vacancy, V_N, and gallium interstitials**,** Ga_i). Therefore, undoped GaN films are n-type with a free carrier concentration around 10^{16} cm^{-3} and p-type doping of the films is typically difficult. Magnesium (Mg) is the common p-type dopant in GaN. However, Mg often incorporates during growth as a Mg-H complex, which is also a donor-type defect. To remove the hydrogen and activate the Mg as an acceptor, a subsequent annealing step under H_2 is required.[13]

2.2 Introduction to laser chemistry control

Controlling the outcome and product of the chemical reactions is an old dream in chemistry. We would like to steer the reactants into a desired outcome and product. Traditionally, control the dynamics of chemical reactions is done with temperature control or finding an appropriate catalyst. [30-44] The energy is traditionally supplied into

the reaction as heat. With changing the temperature, the average energy of all molecules in the sample is changed and the energy is only controlled on an average macroscopic level. The energy is universally injected into all molecule modes including external and internal (electronic, vibrational, rotational) modes and affects the dynamics and the outcome of the reaction.

Laser chemistry concentrates the challenging objective of using lasers to control the outcome of chemical reactions by breaking particular bond in a large molecule. High intensity laser can supply energy into specific reactant bonds, leaving rest cold. For instance, using the infrared (IR) laser, we can selectively supply energy into the internal state (vibrational/rotational) of the reactants because the frequencies of vibrational modes of molecules fall in the IR region. A vibrational mode which is in resonance with an IR laser frequency can be selectively excited via single- or multi-photon processes.[62]

Several experimental studies have revealed the ability of vibrational excitation of molecules to control and promote the chemical reactions.[45-53] S. Nave *et al.* showed the vibrational excitation of the methane molecule significantly enhances its reactivity when the molecule undergoes transitions to the ground or lower-energy vibrational states.[45] They found the υ_1 vibration has the largest efficiency for promoting reaction, however, the υ_3 vibration has smaller efficiency, but significant.[45] F.F. Crim *et al.* showed different vibrational modes, such as the symmetric and antisymmetric stretches in CH_3D, lead to very different reactivities.[46,47] The symmetric stretching vibration excitation of molecules leads the molecules be 10 times more reactive than antisymmetric stretch excitation of molecules.[46,47] Several other studies of laser chemistry control using vibrational excitations contain $Cl + CHD_3$,[48] $Cl + HCN$,[49] $NH_3+ + ND_3$,[50] and $C_2H_2+ + CH_4$.[51]

2.3 Introduction to laser-assisted material synthesis

The use of lasers for synthesis of material and thin films has been obtained increasing interests. It is necessary to understand the species and molecule modes of excitation and energy relaxation during laser interaction with gases and precursors to know how lasers promote material deposition. Laser chemical vapor deposition (LCVD) is a suitable method for thin-film synthesis and enables us to study new reaction pathways. When metalloorganic compounds are used as reactants, LCVD is usually called laser metal organic chemical vapor deposition (LMOCVD).

The overall reaction mechanisms in laser material synthesis are generally complicated. The laser can induce thermal reactions on the substrate surface by heating the substrate and deposition occurs, which is known as pyrolytic or thermochemical deposition like that in conventional CVD synthesis of thin films. In pyrolytic process precursor gases are thermally activated.[52-62] The energy is first deposited to the translational modes of reactant molecules, and then distributed to their internal modes. An enough internal energy is required for overcoming reaction barrier and gas dissociation. When high surface temperatures are required to induce deposition, the pyrolytic process can cause more structural damage in thin films due to high temperatures and thermally induced stresses. Additionally, pyrolytic process is inefficient in energy coupling to drive gas reactions and short of selectivity.

In another arrangement, the laser is absorbed directly by the reactants and dissociates gas-phase or surface-adsorbed molecules without heating the substrate surface. This method is known as photolytic or photochemical deposition. The monochromaticity of lasers

enables narrow-band excitations of selective reactants. Laser excitation can occur by stimulating molecule vibrational or electronic transitions by the absorption of infrared laser multiple-photons and ultraviolet photons. It can selectively control reactions in material synthesis processes. In some cases, the photodissociation products must be decomposed further by conventional heating of the substrate to achieve film depositions.

Two different irradiation geometries can be used in LCVD as shown in Fig. 2.7. In first configuration (Fig. 2.7a), the beam impinges on the surface at nearly normal incidence and gas and substrate surface are both excited. In second configuration, the laser travels parallel to and just above the substrate (Fig. 2.7b). In this case, the laser energy is directly coupled into the gas phase and possible heating of the substrate surface is eliminated. In this dissertation, both parallel and perpendicular irradiation geometries were employed.

Several semiconductor materials, including Silicon (Si), gallium arsenide (GaAs), cadmium telluride (CdTe), indium phosphide (InP), indium antimonide (InSb), and aluminum nitride (AlN), have been grown using the LCVD technique. The LCVD deposition of other films including metal films (W, Al, Cu, and Au), and insulators (Al_2O_3, SiO_2, Si_3N_4) have been also reported.[63-92] Table 2.2 summarizes some typical LCVD processes of various materials.

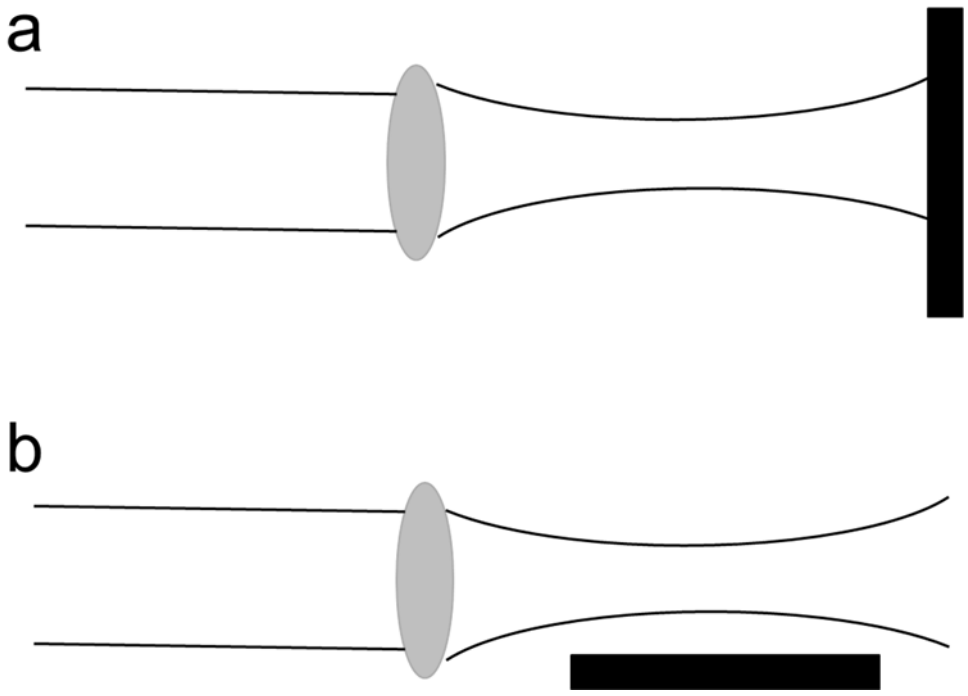

Figure 2.7 (a) Perpendicular and (b) Parallel irradiation geometries employed in a LCVD process.

Table 2.2 Typical LCVD of various materials with specific lasers and precursors.[63-92]

Material	Precursors	Substrate	Laser wavelength(nm)	Ref.
W	WF_6/H_2	GaAs	ArF/193	[64]
Cu	Cu(hfac)tmvs/H_2 /N_2	Si	Ar+/514.5	[66]
Au	$(CH_3)_2Au(hfac)$	Si	XeCl/308	[68]
Al	DMEAA	Si	Ar+/514	[69]
Si	SiH_4/Ar	Si	KrF/248	[72]
Ge	GeH_4/Ar	-	KrF/248	[74]
GaAs	TMG/AsH_3	GaAs	Ar+/514	[75]
InN	HN_3/TMIn	Si	XeCl/308	[77]
ZnSe	DMZ/DMSe/H_2	GaAs	ArF/193	[78]
SiO_2	SiH_4/N_2O	Si	ArF/193	[80]
Si_3N_4	SiH_4/NH_3	-	CO_2/10600	[81]
CNT	C_2H_2/NH_3	Si	CO_2/10600	[89]
Diamond	CH_4/H_2	Silica	Nd:YAG/532	[90]
Graphene	CH_4/H_2	Ni	Nd:YAG/532	[87]

2.4 Challenges in laser-assisted GaN synthesis

Gallium nitride (GaN) has attracted attentions for applications in light-emitting diodes (LEDs), short wavelength optoelectronics, and high-power high-frequency electronics, due to its excellent physical properties such as wide direct bandgap, high thermal stability, and high electron velocities. These conventional growth techniques generally require a sufficiently high temperature to overcome the activation barriers to precursor chemisorption and adatom surface diffusion, which are inefficient energy coupling routes to drive gas reactions. Additionally, high substrate temperatures cause severs adverse effects, such as biaxial stress within GaN films, nitrogen loss, and GaN decomposition, which affect the optical performance of the films and degrade the efficiency of GaN-based devices. As an intensive, coherent and monochromatic light, laser is an ideal candidate for selective promotion of GaN growth and exploring alternative energy coupling pathways. A more efficient energy coupling path can be achieved via directly activating internal motions of reactant molecules. Frequencies of molecular vibrational modes and electronic excitations locate in infrared range and UV-Vis range, respectively. The laser techniques may offer processing advantages that are not available with conventional deposition methods. Laser is a perfect energy source due to its high-energy intensity, wavelength capability from UV to IR, and monochromaticity. In this dissertation, we introduced CO_2 laser for IR-laser vibrational excitations in MOCVD growth of GaN films. We achieved an enhanced energy coupling efficiency and promoted GaN growth rate and crystalline quality.

NH_3 is the common nitrogen precursor used in MOCVD growth of GaN. It has six fundamental vibrational modes as shown in Fig. 2.8, which NH-wagging mode is

strongly infrared active.[62,93] The NH_3 vibrational modes at 932.51 (v_{2+}), 968.32 cm^{-1} (v_{2-}) and 1084.63 cm^{-1} match to the emission lines of a CO_2 IR-laser at 10.719, 10.35 and 9.219 μm, respectively. Therefore, NH_3 is an ideal candidate for studying the IR-laser vibrational excitations in GaN synthesis.

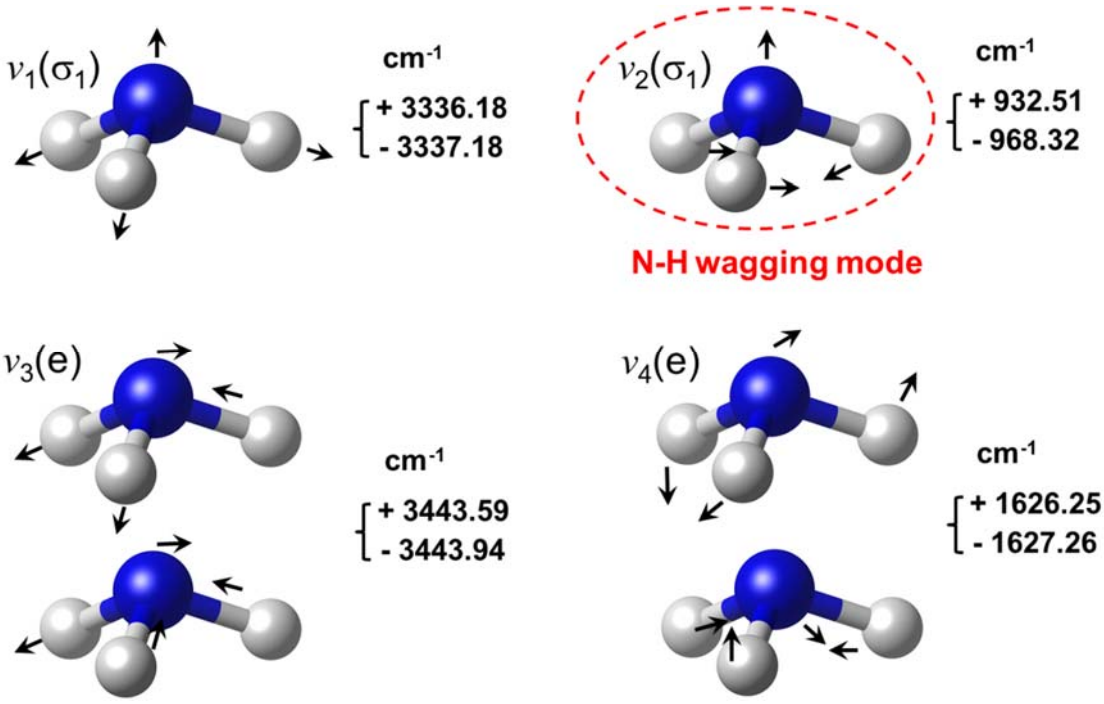

Figure 2.8 Schematic illustration of the NH_3 vibration modes.

2.5 Basic working principles of metal-semiconductor-metal (MSM) UV Photodetectors

Among GaN photodetectors with different device structures, the MSM structure is an attractive candidate for UV photodetector applications, because this type of detector has low dark current, low noise and high response speed characteristics. In addition, its growth and fabrication processes are simplified because n- and p-type doped layers are not required. With lateral and planar structure, these devices have very low capacitance,

suitable for high-speed performance detectors. Additionally, the fabrication process for MSM photodetectors is compatible with field effect transistors, which results an easy integration in an optical detection and amplifier.[94,95]

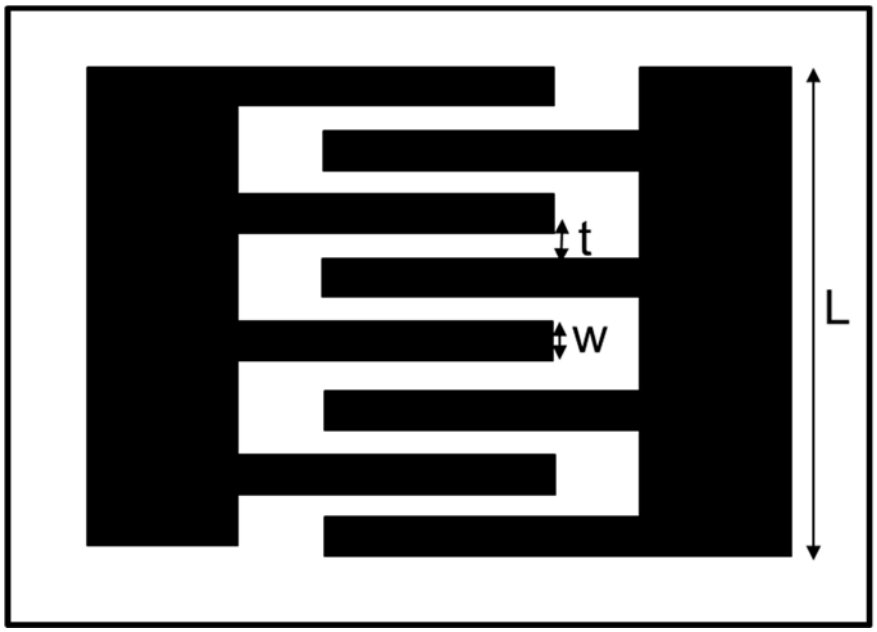

Figure 2.9 Schematic top view of MSM structure.

The schematic of an MSM structure is shown in Fig. 2.9. In this thesis, the finger spacing, *t*, is equal to the finger width, *w*. The MSM photodetector is made by forming Schottky diodes on GaN layer. Two contact pads and interdigitated fingers form the metal structure and the active area of the device. The energy band diagram of the MSM device under thermal equilibrium condition is shown in Fig. 2.10. The MSM photodetector is a two Schottky barriers connected back to back. The electron affinity of GaN is 4.1 eV and the work function of Au is ~5.1 eV which result in electron injection barrier of ~0.9 eV. Under the applied bias, one of the Schottky contacts is in reverse bias, and the other one is in forward bias. With the illumination to the active area of the device, electron-hole pairs are generated in this region. The photo-excited carriers are

collected by contact pads (Ni/Au) under the bias voltage. Responsivity, speed, and dark current are the important parameters of the MSM Photodetectors.[94,95] The relative importance of each parameter depends on the application, and they are not independent of each other.

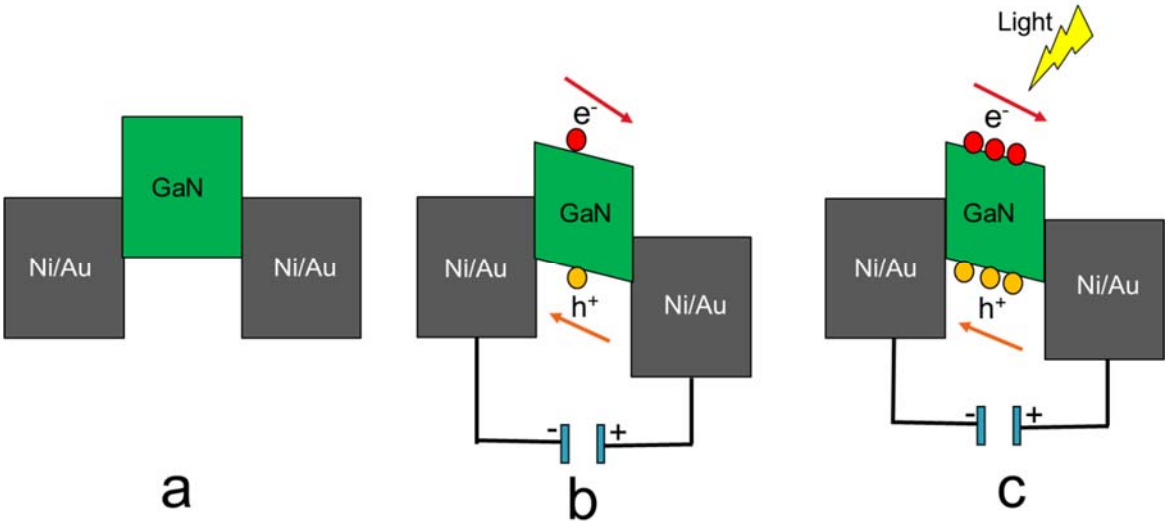

Figure 2.10 Energy band diagram of the GaN MSM photodetectors (a) under thermal equilibrium, (b) with applied voltage bias, (c) under photoexcitation with applied voltage bias. Devices are illuminated from the top.[95]

The growth of high-quality nitride material is the primary obstacle in developing nitride-based UV photodetectors. The UV detectors with low dark currents require the films with very low defect density. In the sections 7 and 8, we introduce improvements in the GaN film crystalline quality and realize the high-performance photodetectors based as grown LMOCVD GaN epilayers.

2.6 References

1. Davis, R. F., III-V nitrides for electronic and optoelectronic applications. Proceedings of the IEEE 1991, 79 (5), 702-712.

2. Bernardini, F.; Fiorentini, V.; Vanderbilt, D., Spontaneous polarization and piezoelectric constants of III-V nitrides. Physical Review B 1997, 56 (16), R10024.

3. Strite, S.; Morkoç, H., GaN, AlN, and InN: a review. Journal of Vacuum Science & Technology B: Microelectronics and Nanometer Structures Processing, Measurement, and Phenomena 1992, 10 (4), 1237-1266.

4. Razeghi, M.; Rogalski, A., Semiconductor ultraviolet detectors. Journal of Applied Physics 1996, 79 (10), 7433-7473.

5. Mauder, C.; Heuken, M. Physics, MOVPE Growth and Investigation of M-plane GaN Films and InGaN/GaN Quantum Wells on γ-LiAlO2 Substrates. Ph. D. Dissertation (Technische Hochschule Aachen, Aachen, 2011), 2011.

6. Lei, T.; Moustakas, T.; Graham, R.; He, Y.; Berkowitz, S., Epitaxial growth and characterization of zinc-blende gallium nitride on (001) silicon. Journal of Applied Physics 1992, 71 (10), 4933-4943.

7. Ramirez-Flores, G.; Navarro-Contreras, H.; Lastras-Martinez, A.; Powell, R.; Greene, J., Temperature-dependent optical band gap of the metastable zinc-blende structure β-GaN. Physical Review B 1994, 50 (12), 8433.

8. Craven, M.; Lim, S.; Wu, F.; Speck, J.; DenBaars, S., Structural characterization of nonpolar (1120) a-plane GaN thin films grown on (1102) r-plane sapphire. Applied physics letters 2002, 81 (3), 469-471.

9. Ghosh, S.; Waltereit, P.; Brandt, O.; Grahn, H.; Ploog, K., Electronic band structure of wurtzite GaN under biaxial strain in the M plane investigated with photoreflectance spectroscopy. Physical Review B 2002, 65 (7), 075202.

10. Waltereit, P.; Brandt, O.; Trampert, A.; Grahn, H.; Menniger, J.; Ramsteiner, M.; Reiche, M.; Ploog, K., Nitride semiconductors free of electrostatic fields for efficient white light-emitting diodes. Nature 2000, 406 (6798), 865-868.

11. Kuokstis, E.; Chen, C.; Gaevski, M.; Sun, W.; Yang, J.; Simin, G.; Asif Khan, M.; Maruska, H.; Hill, D.; Chou, M., Polarization effects in photoluminescence of C-and M-plane GaN/AlGaN multiple quantum wells. Applied Physics Letters 2002, 81 (22), 4130-4132.

12. Miller, D. J.; Harris, J. S.; McGehee, M.; Solomon, G., Gallium nitride epitaxy by a novel hybrid VPE technique. Stanford University: 2011.

13. Kang, H. A Study of the Nucleation and Formation of Multi-functional Nanostructures using GaN-Based Materials for Device Applications. Georgia Institute of Technology, 2006.

14. Kukushkin, S.; Osipov, A.; Bessolov, V.; Medvedev, B.; Nevolin, V.; Tcarik, K., Substrates for epitaxy of gallium nitride: new materials and techniques. Rev. Adv. Mater. Sci 2008, 17 (1/2), 1-32.

15. Gibson, I.; Rosen, D. W.; Stucker, B., Additive manufacturing technologies. Springer: 2010; Vol. 238.

16. Ishikawa, H.; Zhao, G.-Y.; Nakada, N.; Egawa, T.; Jimbo, T.; Umeno, M., GaN on Si substrate with AlGaN/AlN intermediate layer. Japanese journal of applied physics 1999, 38 (5A), L492.

17. Valcheva, E.; Paskova, T.; Persson, P. Å.; Hultman, L.; Monemar, B., Misfit defect formation in thick GaN layers grown on sapphire by hydride vapor phase epitaxy. Applied physics letters 2002, 80 (9), 1550-1552.

18. Usikov, A.; Soukhoveev, V.; Shapovalova, L.; Syrkin, A.; Kovalenkov, O.; Volkova, A.; Sizov, V.; Ivantsov, V.; Dmitriev, V., New results on HVPE growth of AlN, GaN, InN and their alloys. physica status solidi (c) 2008, 5 (6), 1825-1828.

19. Kim, D. S.; Lee, H. J.; Kim, Y. J.; Jung, S. K.; Lee, D. K.; Lee, B. Y. In A thick GaN growth using GaN/Si (111) template by hydride vapor phase epitaxy (HVPE), Integrated Optoelectronic Devices 2008, International Society for Optics and Photonics: 2008; pp 689406-689406-9.

20. Łucznik, B.; Pastuszka, B.; Grzegory, I.; Boćkowski, M.; Kamler, G.; Litwin-Staszewska, E.; Porowski, S., Deposition of thick GaN layers by HVPE on the pressure grown GaN substrates. Journal of crystal growth 2005, 281 (1), 38-46.

21. Tarsa, E.; Heying, B.; Wu, X.; Fini, P.; DenBaars, S.; Speck, J., Homoepitaxial growth of GaN under Ga-stable and N-stable conditions by plasma-assisted molecular beam epitaxy. Journal of Applied Physics 1997, 82 (11), 5472-5479.

22. Nakamura, S., GaN growth using GaN buffer layer. Japanese Journal of Applied Physics 1991, 30 (10A), L1705.

23. Ibach, H.; Lüth, H., Solid-state physics: an introduction to principles of material science. Advanced Texts in Physics, Springer-Verlag berlin Heidelberg New York 2003.

24. Lee, S. K.; Choi, H. J.; Pauzauskie, P.; Yang, P.; Cho, N. K.; Park, H. D.; Suh, E. K.; Lim, K. Y.; Lee, H. J., Gallium nitride nanowires with a metal initiated metal-organic chemical vapor deposition (MOCVD) approach. physica status solidi (b) 2004, 241 (12), 2775-2778.

25. Marchand, H.; Ibbetson, J.; Fini, P. T.; Kozodoy, P.; Keller, S.; DenBaars, S.; Speck, J.; Mishra, U., Atomic force microscopy observation of threading dislocation density reduction in lateral epitaxial overgrowth of gallium nitride by MOCVD. MRS Internet Journal of Nitride Semiconductor Research 1998, 3, e3.

26. Imer, B. M.; Speck, J. S.; DenBaars, S. P.; Nakamura, S., Growth of planar non-polar {1-1 0 0} m-plane gallium nitride with metalorganic chemical vapor deposition (MOCVD). Google Patents: 2008.

27. Wickenden, D.; Kistenmacher, T.; Bryden, W.; Morgan, J.; Wickenden, A. E. In The Effect of Self Nucleation Layers on the Mocvd Growth of Gallium Nitride on Sapphire, MRS Proceedings, Cambridge Univ Press: 1991; p 167.

28. Hirako, A.; Kusakabe, K.; Ohkawa, K., Modeling of reaction pathways of GaN growth by metalorganic vapor-phase epitaxy using TMGa/NH3/H2 system: a

computational fluid dynamics simulation study. Japanese journal of applied physics 2005, 44 (2R), 874.

29. Mihopoulos, T. G.; Gupta, V.; Jensen, K. F., A reaction-transport model for AlGaN MOVPE growth. Journal of Crystal Growth 1998, 195 (1), 733-739.

30. R. N. Zare, “Laser control of chemical reactions”, Science **279**, 1875 (1998).

31. F. F. Crim, “Bond-selected chemistry: Vibrational state control of photodissociation and bimolecular reaction”, J Phys Chem **100**, 12725 (1996).

32. F. F. Crim, “Chemical dynamics of vibrationally excited molecules: Controlling reactions in gases and on surfaces”, P Natl Acad Sci USA **105**, 12654 (2008).

33. D. R. Killelea, V. L. Campbell, N. S. Shuman and A. L. Utz, “Bond-selective control of a heterogeneously catalyzed reaction”, Science **319**, 790 (2008).

34. M. Goez, “Conformation-selective laser chemistry”, Angew Chem Int Edit **42**, 2336 (2003).

35. D. W. Lupo and M. Quack, “IR-laser photochemistry”, Chem Rev **87**, 181 (1987).

36. D. R. Killelea and A. L. Utz, “On the origin of mode- and bond-selectivity in vibrationally mediated reactions on surfaces”, Phys Chem Chem Phys **15**, 20545 (2013).

37. A. H. Zewail, “Laser-selective chemistry and vibrational-energy redistribution in molecules”, J Photochem **17**, 269 (1981).

38. A. Teslija and J.J. Valentini, “State-to-state reaction dynamics: A selective review”, J Chem Phys **125**, 132304 (2006).

39. S. Yoon, R. J. Holiday and F. F. Crim, “Vibrationally controlled chemistry: Mode- and bond-selected reaction of CH3D with CI”, J Phys Chem B **109**, 8388 (2005).

40. F. F. Crim, “Vibrational-state control of bimolecular reactions: Discovering and directing the chemistry”, Acc Chem Res 32, 877 (1999).

41. A. H. Zewail, “Laser selective chemistry - Is it possible”, Phys Today **33**, 27 (1980).

42. P. J. Heggs, “Special topic issue: chemical-reaction engineering”, Chem Eng Res Des **68**, 481 (1990).

43. J. N. Du, K. L. Skubi, D. M. Schultz and T. P. Yoon, “A dual-catalysis approach to enantioselective [2+2] photocycloadditions using visible light”, Science **344**, 392 (2014).

44. P. Kripylo and L. Beck, “Chemical-reaction engineering and development of catalysts for heterogeneous catalyzed gas-phase oxidation of hydrocarbons”, Chem Tech Leipzig **42**, 462 (1990).

45. A. Sinha, M. C. Hsiao and F. F. Crim, “Bond-selected bimolecular chemistry: H+HOD(4*v*OH)->OD+H2”, J Chem Phys **92**, 6333 (1990).

46. M. J. Bronikowski, W. R. Simpson, B. Girard and R. N. Zare, “Bond-specific chemistry: OD-OH product ratios for the reactions H+HOD (100) and H+HOD (001)”, J Chem Phys **95**, 8647 (1991).

47. M. J. Bronikowski, W. R. Simpson and R. N. Zare, “Comparison of reagent stretch vs bend excitation in the H+D2O reaction - an example of mode-selective chemistry”, J Phys Chem **97**, 2204 (1993).

48. S. Yan, Y. T. Wu, B. L. Zhang, X. F. Yue and K. P. Liu, "Do vibrational excitations of CHD3 preferentially promote reactivity toward the chlorine atom?", Science **316**, 1723 (2007).

49. C. Kreher, R. Theinl and K. H. Gericke, "State-to-state reaction dynamics of R+HCN ($v1v$l22$v3$)->RH+CN(v, J) with R=Cl, H", J Chem Phys **104**, 4481 (1996).

50. R. D. Guettler, G. C. Jones, L. A. Posey and R. N. Zare, "Partial control of an ion-molecule reaction by selection of the internal motion of the polyatomic reagent ion", Science **266**, 259 (1994).

51. Y. H. Chiu, H. S. Fu, J. T. Huang and S. L. Anderson, Large, "Mode-selective vibrational effect on the reaction of C2H2+ with methane", J Chem Phys **101**, 5410 (1994).

52. L. J. Butler, E. J. Hintsa and Y. T. Lee, "Bond selective photochemistry in CH2BrI through electronic excitation at 210 nm", J Chem Phys **84**, 4104 (1986).

53. L. J. Butler, E. J. Hintsa, S. F. Shane and Y. T. Lee, "The electronic state-selective photodissociation of CH2BrI at 248, 210, and 193 nm, J Chem Phys **86**, 2051 (1987).

54. R. Haubner and B. Lux, "Diamond growth by hot-gas breakdown chemical-vapor-deposition: State-of-the-art", Diam Relat Mater **2**, 1277 (1993).

55. J. A. Smith, K. N. Rosser, H. Yagi, M. I. Wallace, P. W. May and M. N. R. Ashfold, "Diamond deposition in a DC-arc jet CVD system: investigations of the effects of nitrogen addition", Diam Relat Mater **10**, 370 (2001).

56. J. K. Lee, K. Y. Eun, Y. J. Baik, H. J. Cheon, J. W. Rhyu, T. J. Shin and J. W. Park, "The large area deposition of diamond by the multi-cathode direct current plasma assisted chemical vapor deposition (DC-PACVD) method", Diam Relat Mater **11**, 463 (2002).

57. D. E. Meyer, R. O. Dillon and J. A. Woollam, "Radio-frequency plasma chemical vapor deposition growth of diamond", J Vac Sci Technol A **7**, 2325 (1989).

58. S. Matsumoto, M. Hino and T. Kobayashi, "Synthesis of diamond films in a RF induction thermal plasma", Appl Phys Lett **51**, 737 (1987).

59. K. Kobashi, K. Nishimura, Y. Kawate and T. Horiuchi, "Synthesis of diamonds by use of microwave plasma chemical-vapor deposition: morphology and growth of diamond films", Phys Rev B **38**, 4067 (1988).

60. A. Ono, T. Baba, H. Funamoto and A. Nishikawa, "Thermal-conductivity of diamond films synthesized by microwave plasma CVD", Jpn J Appl Phys **25**, L808 (1986).

61. Y. Hirose, S. Amanuma and K. Komaki, "The synthesis of high-quality diamond in combustion flames", J Appl Phys **68**, 6401 (1990).

62. Fan, Lisha. "Diamond film deposition using laser-assisted combustion flames." (2014).

63. P. Heszler, L. Landstrom, M. Lindstam and J. O. Carlsson, “Light emission from tungsten nanoparticles during laser-assisted chemical vapor deposition of tungsten”, J Appl Phys **89**, 3967 (2001).

64. P. Heszler, J. O. Carlsson and P. Mogyorosi, “Reaction pathways for ArF excimer-laser assisted tungsten chemical-vapor-deposition from a WF6-H2 gas-mixture”, J Vac Sci Technol A **11**, 2924 (1993).

65. H. Zama, T. Miyake, T. Hattori and S. Oda, “Preparation of highly oriented copper-films by photo-assisted chemical vapor deposition using beta-diketonate complex”, Jpn J Appl Phys **31**, L588 (1992).

66. J. S. Han and K. F. Jensen, “Combined experimental and modeling studies of laser-assisted chemical-vapor-deposition of copper from copper(I)-hexafluoroacetylacetonate trimethylvinylsilane”, J Appl Phys **75**, 2240 (1994).

67. B. Markwalder, M. Widmer, D. Braichotte and H. Vandenbergh, “High-speed laser chemical vapor deposition of copper - a search for optimum conditions”, J Appl Phys **65**, 2470 (1989).

68. D. Wexler, J. I. Zink, L. W. Tutt and S. R. Lunt, “Laser-assisted deposition of pure gold from (CH3)2Au-hexafluoroacetylacetonate and gas-phase luminescence identification of photofragments”, J Phys Chem **97**, 13563 (1993).

69. J. S. Han, K. F. Jensen, Y. Senzaki and W. L. Gladfelter, “Pyrolytic laser-assisted chemical-vapor-deposition of Al from dimethylethylamine-alane: characterization and a new 2-step writing Process”, Appl Phys Lett **64**, 425 (1994).

70. D. C. Skouby and K. F. Jensen, “Modeling of pyrolytic laser-assisted chemical vapor-deposition: mass-transfer and kinetic effects influencing the shape of the deposit”, J Appl Phys **63**, 198 (1988).

71. R. Bilenchi, I. Gianinoni, M. Musci, R. Murri and S. Tacchetti, “CO2 laser-assisted deposition of boron and phosphorus-doped hydrogenated amorphous-silicon”, Appl Phys Lett **47**, 279 (1985).

72. K. Suzuki, D. Lubben and J. E. Greene, “Laser-assisted chemical vapor deposition of Si (low-temperature (< 600℃) growth of epitaxial and polycrystalline layers”, J Appl Phys **58**, 979 (1985).

73. A. Yamada, A. Satoh, M. Konagai and K. Takahashi, “Low-temperature (600-650℃) silicon epitaxy by excimer laser assisted chemical vapor deposition”, J Appl Phys **65**, 4268 (1989).

74. J. F. Osmundsen, C. C. Abele and J. G. Eden, “Activation-energy and spectroscopy of the growth of germanium films by ultraviolet laser-assisted chemical vapor deposition”, J Appl Phys **57**, 2921 (1985).

75. N. H. Karam, H. Liu, I. Yoshida, B. L. Jiang and S. M. Bedair, “Low-temperature selective epitaxy of III-V compounds by laser assisted chemical vapor deposition”, J Cryst Growth **93**, 254 (1988).

76. J. Kikawa, S. Yoshida and Y. Itoh, “Hexagonal GaN1-xPx growth by laser-assisted metalorganic chemical vapor deposition’, J Cryst Growth **229**, 48 (2001).

77. Y. Bu, L. Ma and M. C. Lin, “Laser-assisted chemical vapor deposition of InN on Si(100)”, J Vac Sci Technol A **11**, 2931 (1993).

78. G. B. Shinn, P. M. Gillespie, W. L. Wilson and W. M. Duncan, “Laser-assisted metalorganic chemical vapor-deposition of zinc selenide epitaxial-films”, Appl Phys Lett **54**, 2440 (1989).

79. H. Demiryont, L. R. Thompson and G. J. Collins, “Optical-properties of aluminum oxynitrides deposited by laser-assisted CVD”, Appl Optics **25**, 1311 (1986).

80. P. K. Boyer, G. A. Roche, W. H. Ritchie and G. J. Collins, “Laser-induced chemical vapor deposition of SiO2”, Appl Phys Lett **40**, 716 (1982).

81. H. S. Tsai, G. J. Jaw, S. H. Chang, C. C. Cheng, C. T. Lee and H. P. Liu, “Laser-assisted plasma-enhanced chemical vapor deposition of silicon nitride thin film”, Surf Coat Tech **132**, 158 (2000).

82. R. Banal, T. Kimura and T. Goto, “High speed deposition of Y2O3 films by laser-assisted chemical vapor deposition”, Mater Trans **46**, 2114 (2005).

83. J. C. Oliveira, M. N. Oliveira and O. Conde, “Structural characterization of B4C films deposited by laser-assisted CVD”, Surf Coat Tech **80**, 100 (1996).

84. R. Longtin, C. Fauteux, J. Pegna and M. Boman, “Micromechanical testing of carbon fibers deposited by low-pressure laser-assisted chemical vapor deposition”, Carbon **42**, 2905 (2004).

85. M. Lindstam, M. Boman and K. Piglmayer, “Room temperature deposition of hydrogenated amorphous carbon films from laser-assisted photolytic chemical vapor deposition at 248 nm”, Thin Solid Films **394**, 115 (2001).

86. J. H. D. Rebello, D. L. Straub and V. V. Subramaniam, “Diamond growth from a CO/CH4 mixture by laser excitation of CO: Laser-excited chemical vapor deposition”, J Appl Phys **72**, 1133 (1992).

87. J. B. Park, W. Xiong, Y. Gao, M. Qian, Z. Q. Xie, M. Mitchell, Y. S. Zhou, G. H. Han, L. Jiang and Y. F. Lu, “Fast growth of graphene patterns by laser direct writing”, Appl Phys Lett **98**, 123109 (2011).

88. K. Kasuya, K. Nagato, Y. Jin, H. Morii, T. Ooi and M. Nakao, “Rapid and localized synthesis of single-walled carbon nanotubes on flat surface by laser-assisted chemical vapor deposition”, Jpn J Appl Phys **46**, L333 (2007).

89. M. Mahjouri-Samani, Y. S. Zhou, W. Xiong, Y. Gao, M. Mitchell, L. Jiang and Y. F. Lu, “Diameter modulation by fast temperature control in laser-assisted chemical vapor deposition of single-walled carbon nanotubes”, Nanotechnology **21**, 395601 (2010).

90. Z. Toth, A. Mechler and P. Heszler, “Local laser-assisted chemical vapor deposition of diamond”, Appl Surf Sci **168**, 5 (2000).

91. J. Shi, Y. F. Lu, K. J. Yi, Y. S. Lin, S. H. Liou, J. B. Hou and X. W. Wang, “Direct synthesis of single-walled carbon nanotubes bridging metal electrodes by laser-assisted chemical vapor deposition”, Appl Phys Lett **89,** 083105 (2006).

92. E. Plonjes, P. Palm, G. B. Viswanathan, V. V. Subramaniam, I. V. Adamovich, W. R. Lempert, H. L. Fraser and J. W. Rich, “Synthesis of single-walled carbon nanotubes in vibrationally non-equilibrium carbon monoxide”, Chem Phys Lett **352**, 342 (2002).

93. C. W. David, “IR vibration-rotation spectra of the ammonia molecule”, J Chem Educ **73**, 46 (1996).

94. Li, Jianliang. "Ultrafast Metal-Semiconductor-Metal UV Photodetectors on GaN." PhD diss., University of Rochester, (2004).

95. Tekcan, B.; Ozgit-Akgun, C.; Bolat, S.; Biyikli, N.; Okyay, A. K., Metal-semiconductor-metal ultraviolet photodetectors based on gallium nitride grown by atomic layer deposition at low temperatures. *Optical Engineering***,** *53* (10), 107106-107106 (2014).

CHAPTER 3 THEORETICAL OVERVIEW AND CHARACTERIZATION TECHNIQUES

3.1 Sample preparation

We used two general types of irradiation geometries in laser-assisted metal organic chemical vapor deposition (LMOCVD) of gallium nitride (GaN), represented in Fig. 3.1. In first irradiation geometry used in chapter 6, large GaN films were formed at low temperatures by a laser-initiated homogeneous reaction above the surface. A wavelength-tunable carbon dioxide (CO_2) laser (PRC, wavelength range from 9.2 to 10.9 μm) was used as the irradiation sources. The laser beam, with a diameter of around 10-12 mm, was irradiated in parallel to the substrate surface inside the chamber through a zinc selenide (ZnSe) window, as shown in Fig. 3.1a. The laser was tuned at a wavelength of 9.219 μm to resonantly excite the wagging mode of ammonia (NH_3) molecules, couple the laser energy into the reaction. The distance between the laser beam and substrate surface was maintained at about 20 mm. In this case, the laser initiates chemistry in the gas only and not on the substrate surface. In another irradiation geometry and configuration of laser-assisted metal organic chemical vapor deposition of gallium nitride in chapters 4, 5, 7 and 8, the continuous-wave (CW) CO_2 laser beam irradiates on the substrate surface at nearly normal incidence (Fig. 3.1b). In chapter 4, the Si substrate was shined and heated with a CO_2 laser beam of diameter 2.5 ± 0.5 mm. In chapter 6, CW CO_2 laser (PRC, Inc., 9.2-10.9 μm) was used as the irradiation source at laser wavelengths of 10.719, 10.350, and 9.219 μm, achieving a reactant excitation of NH_3 molecules and substrate heating. In chapters 7 and 8, a continuous-wave wavelength-tunable CO_2 laser (PRC Inc., λ = 9.201 μm) was also used for substrate heating. However, in this new setup, a flat top laser beam shaper (Edmund Optics) was used for generating a wider beam with uniform power distribution (beam diameter ~ 20 mm) from

a Gaussian CO_2 laser beam (wavelength-tunable PRC CO_2 laser Inc., $\lambda = 9.201$ μm). The temperature of the substrates during the deposition was monitored by a noncontact pyrometer (OS3752, Omega Engineering, Inc.).

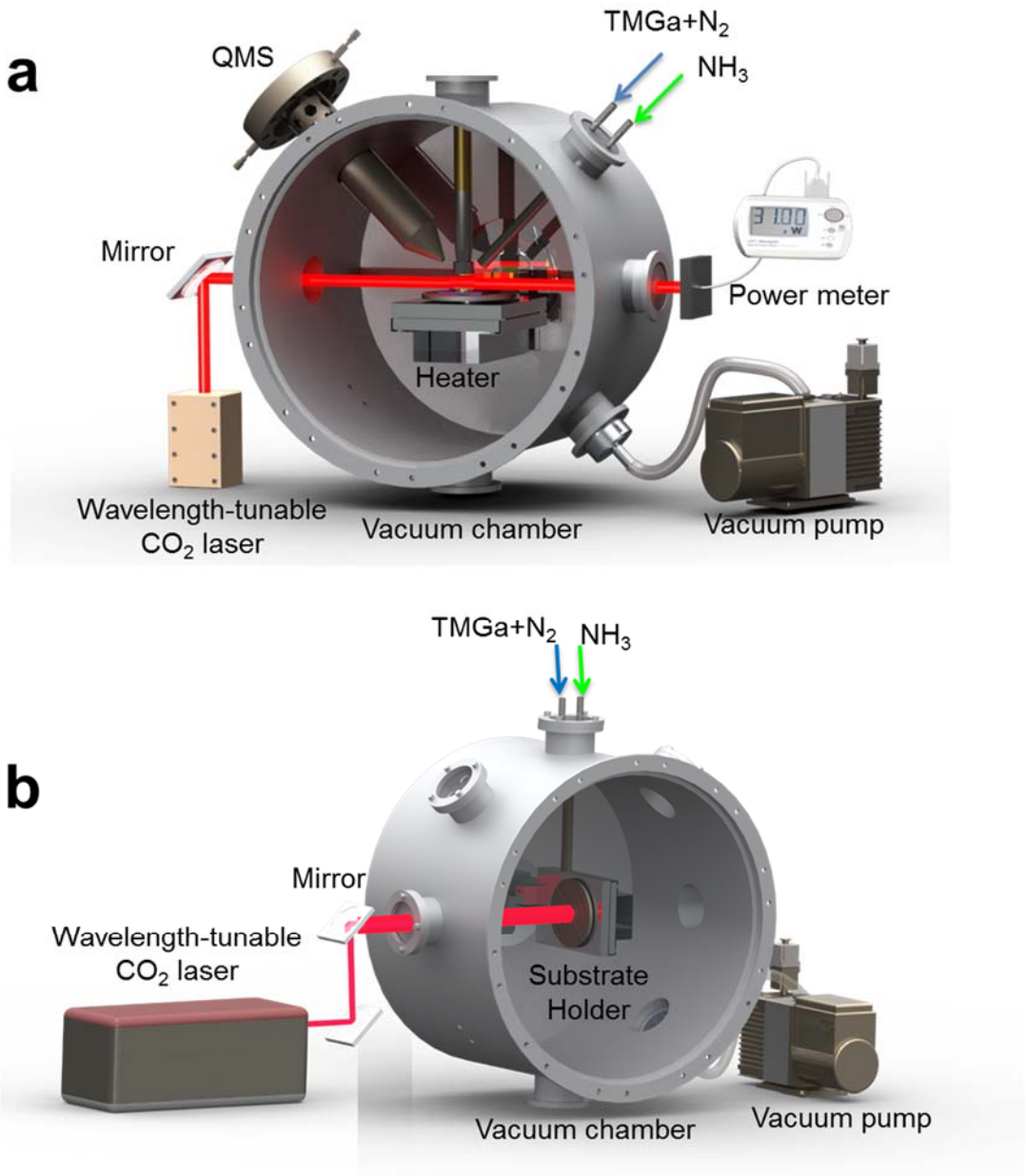

Figure 3.1 (a) Illustration of the experimental setup for the CO_2 laser-assisted MOCVD growth of GaN films with: (a) parallel irradiation geometry and (b) perpendicular irradiation geometry.

In all experiments, the silicon and sapphire substrates (10 × 10 mm^2) were cleaned and dried before loading into the LMOCVD chambers. Trimethylgallium (TMGa) and NH_3 were used as the Ga and N precursors, respectively. The experimental details were explained in each chapter.

The applications of GaN films are based on their remarkable properties. For these applications to be realized, the structural, optical and electronic qualities of films need to be more thoroughly characterized. Numerous techniques are useful in GaN characterizations.

3. 2 Structural characterization

3.2.1 X-ray diffraction

X-Ray diffraction (XRD) is a non-destructive method used to characterize the structures of GaN film. The Bragg's law describes the diffraction of X-rays from a crystal by:[1-3]

$$n\lambda = 2d \times \sin\theta \qquad (3.1)$$

where n is an integer, λ is the X-ray wavelength, and d is the spacing between atoms. With a given X-ray wavelength and the angle that X-rays are diffracted, θ, the atomic spacing d can be calculated, as shown in Fig. 3.2. Because the exact atomic spacing, d, is unique for a material, the unknown materials can be identified by comparing their XRD spectrum with that of a known standard. The Fig. 3.2 illustrates the schematic illustration of the geometrical parameters of the XRD characterization.

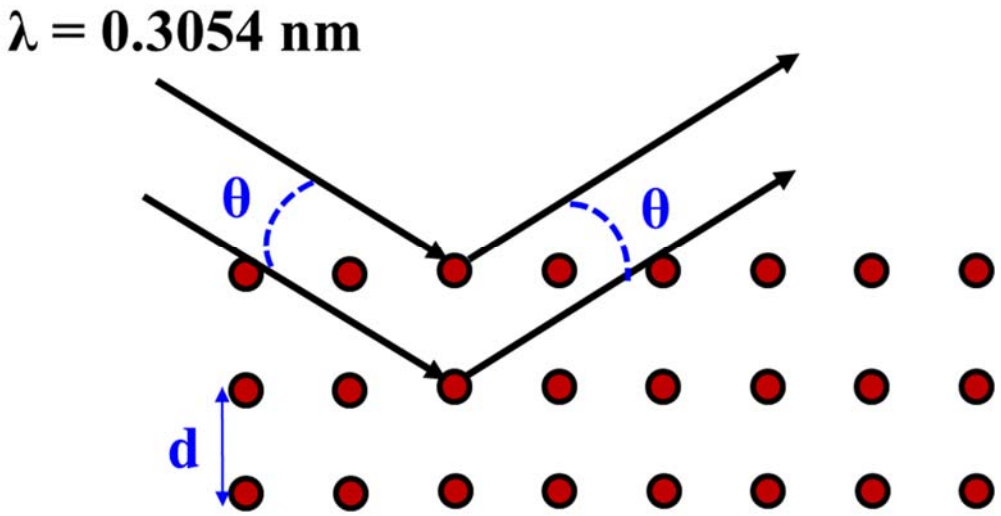

Figure 3.2. Diffraction of X-rays from a thin film surface showing the Bragg angle, θ.[1]

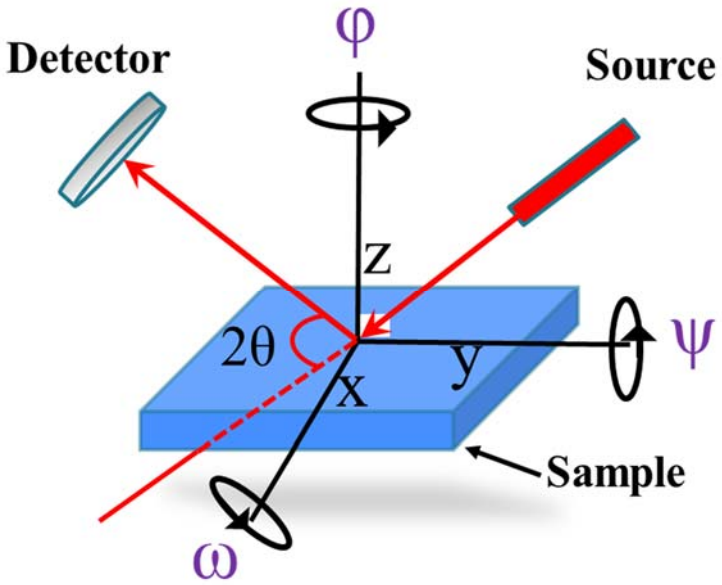

Figure 3.3 The schematic illustration of the geometrical parameters of the XRD characterization.

3.2.1.1 θ-2θ scan

The lattice constant and mole fraction of the materials can be identified using the XRD *θ-2θ* scan measurement. In *θ-2θ* scan, the X-ray source is fixed and the sample rotates a certain angle, *θ*, with respect to the axis of X-ray beam. The detector rotates

twice of the angle θ as shown in Fig. 3.3, and collects the reflected X-ray beam. The material information such as orientation can be calculated from this type of XRD scan. For example, the (0002) reflection plane is indexed to the *c*-plane GaN. This reflection is perpendicular to the growth direction and is a good gauge of GaN crystal orientation and qaulity.[1-3] Figs. 3.4a and b show a photo of Rigaku Smartlab, a multifunctional X-Ray diffractometer system, and XRD θ-2θ spectrum of *c*-oriented GaN on sapphire, respectively.

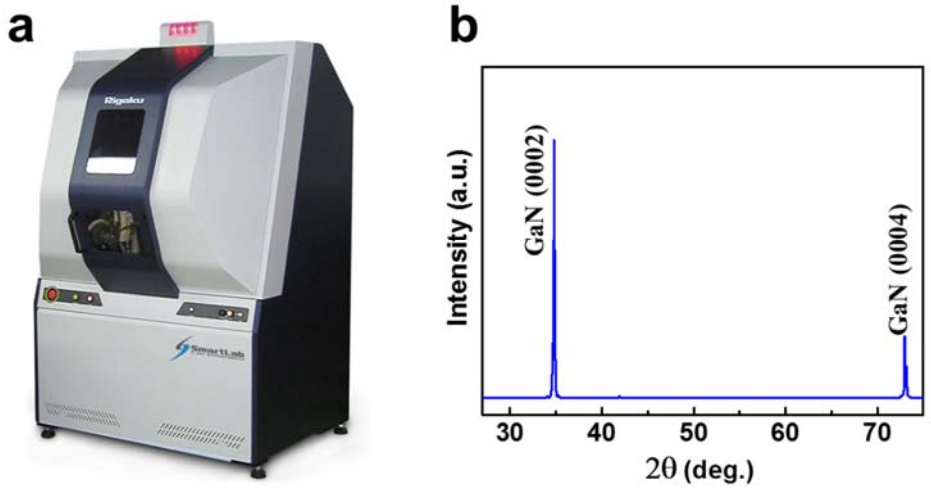

Figure 3.4 (a) A photo of Rigaku Smartlab, a multifunctional X-Ray diffractometer system. (b) XRD θ-2θ spectrum of *c*-oriented GaN on sapphire.

3.2.1.2 Rocking curve scan (ω-scan)

The XRD rocking curve (XRC) measurement is commonly used for quantitative measurement of the film quality while the θ-2θ XRD only gives the information on the crystalline orientation of the thin films. The inter-planar spacing of the grown films is measured using XRC.[4-7] In this experiment, the detector and the X-ray source are fixed at certain angle, which receive the x-ray signal in θ-2θ scan. Then, the sample is rocked about ω axis. The strong diffraction peak is only observed when a particular crystal is

aligned at the angle matching to Bragg's Law. The full width at half maximum (FWHM) of XRC is typically used to measure the film threading dislocation density and determine the film quality.[4-7]

3.2.1.3 In-plane φ-scan

The XRD φ-scans are conducted to reveal the in□plane orientation and epitaxial details of films.[4-7] The in□plane orientation can be measured by four□circle diffractometer. In φ-scan experiment, first, a crystallographic plane inclined to the growth plane is identified. The θ and 2θ angles are constant to corresponding to Bragg angle for the identified plane. The ψ, sample tilt, is set equal to the crystallographic angle between the growth plane and the identified plane for the φ-scan. The diffraction spectra are collected with the sample rotation along φ-axis. In an epitaxial film, the φ spectra have sharp diffraction peaks at certain φ-angles.[4-7]

3.2.2 Raman spectroscopy

Raman spectroscopy is a common technique for studying the quality and residual stress of thin films.[8-10] In Raman spectroscopy, an incident beam with a single wavelength is irradiated on the sample and a photon with different energy from the incident photon is scattered. The different between the energy of scattered photon and incident photon is one vibrational energy unit which forms the basis of Raman scattering.

The theoretical studies show that the hexagonal structure has eight sets of phonon modes at k ~ 0 (Γ point in Brillouin zone), $2A_1 + 2E_1 + 2B_1 + 2E_2$. The A_1 and E_1 modes are acoustic and other six modes, $A_1 + E_1 + 2B_1 + 2E_2$, are optical.[8-11] The schematic of the atomic displacement of the optical modes is seen in Fig. 3.5. The A_1 and B_1 modes represent atomic displacements along the *c*-axis and the E_1 and E_2 are atomic

displacements perpendicular to the *c*-axis. The A_1 and E_1 modes are both Raman and infrared (IR) active, while the two E_2 modes are only Raman active, and the two B_1 modes are neither Raman nor IR active.

Raman configurations of allowed modes in hexagonal nitrides are shown in Table 3.1. The symbols from left to right outside the bracket show the direction of incident and scattered light, respectively, and the ones from left to right inside the bracket represent the polarization direction of the incident and scattered light, respectively. In wurtzite nitride structures studied under a *z(x,x)-z* geometry, E_2(high) mode is the strongest and is very sensitive to the inplane strain. The A_1(LO) phonon mode has atomic displacement parallel to the *c*□axis. If we suppose the *c*-axis is along the *z* direction and *x* and *y* directions are perpendicular to *c*-axis, the A_1(LO) mode can be detected from *c*□plane wurtzite nitrides under a *z(x,x)-z* backscattering geometry.[8-10]

In this work, Raman spectroscopic studies were conducted under a *z(x,x)-z* backscattering geometry, where *z* and *-z* represent the projection direction of the incoming and scattered light, and x represents the polarization direction of the incoming and scattered light. Figs. 3.6a and b show a picture of the Raman spectroscopy system (inVia Raman microscopy, Renishaw) and Raman spectrum of a wurtzite GaN film grown by LMOCVD, respectively.[8-11]

Table 3.1 Raman configurations of allowed modes in hexagonal nitrides[11]

Configuration	*x*(*y*, *y*)-*x*	*x*(*z*, *z*)-*x*	*x*(*z*, *y*)-*x*	*x*(*y*, *z*)*y*	*x*(*y*, *y*)*z*	*z*(*y*, *x*)-*z*	*z*(*y*, *y*)-*z*
Mode	A_1(TO), E_2	A_1(TO)	E_1(TO)	E_1(TO), E_1(LO)	E_2	E_2	A_1(LO), E_2

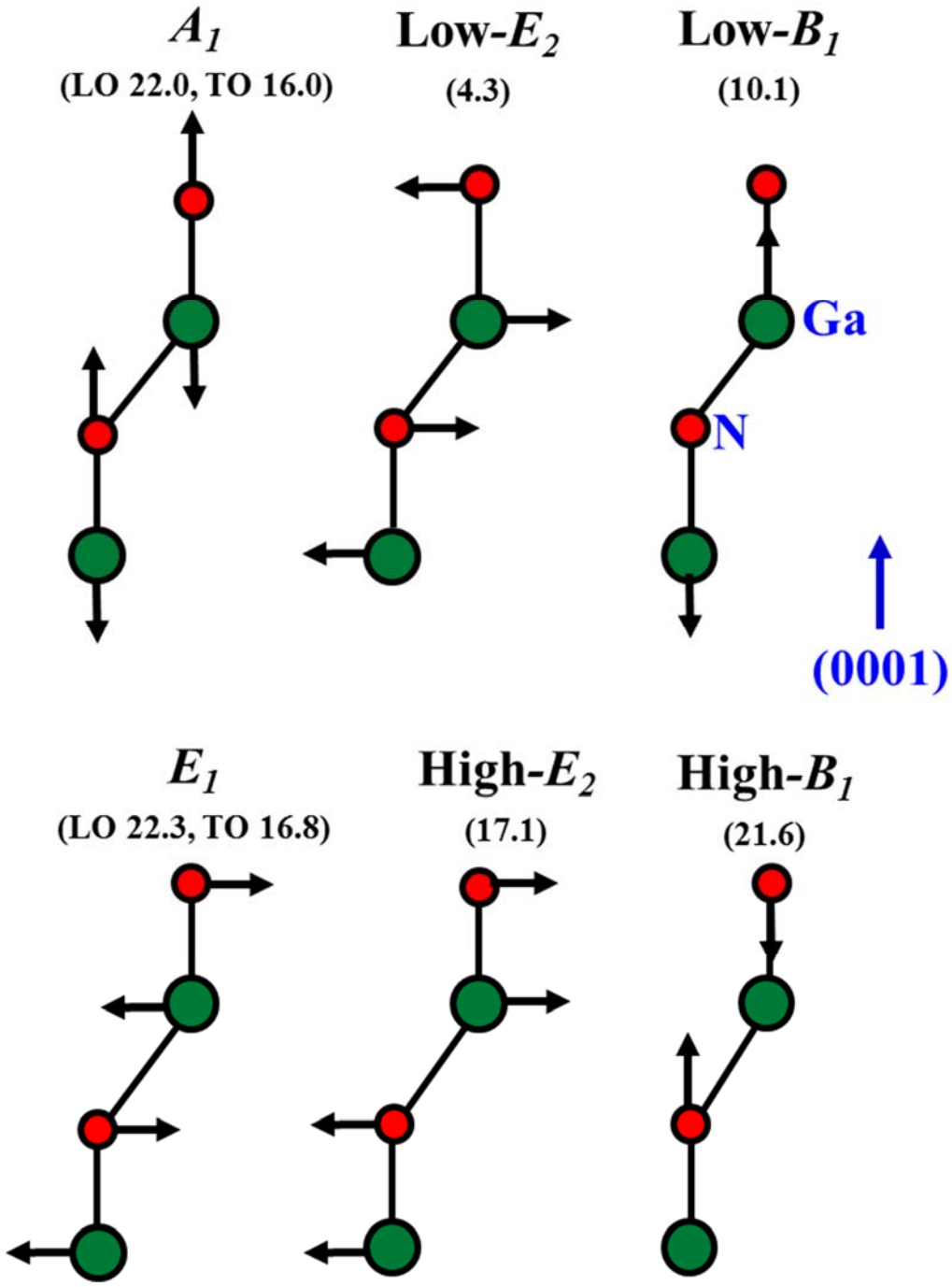

Figure 3.5. Atomic displacements of the Γ-point phonons in wurtzite GaN. Low-E_2 (low-B_1) and high-E_2 (high-B_1) represent the low- and high-frequency E_2 (B_1) modes, respectively. The frequency numbers inside the parentheses are in THz obtained from previous studies.[11]

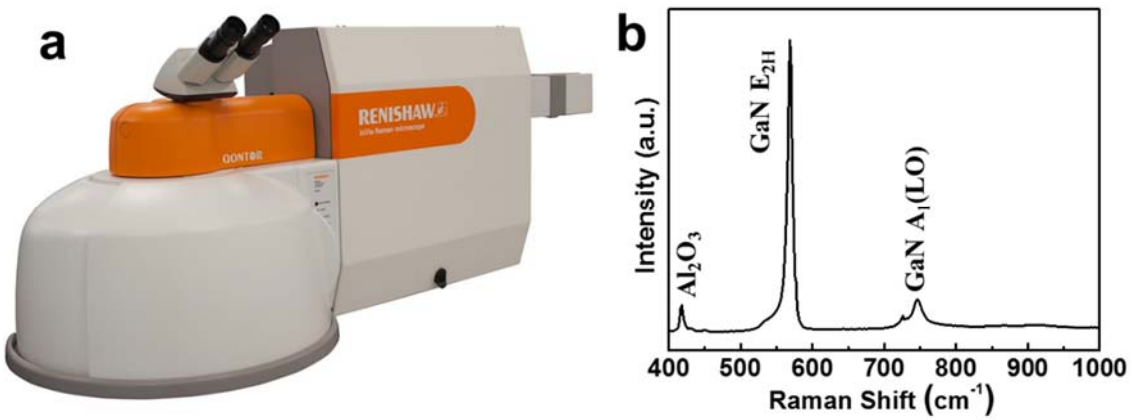

Figure 3.6 (a) A picture of the Raman spectroscopy system (inVia Raman microscopy, Renishaw); (b) A Raman spectrum of a wurtzite GaN film grown by LMOCVD.

3.3 Surface characterization

3.3.1 Scanning Electron Microscopy (SEM)/Energy Dispersive X-ray Spectroscopy (EDS)

Using the interaction between a beam of high energy electrons and the sample, a thin film can be imaged. The interaction between the sample and the electrons has different types including transmitted electrons, secondary electrons, and backscattered electrons. In a SEM, high-energy beam of electrons scan the sample surface. Depending on the desired image, various types of the electrons can be detected. SEM images are very useful in investigating the microstructure of a GaN film surface. Incident a beam of high energy electrons can also generate X-rays with a specific wavelength which is used for the characterization of the thin film composition. In EDS, the relative intensities of these X-rays are measured to study the composition of sample surface.

3.3.2 Transmission Electron Microscopy (TEM)

TEM, a high-resolution imaging method, is known as a very powerful method for studying the crystal quality of thin films and interfaces. In TEM, a beam of electrons transmitted through a very thin sample (10-100 nm thickness).[13] Very high magnification

images are obtained from the patterns produced from the interaction of the electrons with the sample. Electrons can be diffracted, absorbed or transmitted through the sample. The diffracted electron patterns can help for studying the crystal structure and quality, and the absorbed electron patterns are useful to create contrast in both bright-field and dark-field TEM images.

3.3.3 Atomic Force Microscope (AFM)

AFM is a simple and non-destructive method to determine the film surface roughness and average threading dislocations in gallium nitride. In AFM technique, a sharp tip runs over the surface to scan and takes AFM images. The AFM tips are typically from silicon nitride or silicon attached to a cantilever. A laser beam is used to detect cantilever deflections towards or away from the surface. A position-sensitive photo diode (PSPD) is used to detect these changes and generate an electric signal. This signal is sent via a feedback loop to a piezoelectric ceramic to control the height of the tip above the surface and maintain the position of laser constant. The interaction force around 10^{-11}-10^{-6} N between tip and film surface can detect the topography of sample.[12]

The AFM measurements in GaN can be done either in tapping or contact mode. Since, the GaN is a very hard material compared to the tip, the dragging motion of the probe tip in contact mode can break the tip. The measurements in this work were done at Nebraska Center for Materials and Nanoscience using Bruker Dimension ICON SPM. The resonance frequency was set on 220-320 kHz, and a scan rate of 2 Hz was used for scanning GaN film surface using a silicon tip.

3.4 Optical characterization

The information about the quality, strain, impurities, and native defects of GaN can be obtained using optical characterization of films. The information about energy level of impurities can be also achieved form the temperature dependence of these properties. Photoluminescence spectroscopy and optical transmission/absorption spectroscopy are the common methods for investigating optical properties in semiconductors materials. Photoluminescence spectroscopy was employed in this work, along with optical transmission and absorption, to study the optical properties of the grown GaN layers.

3.4.1 Photoluminescence Spectroscopy (PL)

In photoluminescence process, a material absorbs photons of one wavelength and emits photons of another wavelength. The electrons are excited to higher energy states by absorbing photon energy from a photoexcitation source like laser.[14-16] When the electrons return to their ground state through a radiative recombination, they emit photons. PL is the investigation of radiative recombination mechanisms in materials. Many semiconductor material properties including bandgap energy, electronic defects, strain, and optical quality can be determined using PL spectroscopy.

PL spectrum of a semiconductor material shows two prominent features, near-bandgap emission that gives the semiconductor band gap, and radiative transitions which involve semiconductor impurities and electronic defects.[14-16] PL spectra of wide bandgap semiconductors typically contain several radiative transitions including near-band edge transitions, donor-acceptor pair transitions, defect levels to the bandedge transitions and

bandedge to defect levels transitions. Using the energy of such transitions, the defect levels in semiconductors are determined.

In our work, the PL spectroscopy of GaN films was studied using a photoluminescence spectrometer (a 325 nm Melles-Griot He-Cd laser as photoexcitation source and a iHR320 photoluminescence spectrometer with Si and indium gallium arsenide (InGaAs) detectors).

3.4.2 Optical transmission

Another useful technique to examine the optical properties of a material is optical transmission. The GaN is transparent throughout the visible spectrum, allowing light of a lower energy than the bandgap to pass through the material. Examining the percent transmission as a function of wavelength give information about the bandedge as well as electronic defects that are not visible in PL spectra.

Defects are often visible in a transmission spectrum as an absorption band that causes a drop in the transmission signal below the bandgap energy. Optical transmission also provides information about intra-atomic transitions. These measurements require a smooth surface on both top and bottom of the film, however, as a rough surface will scatter the transmitted light and decrease signal intensity significantly. Optical transmission data were collected using a Perkin-Elmer LAMBDA 1050 UV/Vis/NIR spectrophotometer.

3.5 Electrical characterization

Electrical characterization techniques are performed to measure the free carrier concentration, conductivity and resistivity of the thin films. This information helps to determine the impurity levels and quality of GaN films. For example, the important

impurities in GaN, such as oxygen, silicon, and carbon contribute to high carrier concertation and conduction.

3.5.1 Hall effect measurement

The Hall effect is measured with applying a magnetic field perpendicular to the flow of current in a semiconductor bar to deflect the path of the carriers.[17,18] If we suppose that the magnetic field is applied in the *z* direction in a right-handed coordinated system, and current flows in the *x* direction, then the force applied to the carriers is given as:

$$F_y = q(E_y - V_x B_z) \tag{3.2}$$

where E_y is the electric field (*y* direction), V_x is carrier velocity (*x* direction), and B_z is the magnetic field (*z* direction). The carriers will face a net force F_y (–*y* direction) except an electric field with magnitude equal to $V_x B_z$ is caused to compensate. The compensating electric field is created with the shift of the carriers along the *y*-axis which it causes the carriers to keep the *x*-axis as their overall direction. The compensating electric field generated by the Hall effect is measured with the product of current density and magnetic flux density. The Hall coefficient is calculated by:[17,18]

$$R_H = \frac{1}{\mathrm{q}p_0} \tag{3.3}$$

where p_o is the carrier density. With given the values of current and magnetic field, and measuring the induced voltage across the sample, the free carrier concentration can be computed. Hall effect measurements are useful to determine information, including the resistivity, conductivity, and carrier mobility of GaN films. In this work, Hall effect measurements were performed using the Van der Pauw technique with cloverleaf geometry at room temperature.

3.6 Optical emission spectroscopy

The optical emission spectra (OES) of laser irradiated NH_3 were taken in open air using a spectrometer (Shamrock SR-303i-A, Andor Technology) coupled with an intensified charged coupled device (ICCD) (iStar DH-712, Andor Technology). Fig. 3.7a and b show the schematic experimental setup for the OES measurements in open air and OES of the NH_3 under laser irradiation at wavelength of 9.219 μm in open air, respectively.

The IR laser beam was focused to a diameter around 1 mm using a ZnSe convex lens (f = 25.4 cm). A welding torch with a nozzle diameter of 1.5 mm was used to introduce the NH_3 gas at a flowrate of 50 sccm. The CO_2 laser beam was directed perpendicularly to the NH_3 flow. The laser incident power density was fixed at 1.4 × 104 W/cm^2 for all laser wavelengths. All spectra were taken with a vertical collecting length of 0.5 mm along the emission, centered at the tip of the emission, and with a horizontal slit width of 30 μm centered at the tip apex of the emission. A background spectrum captured before collecting the emission spectra was subtracted from all spectra.

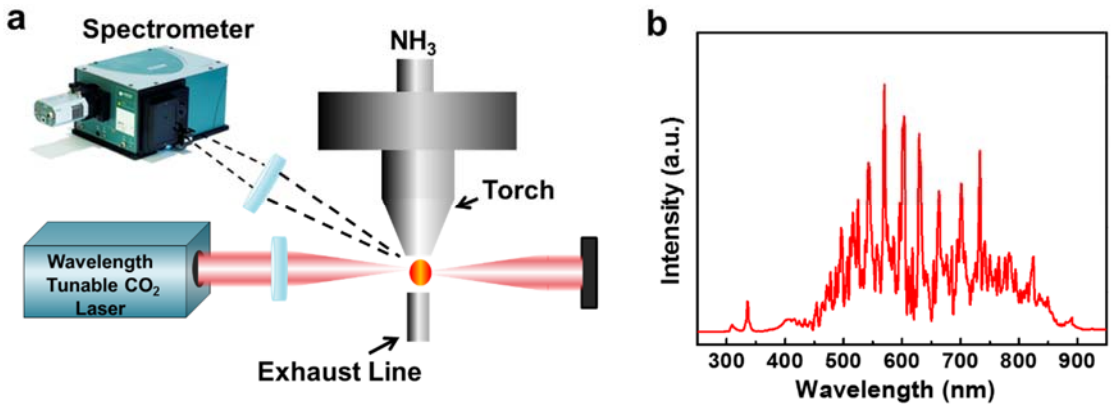

Figure 3.7 (a) schematic experimental setup for the OES measurements in open air. b) OES of the NH_3 under laser irradiation at wavelength of 9.219 μm in open air.

3.7 Device processing and characterization

Once LMOCVD GaN films were grown, the metal semiconductor metal (MSM) device was fabricated on as-grown films. The interdigitated finger of MSM device was 50 μm long, with 10 μm finger width and 10 μm finger spacing, and a detection area of 10×10 μm^2. The devices were fabricated using standard photolithography with patterning photoresist for subsequent metallization of metal Schottky contacts on the GaN. With the high metal work function and the good adhesion with GaN, Ni and Au metals were chosen as the Schottky contacts.[19,20] Schottky contacts were 100 nm Au/20 nm Ni, deposited using magnetron sputtering. To improve the Schottky characteristics, a pre-cleaning step was used to remove the oxide on the GaN surface prior to metallization. The film cleaing process has been done using hydrofluoric (HF) acid for 1 min and warm ammonium hydroxide (NH_4OH) for 15 min.

The current-voltage (*I-V*) measurements of the GaN UV photodetectors were carried out using a Keithley 237 electrometer. Photoresponse measurements were realized by using a Xe arc lamp with power of 150 W as UV light source. External quantum efficiency (EQE) measurement was performed by using an incident monochromatic light beam directed onto the photodetector and the data was collected via a Newport QE measurement kit. Transient response measurements were taken using a 337 nm, 4 ns pulsed laser as light source, and voltage variations were collected using an oscilloscope (LeCroy WaveRunner).

3.8 References

1. Baker, T. J.; Haskell, B. A.; Wu, F.; Speck, J. S.; Nakamura, S., Characterization of planar semipolar gallium nitride films on sapphire substrates. Japanese Journal of Applied Physics 2006, 45 (2L), L154.

2. Chwang, R.; Smith, B.; Crowell, C., Contact size effects on the van der Pauw method for resistivity and Hall coefficient measurement. Solid-State Electronics 1974, 17 (12), 1217-1227.

3. Davydov, V. Y.; Kitaev, Y. E.; Goncharuk, I.; Smirnov, A.; Graul, J.; Semchinova, O.; Uffmann, D.; Smirnov, M.; Mirgorodsky, A.; Evarestov, R., Phonon dispersion and Raman scattering in hexagonal GaN and AlN. Physical Review B 1998, 58 (19), 12899.

4. Fang, Y.; Huang, J., Resolving Weak Light of Sub-picowatt per Square Centimeter by Hybrid Perovskite Photodetectors Enabled by Noise Reduction. Advanced Materials 2015, 27 (17), 2804-2810.

5. Harima, H., Properties of GaN and related compounds studied by means of Raman scattering. Journal of Physics: Condensed Matter 2002, 14 (38), R967.

6. Heying, B.; Wu, X.; Keller, S.; Li, Y.; Kapolnek, D.; Keller, B.; DenBaars, S. P.; Speck, J., Role of threading dislocation structure on the x-ray diffraction peak widths in epitaxial GaN films. Applied Physics Letters 1996, 68 (5), 643-645.

7. Hong, C.; Pavlidis, D.; Brown, S.; Rand, S., Photoluminescence investigation of GaN films grown by metalorganic chemical vapor deposition on (100) GaAs. Journal of applied physics 1995, 77 (4), 1705-1709.

8. Ishioka, K.; Kato, K.; Ohashi, N.; Haneda, H.; Kitajima, M.; Petek, H., The effect of n-and p-type doping on coherent phonons in GaN. Journal of Physics: Condensed Matter 2013, 25 (20), 205404.

9. Kang, H. A Study of the Nucleation and Formation of Multi-functional Nanostructures using GaN-Based Materials for Device Applications. Georgia Institute of Technology, 2006.

10. Kuball, M., Raman spectroscopy of GaN, AlGaN and AlN for process and growth monitoring/control. Surface and Interface Analysis 2001, 31 (10), 987-999.

11. Li, J. Ultrafast Metal-Semiconductor-Metal UV Photodetectors on GaN. University of Rochester, 2004.

12. Marchand, H.; Ibbetson, J.; Fini, P. T.; Kozodoy, P.; Keller, S.; DenBaars, S.; Speck, J.; Mishra, U., Atomic force microscopy observation of threading dislocation density reduction in lateral epitaxial overgrowth of gallium nitride by MOCVD. MRS Internet Journal of Nitride Semiconductor Research 1998, 3, e3.

13. Miller, D. J.; Harris, J. S.; McGehee, M.; Solomon, G., Gallium nitride epitaxy by a novel hybrid VPE technique. Stanford University: 2011.

14. Moram, M.; Vickers, M., X-ray diffraction of III-nitrides. Reports on progress in physics 2009, 72 (3), 036502.

15. Okumura, H.; Yoshida, S.; Okahisa, T., Optical properties near the band gap on hexagonal and cubic GaN. Applied physics letters 1994, 64 (22), 2997-2999.

16. Reimer, L., Transmission electron microscopy: physics of image formation and microanalysis. Springer: 2013; Vol. 36.

17. Reshchikov, M. A.; Morkoç, H., Luminescence properties of defects in GaN. Journal of applied physics 2005, 97 (6), 5-19.

18. van der PAUYV, L., A method of measuring specific resistivity and Hall effect of discs of arbitrary shape. Philips Res. Rep 1958, 13, 1-9.

19. Vickers, M.; Kappers, M.; Datta, R.; McAleese, C.; Smeeton, T.; Rayment, F.; Humphreys, C., In-plane imperfections in GaN studied by x-ray diffraction. Journal of Physics D: Applied Physics 2005, 38 (10A), A99.

20. Zheng, X.; Chen, H.; Yan, Z.; Han, Y.; Yu, H.; Li, D.; Huang, Q.; Zhou, J., Determination of twist angle of in-plane mosaic spread of GaN films by high-resolution X-ray diffraction. Journal of crystal Growth 2003, 255 (1), 63-67.

CHAPTER 4 GROWTH OF M-PLANE GAN NANOPLATE USING LASER-ASSISTED METAL ORGANIC CHEMICAL VAPOR DEPOSITION

4.1 Introduction

The growth of GaN nanostructures including nanowires and nanorods is predominant along the ⟨0001⟩ direction (*c*-plane) due to the high surface free energy of the *c*-plane.[1–3] Several attempts were made to grow the gallium nitride (GaN) nanostructures oriented along the <10-10> direction (*m*-plane).[1,2] The <10-10> oriented GaN nanostructures can be utilized to overcome the quantum-confined stark effect (QCSE) [i.e., separation of the electron and hole wave functions within the quantum wells (QWs)], which degrades the recombination efficiency of GaN-based photonic devices.[4–6] However, the growth of <10-10> oriented GaN nanostructures requires expensive lattice-matched substrates, including lithium aluminate (γ-$LiAlO_2$), *m*- and *r*-plane sapphire (Al_2O_3), and m-plane silicon carbide (4H-SiC).[4,5] In addition, the growth of GaN involves high-temperature methods, including metal organic chemical vapor deposition (MOCVD, ~930 °C), molecular beam epitaxy (MBE, ~800 °C), and hydride vapor phase epitaxy (HVPE, ~750 °C).[7–9] All of these methods require a long processing time of ~2 h.[1–10] The growth rates of GaN were reported to be 200, 4, and 1 μm/h in HVPE, MOCVD, and MBE techniques, respectively.[10,11]

The potential applications of GaN demand a simple approach for the rapid and selective growth of GaN nanostructures. Laser-assisted MOCVD (L-MOCVD) is a suitable method for enabling the rapid growth of materials at a low temperature in a predefined area.[12–16] In addition, another obvious advantage of the L-MOCVD over conventional MOCVD is the ability to generate patterned material deposition on substrates without involving complex lithography steps.[14,17] Several semiconductor

materials, including gallium arsenide (GaAs), cadmium telluride (CdTe), indium phosphide (InP), indium antimonide (InSb), and aluminum nitride (AlN), were grown using the L-MOCVD technique.[15] Similarly, GaN can be grown at low substrate temperatures using L-MOCVD compared to conventional growth methods. The growth rate can be remarkably enhanced due to the rapid processing nature of L-MOCVD. There are few reports available discussing the growth of GaN using L-MOCVD.[16] In this study, the *m*-plane oriented GaN nanoplates have been successfully grown on lattice-mismatched (Si) substrates using L-MOCVD. The rapid growth of GaN was realized by pyrolytically decomposing the source precursors at 450 °C.

4.2 Experimental methods

GaN nanoplates were grown on Si substrates at 450 ^{o}C using a home-built L-MOCVD system. Fig. 4.1 shows the schematic diagram and real-time image of the L-MOCVD system. Initially, the vacuum chamber was evacuated to a base pressure of 1 x 10^{-3} Torr. The TMGa and NH_3 were used as gas precursors in L-MOCVD. The flow rate of NH_3 was maintained at 2.2 mmol/min. The TMGa was carried into the growth chamber using nitrogen (N_2) as a carrier gas at a flow rate of 0.4 mmol/min. The chamber pressure was maintained at 450 Torr during the deposition process. Once the chamber pressure is stabilized, a CO_2 laser beam was shined on to the Si substrate. The power of the laser beam was fixed at 14 W. GaN nanostructures were grown at different deposition times from 1 to 5 min. The temperature of the growth region was monitored using a pyrometer (Omega, OS3752). After the growth process, the GaN nanoplates were characterized as follows. The morphology of the GaN films was examined using a field-emission scanning electron microscope (FESEM, S4700) and a high-resolution

transmission electron microscope (HRTEM, FEI Tecnai). The composition of the nanoplates was analyzed using an energy dispersive X-ray spectrometer (EDX, Oxford X-max 20 mm^2). The crystallinity and structure of the GaN nanoplates was studied using a micro-Raman spectroscope (Renishaw Invia, Argon ion laser, λ = 514 nm) and a powder X-ray diffractometer (Rigaku D/Max B diffractometer, Co Kα1 λ = 1.788 Å). The optical properties of the nanoplates were examined using a home-built photoluminescence spectrometer (Spectra Physics, wavelength-tunable Argon ion laser, λ_{ex} = 244 nm).

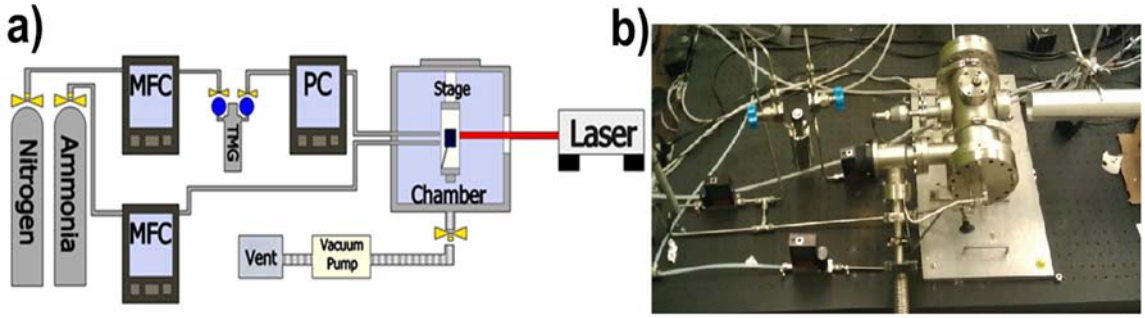

Figure 4.1 (a) Schematic diagram and (b) the real-time image of the L-MOCVD system.

4.3 Results and discussion

4.3.1 Morphological analysis

The morphology of the GaN films was examined using a field-emission scanning electron microscope (FESEM) and high-resolution transmission electron microscope (HRTEM). The FESEM images in Fig. 4.2a-d show the micrographs of GaN nanoplates grown at 1, 3, 5 and 7 min, respectively. The GaN film deposited at 1 min revealed the formation of nanoplates as shown in Fig. 4.2a. The shape of the nanoplates was similar to a semi-hexagonal and hexagonal. The arrows in Fig. 4.2a show the hexagonal shape of nanoplates. GaN nanoplates grown at 3 min had similar shape compared to the nanoplates grown at 1 min as shown in Fig. 4.2b. As the growth time was further increased to 5 and

7 min, the nanoplates overlapped with the adjacent nanoplates and formed interlinked GaN nanoplates as shown in Fig. 4.2c and d. The diameters of the GaN nanoplates were ~200 ± 50, 250 ± 50, 900 ± 50, 1500 ± 50 nm at 1, 3, 5 and 7 min, respectively. The thicknesses of the GaN nanoplates were 40 ± 10 nm, 50 ± 10 nm, 90 ± 10 nm and 900 ± 10 nm at 1, 3, 5 and 7 min, respectively. As the growth time increased the thickness of the nanoplates increases. The nanoplates join with the adjacent counterparts in all directions. The orientation of the GaN crystals on the Si substrate was similar to the GaN nanoplates, i.e., the c-axis of GaN was perpendicular to the substrate normal. The EDX results confirmed the presence of Ga and N elements in the nanoplates.[18] The atomic concentrations of Ga and N were 52.63 and 43.42, respectively.

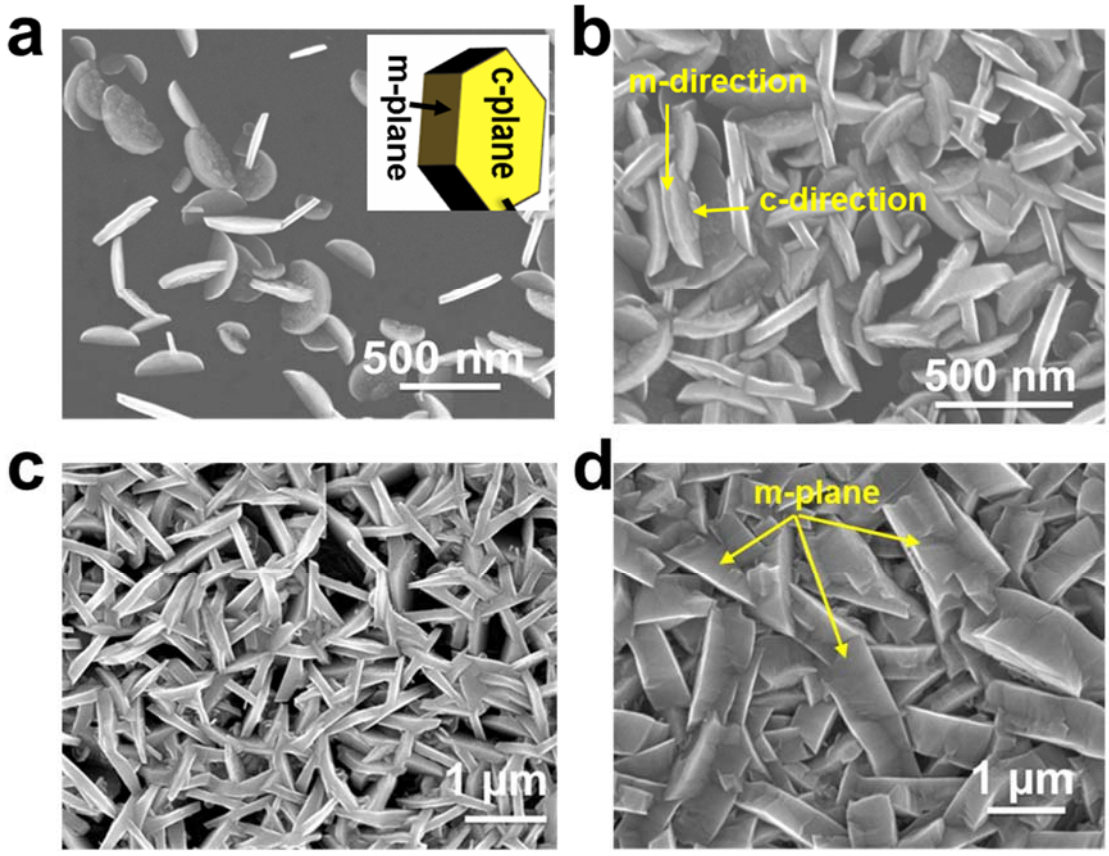

Figure 4.2 FESEM images of m-plane GaN nanoplates grown at (a) 1, (b) 3, (c) 5 min and (d) 7 min.

Figs. 4.3a and 4.3b show the selected-area electron diffraction (SAED) and high-magnification TEM images of a GaN nanoplate. SAED pattern of the GaN nanoplates revealed the array of spots indexed to the reflection of GaN with the wurtzite structure along the *m*-direction. The lattice fringes in Fig. 4.3b further confirm the single crystallinity of the GaN nanoplate. The interplanar spacing of 0.28 nm can be assigned to (10-10) plane, which corresponds to the m-plane of GaN.[19]

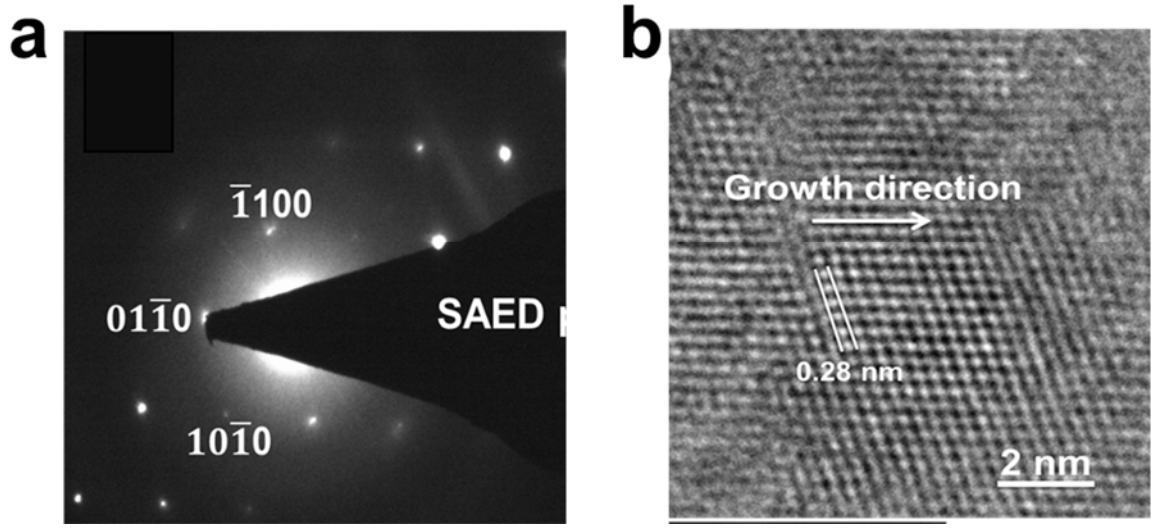

Figure 4.3 TEM images of a GaN nanoplate: (a) SAED pattern of the GaN nanoplate, (b) lattice fringes of the GaN nanoplate.

4.3.2. Growth Mechanism

The growth rates of different planes of the hexagonal GaN crystals were reported to have the following tendency [0001] > [01-1-1] > [10-10] > [01-11].[20-21] Typically, due to high growth rate of c-plane, the GaN nanostructures grow along <0001> direction.[20] However, in this study the GaN nanoplates were grown along <10-10> direction. The growth orientations other than (0001) can be achieved for the films deposited at low-temperature and/or high deposition rate.[3,22,23] The estimated growth rate of GaN was ~ 38 μm/h. The high growth rate can be attributed to the three-dimensional (3-D) diffusion

path of the reactive gases in LMOCVD. In addition, in this study GaN nanoplates were grown at a low temperature (450 ^{o}C) compared to GaN nanostructures grown by MOCVD at 930 ^{o}C.

The schematic diagram in Fig. 4.4a represents the growth of *m*-plane GaN nanoplates. Once the substrate is completely covered by the nanoplates, the upcoming species have to nucleate either on c-plane or m-plane of the nanoplates.[24-29] The GaN nanoplates served as seed crystals for the subsequent growth of m-plane oriented interlinked nanoplates. At an increased growth time, the growth continued on the different facets of the GaN nanoplates. Due to the negligible lattice mismatch between the c-plane and m-plane of GaN, the m-plane oriented nanoplates were dominant at a longer growth time. At an increased growth time, the overlap of the nanoplates led to the formation of nanoplate networks whose m-plane was orienting parallel to the Si substrate as shown in Figs. 4.4a and b. The FESEM images in Fig. 4.4b clearly revealed the growth of m-oriented GaN nanoplates.

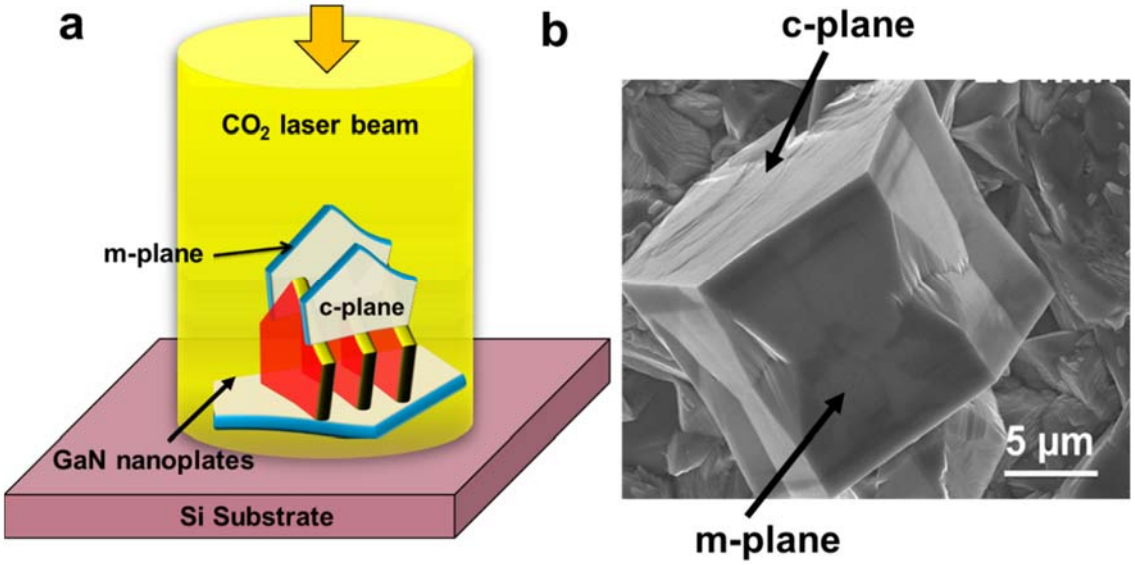

Figure 4.4 (a) Schematic diagram demonstrates the growth of m-plane GaN nanoplates on Si substrate. (b) FESEM images of m-direction GaN nanoplates grown on Si substrate.

4.3.3. Structural and optical properties

According to the group theory the Raman active modes of GaN are $A_1+E_1+2E_2$, where two non-polar E_2 modes are Raman active, A_1 and E_1 modes are both Raman and infrared active.[30-33] The vibrational modes of the GaN nanoplates were examined using a micro-Raman spectrometer under a Z(X,X)-Z backscattering geometry. Where, Z and -Z represents the projection direction of the incoming and scattered light, while X represent the polarization direction of the incoming and scattered light. Fig. 4.5 shows the micro-Raman spectra of the GaN nanoplates grown at 1and 5 min, respectively.

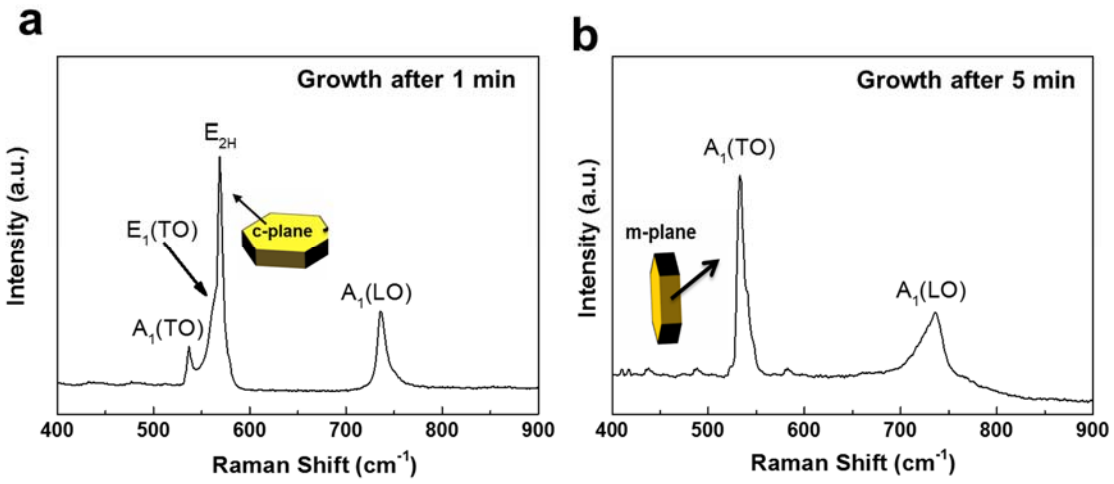

Figure 4.5 Raman spectra of GaN nanoplates grown at 1 and 5 min.

The GaN nanoplates grown at 1 min showed strong E_{2H} mode at 569 cm^{-1} and relatively weak A_1(TO), E_1(TO) and A_1(LO) modes at 530, 560, 738 cm^{-1}, respectively.[30-33] The strong E_{2H} mode is characteristic of wurtzite GaN. The c-plane GaN showed strong E_{2H} at 569 cm^{-1} as shown in Fig. 4.5a. The strong A_1(TO) mode was obtained for GaN nanoplates grown at 5 min as shown in Fig. 4.5b. The GaN nanoplates grown at 5

min did not show E_{2H} mode. According to the Raman selection rule, the m-plane GaN will show strong A_1(TO) mode along the *Z(X,X)-Z* geometry. This can be attributed to the absence of E_{2H} mode and presence of strong A_1(TO) mode for GaN film grown at 5 min.

Fig. 4.6 compares the XRD patterns of GaN nanoplates grown at 1 and 5 min. The XRD peaks including (10-10), (0002) and (10-11) can be indexed to wurtzite GaN with the hexagonal structure, which are in good agreement with Joint Committee on Powder Diffraction Standards (JCPDS) card no. 01-070-2546. GaN nanoplates grown at 1 min showed a strong (0002) peak which indicates the c-axis orientation of the nanoplates as shown in Fig. 4.6a.

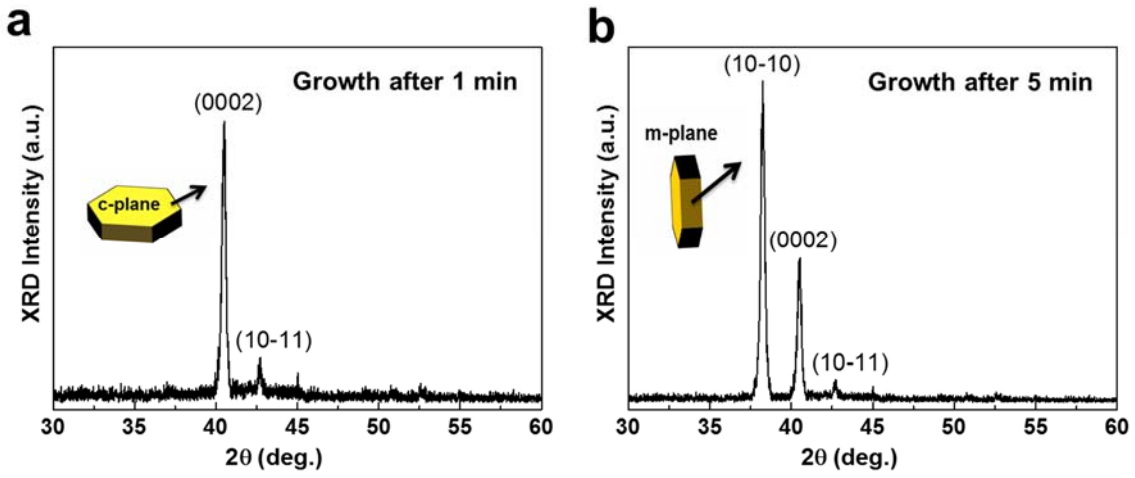

Figure 4.6 XRD patterns of GaN nanoplates grown at 1and 5 min.

The degree of orientation can be estimated by the relative texture coefficient which is given as:[19,34]

$$TC_{0002} = \frac{I_{0002} / I^{0}{}_{0002}}{I_{0002} / I^{0}{}_{0002} \Big/ I_{10\bar{1}0} / I^{0}{}_{10\bar{1}0}} \tag{4.1}$$

where TC_{0002} is the relative texture coefficient of (0002) peak over (10-10) peak. $I_{(0002)}$ and $I_{(10\text{-}10)}$ are the measured intensities of (0002) and (10-10) peaks, respectively.

$I^0_{(0002)}$ and $I^0_{(10\text{-}10)}$ are the intensity values of (0002) and (10-10) peaks of GaN powders obtained from the JCPDS card no. 01-070-2546, respectively. The textured coefficient of GaN powders with random crystallographic orientation is 0.5. The textured coefficient of GaN nanoplates grown at 1 min is 0.923, which indicates strong *c*-axis orientation of the GaN nanoplates. This is obvious from Fig. 4.2a which clearly showed the formation of GaN nanoplates and *c*-axis of most of the nanoplates are parallel to the substrate normal. On the other hand, GaN film grown at 5 min showed a strong (10-10) peak as shown in Fig. 4.6b which corresponds to the *m*-plane of GaN. The relative texture coefficient was used to estimate their degree of orientation using the following relation:[19,34]

$$TC_{10\bar{1}0} = \frac{I_{10\bar{1}0} / I^0_{10\bar{1}0}}{I_{10\bar{1}0} / I^0_{10\bar{1}0} \Big/ I_{0002} / I^0_{0002}} \qquad (4.2)$$

where $TC^{10\bar{1}0}$ is the relative texture coefficient of (10-10) peak over (0002) peak. The estimated $TC_{(10\text{-}10)}$ of interlinked GaN nanoplates grown at 5 min was 0.563. This result indicates that the as grown interlinked GaN nanoplates are preferentially oriented along the <10-10> direction. The XRD data are in good correlation with the FESEM, HRTEM and Raman results.

The optical properties of the nanoplates were examined using a photoluminescence (λ= 244 nm) set up. The GaN nanoplates grown at 5 min showed near-band-edge (NBE) emission at 3.4 eV which is closer to the NBE emission of bulk GaN (3.47 eV).[35,36] In addition, GaN nanoplates showed a broad deep level emission (DLE) at 2.21 eV. The DLE emission at 2.21 eV can be attributed to nitrogen vacancies and gallium interstitials of the GaN nanoplates.[35,37] The NBE emission peaking at 3.4 eV confirmed the good optical quality of the GaN nanoplates.

4.4 Conclusions

The interlinked m-plane-oriented GaN nanoplates can rapidly be grown on a Si substrate using the L-MOCVD method. The FESEM and HRTEM images confirmed the formation of GaN nanoplates. The growth direction of GaN nanoplates was found to be the <10-10> direction. The A_1 (TO) mode of Raman further confirmed the m-plane orientation of the GaN nanoplates. The high deposition rate, low-growth temperature, and repeated growth on the different facets of the nanoplates resulted in the formation of m-plane-oriented interlinked GaN nanoplates. Therefore, the LMOCVD is a suitable technique for the rapid growth of m-plane-oriented GaN nanoplates on Si substrate at low-growth temperatures. This method can be extended to the rapid growth of other III-nitride materials.

4.5 References

1. Yeh, T.-W.; Lin, Y.-T.; Ahn, B.; Stewart, L. S.; Daniel Dapkus, P.; Nutt, S. R., Vertical nonpolar growth templates for light emitting diodes formed with GaN nanosheets. Applied Physics Letters 2012, 100 (3), 033119.

2. Fujito, K.; Kiyomi, K.; Mochizuki, T.; Oota, H.; Namita, H.; Nagao, S.; Fujimura, I., High‐quality nonpolar m‐plane GaN substrates grown by HVPE. physica status solidi (a) 2008, 205 (5), 1056-1059.

3. Lu, J.; Ye, Z.; Huang, J.; Wang, L.; Zhao, B., Synthesis and properties of ZnO films with (1 0 0) orientation by SS-CVD. Applied Surface Science 2003, 207 (1), 295-299.

4. Ni, X.; Wu, M.; Lee, J.; Li, X.; Baski, A.; Özgür, Ü.; Morkoç, H., Nonpolar m-plane GaN on patterned Si (112) substrates by metalorganic chemical vapor deposition. Applied Physics Letters 2009, 95 (11), 111102.

5. Chou, M. M.; Chen, C.; Hang, D.; Yang, W.-T., Growth of nonpolar m-plane GaN epitaxial film on a lattice-matched (100) β-LiGaO 2 substrate by chemical vapor deposition. Thin Solid Films 2011, 519 (15), 5066-5069.

6. Sun, Y. J.; Brandt, O.; Ploog, K. H., Growth of M-plane GaN films on γ-LiAlO 2 (100) with high phase purity. Journal of Vacuum Science & Technology B: Microelectronics and Nanometer Structures Processing, Measurement, and Phenomena 2003, 21 (4), 1350-1356.

7. Kuykendall, T.; Pauzauskie, P.; Lee, S.; Zhang, Y.; Goldberger, J.; Yang, P., Metalorganic chemical vapor deposition route to GaN nanowires with triangular cross sections. Nano Letters 2003, 3 (8), 1063-1066.

8. Seryogin, G.; Shalish, I.; Moberlychan, W.; Narayanamurti, V., Catalytic hydride vapour phase epitaxy growth of GaN nanowires. Nanotechnology 2005, 16 (10), 2342.

9. Ambacher, O., Growth and applications of group III-nitrides. Journal of Physics D: Applied Physics 1998, 31 (20), 2653.

10. Nasser, N.; Zhen, Y. Z.; Jiawei, L.; Bou, X. Y., GaN Heteroeptaxial Growth Techniques. Journal of Microwaves, Optoelectronics and Electromagnetic Applications (JMOe) 2001, 2 (3), 22-31.

11. Iga, R.; Sugiura, H.; Yamada, T., Selective growth of III-V semiconductor compounds by laser-assisted epitaxy. Semiconductor science and technology 1993, 8 (6), 1101.

12. Kesaria, M.; Shetty, S.; Shivaprasad, S., Spontaneous formation of GaN nanostructures by molecular beam epitaxy. Journal of Crystal Growth 2011, 326 (1), 191-194.

13. Shinn, G. B.; Gillespie, P.; Wilson Jr, W.; Duncan, W. M., Laser‐assisted metalorganic chemical vapor deposition of zinc selenide epitaxial films. Applied Physics Letters 1989, 54 (24), 2440-2442.

14. Allen, S., Laser chemical vapor deposition: A technique for selective area deposition. Journal of Applied Physics 1981, 52 (11), 6501-6505.

15. Herman, I. P., Laser-assisted deposition of thin films from gas-phase and surface-adsorbed molecules. Chemical Reviews 1989, 89 (6), 1323-1357.

16. Lee, S. S.; Park, S. M.; Chong, P. J., Single-phase deposition of α-gallium nitride by a laser-induced transport process. Journal of Materials Chemistry 1993, 3 (4), 347-351.

17. Duty, C.; Jean, D.; Lackey, W., Laser chemical vapour deposition: materials, modelling, and process control. International Materials Reviews 2001, 46 (6), 271-287.

18. Lin, L.; Lai, C.-H.; Hu, Y.; Zhang, Y.; Wang, X.; Xu, C.; Snyder, R. L.; Chen, L.-J.; Wang, Z. L., High output nanogenerator based on assembly of GaN nanowires. Nanotechnology 2011, 22 (47), 475401.

19. Yang, F.; Liu, W.-H.; Wang, X.-W.; Zheng, J.; Shi, R.-Y.; Zhao, H.; Yang, H.-Q., Controllable low temperature vapor-solid growth and hexagonal disk enhanced field emission property of ZnO nanorod arrays and hexagonal nanodisk networks. ACS applied materials & interfaces 2012, 4 (8), 3852-3859.

20. Li, W.-J.; Shi, E.-W.; Zhong, W.-Z.; Yin, Z.-W., Growth mechanism and growth habit of oxide crystals. Journal of crystal growth 1999, 203 (1), 186-196.

21. Jeong, J. S.; Lee, J. Y.; Cho, J. H.; Lee, C. J.; An, S.-J.; Yi, G.-C.; Gronsky, R., Growth behaviour of well-aligned ZnO nanowires on a Si substrate at low temperature and their optical properties. Nanotechnology 2005, 16 (10), 2455.

22. Tran, N. H.; Hartmann, A. J.; Lamb, R. N., Structural order of nanocrystalline ZnO films. The Journal of Physical Chemistry B 1999, 103 (21), 4264-4268.

23. Aggarwal, R.; Zhou, H.; Jin, C.; Narayan, J.; Narayan, R. J., Semipolar r-plane ZnO films on Si (100) substrates: Thin film epitaxy and optical properties. Journal of applied physics 2010, 107 (11), 113530.

24. Hersee, S. D.; Sun, X.; Wang, X., The controlled growth of GaN nanowires. Nano letters 2006, 6 (8), 1808-1811.

25. Colby, R.; Liang, Z.; Wildeson, I. H.; Ewoldt, D. A.; Sands, T. D.; García, R. E.; Stach, E. A., Dislocation filtering in GaN nanostructures. Nano letters 2010, 10 (5), 1568-1573.

26. Premkumar, T.; Zhou, Y.; Lu, Y.; Baskar, K., Optical and field-emission properties of ZnO nanostructures deposited using high-pressure pulsed laser deposition. ACS applied materials & interfaces 2010, 2 (10), 2863-2869.

27. Kim, S.-W.; Park, H.-K.; Yi, M.-S.; Park, N.-M.; Park, J.-H.; Kim, S.-H.; Maeng, S.-L.; Choi, C.-J.; Moon, S.-E., Epitaxial growth of ZnO nanowall networks on GaN/sapphire substrates. Applied physics letters 2007, 90 (3), 033107.

28. Yang, H.; Fan, N.; Luan, W.; Tu, S.-t., Synthesis of monodisperse nanocrystals via microreaction: open-to-air synthesis with oleylamine as a coligand. Nanoscale research letters 2009, 4 (4), 344.

29. Wang, Y.; Hu, F.; Zhu, H.; Hane, K., III‐nitride grown on freestanding GaN nanostructures. physica status solidi (c) 2012, 9 (3‐4), 554-557.

30. Zhu, T.; Martin, D.; Grandjean, N., M-plane gan grown on m-plane sapphire by hydride vapor phase epitaxy. Japanese Journal of Applied Physics 2009, 48 (2R), 020226.

31. Thirugnanam, P.; Xiong, W.; Mahjouri-Samani, M.; Fan, L.; Raju, R.; Mitchell, M.; Gao, Y.; Krishnan, B.; Zhou, Y.; Jiang, L., Rapid growth of m-plane oriented gallium nitride nanoplates on silicon substrate using laser-assisted metal organic chemical vapor deposition. Crystal Growth & Design 2013, 13 (7), 3171-3176.

32. Harima, H., Properties of GaN and related compounds studied by means of Raman scattering. Journal of Physics: Condensed Matter 2002, 14 (38), R967.

33. Hsu, H.-C.; Hsu, G.-M.; Lai, Y.-s.; Feng, Z. C.; Tseng, S.-Y.; Lundskog, A.; Forsberg, U.; Janzén, E.; Chen, K.-H.; Chen, L.-C., Polarized and diameter-dependent Raman scattering from individual aluminum nitride nanowires: The antenna and cavity effects. Applied Physics Letters 2012, 101 (12), 121902.

34. Yang, H.; Song, Y.; Li, L.; Ma, J.; Chen, D.; Mai, S.; Zhao, H., Large-scale growth of highly oriented ZnO nanorod arrays in the Zn-NH3· H2O hydrothermal system. Crystal Growth and Design 2008, 8 (3), 1039-1043.

35. Chin, A. H.; Ahn, T. S.; Li, H.; Vaddiraju, S.; Bardeen, C. J.; Ning, C.-Z.; Sunkara, M. K., Photoluminescence of GaN nanowires of different crystallographic orientations. Nano letters 2007, 7 (3), 626-631.

36. Li, Q.; Wang, G. T., Spatial distribution of defect luminescence in GaN nanowires. Nano letters 2010, 10 (5), 1554-1558.

37. Hofmann, D.; Kovalev, D.; Steude, G.; Meyer, B.; Hoffmann, A.; Eckey, L.; Heitz, R.; Detchprom, T.; Amano, H.; Akasaki, I., Properties of the yellow luminescence in undoped GaN epitaxial layers. Physical Review B 1995, 52 (23), 16702. 1879.

CHAPTER 5 ENHANCED GAN FILMS GROWTH ON SILICON SUBSTATES WITH RESONANT VIBRATIONAL EXCITATIONS OF AMMONIA MOLECULES

5.1 Introduction

In this chapter, the influence of exciting ammonia (NH_3) molecular vibration in the growth of gallium nitride (GaN) on silicon (100) substrates is investigated by using an infrared laser-assisted metal organic chemical vapor deposition (LMOCVD) method. High-quality commercial GaN films are usually grown by the metalorganic chemical vapor deposition (MOCVD) technique on expensive lattice-mismatched substrates such as sapphire and SiC substrates at a growth rate around 2 μm/h.[1-14] Recently, interests in the epitaxial growth of thick GaN films on Si (100) substrates arose for scalable production of power-switching devices at an affordable cost.[6,8] However, the MOCVD technique is accompanied with a parasitic reaction between the precursors at high temperatures, which restricts the growth rates and impairs the epitaxial growth of thick GaN films.[13-16] In addition, the high growth temperatures (~ 900 - 1200 ˚C) lead to GaN decomposition and nitrogen reevaporation therefore result in reduced GaN growth rates and degraded crystalline quality.[17,18] Moreover, there is a series of Ga-Si reactions at elevated temperatures that could directly deter the growth of GaN on Si.[19] However, a high reaction temperature is required for effective NH_3 decomposition and overcoming the energy barriers on precursor adsorption and surface adatom migration.[13-16]

Ultraviolet laser-induced MOCVD growth of group-III nitrides was developed [20,21] with the potential to overcome these disadvantages and was principally intended to provide the reactive radicals Ga and N by photolysis of their precursors at low substrate temperature. However, the density of the reactive N-containing fragments from NH_3 was not very high even at high volume ratios and GaN growth rate was low. To address the challenges without introducing hetero catalysts, we have developed an infrared laser

LMOCVD method to achieve thick GaN on Si (100).[22] Selective NH_3 decomposition at room temperatures is realized by resonantly exciting the rotational-vibrational transition of the NH-wagging modes using a CO_2 laser beam. The roles of vibrational excitation in NH_3 decomposition and GaN formation is discussed. There are six vibrational modes and numerous vibrational bands in NH_3 molecules. Will vibrational excitation of each mode contribute equally to the NH_3 decomposition and GaN growth? How will each mode impact the NH_3 decomposition and GaN growth?

Based on the available irradiation lines, the NH_3 NH-wagging modes at 932.51 (ν_2+) and 968.32 cm^{-1} (ν_2-), and the NH rotational-vibrational transition at 1084.63 cm^{-1} were resonantly excited leading to significantly improved GaN growth rates. Compared to laser-induced thermal heating at nonresonant wavelengths, the resonant excitations lead to more effective NH_3 decomposition, higher concentrations of active species, higher GaN deposition rates, and better GaN crystalline quality.

5.2 Experimental details

5.2.1 Sample preparation

The schematic experimental setup of a home-built LMOCVD system is shown in Fig. 5.1. GaN films were grown on p-type Si(100) substrates. From the point of view of integrating GaN devices with silicon technology, the Si(100) substrate is preferred because Si(100) is the most widely used in silicon mainstream technology. The Si substrates (10 × 10 mm^2) were etched with 10% hydrofluoric to remove oxide layers, cleaned and dried before loading into the LMOCVD chamber. Trimethylgallium (TMGa) and NH_3 were used as the Ga and N precursors, respectively. The LMOCVD chamber was evacuated to a base pressure of 1×10^{-3} Torr. Then, laser thermal cleaning of Si

substrates was carried out at 900 ^{o}C under H_2 flow for 5 min to remove the native oxide on the substrate surface followed by one step nitridation at 750 ^{o}C. The nitridation was lasted for 5 min under 54 mmol/min NH_3 flow at a reactor pressure of 100 Torr. It has widely been reported that a silicon nitride layer is formed due to the nitridation surface treatment process on the silicon substrate. [23,24] Nitridation of Si surface helps to release strain in GaN-on-Si growth and favours the growth of wurtzite GaN.[25-27]

The molar flow rate of NH_3 was maintained at 54 mmol/min. The TMGa was carried into the growth chamber using a nitrogen carrier gas (N_2) at a molar flow rate of 88 μmol/min. The chamber pressure during the growth process was maintained at ~ 10 Torr. A continuous-wave wavelength-tunable CO_2 laser (PRC Inc., 9.2 - 10.9 μm) was used as the irradiation source, achieving reactant excitation and substrate heating. Based on the available emission lines of the CO_2 laser, the NH-wagging modes (v_2, at 932.51, 968.32, and 1084.71 cm^{-1}) of NH_3 molecules were selected to be resonantly excited at corresponding laser wavelengths of 10.719, 10.350, and 9.219 μm. Two other wavelengths at 9.201 and 10.591 μm were selected as nonresonant wavelength references realizing only conventional laser heating. GaN nucleation layers (40 - 60 nm in thickness) were deposited at 500 ^{o}C for 30 seconds followed by epilayer growth at 750 ^{o}C for 5 min. The laser incident power was tuned to keep the substrate temperature same for all GaN samples grown at different laser wavelengths. The substrate temperature was monitored using a pyrometer (Omega, OS3752).

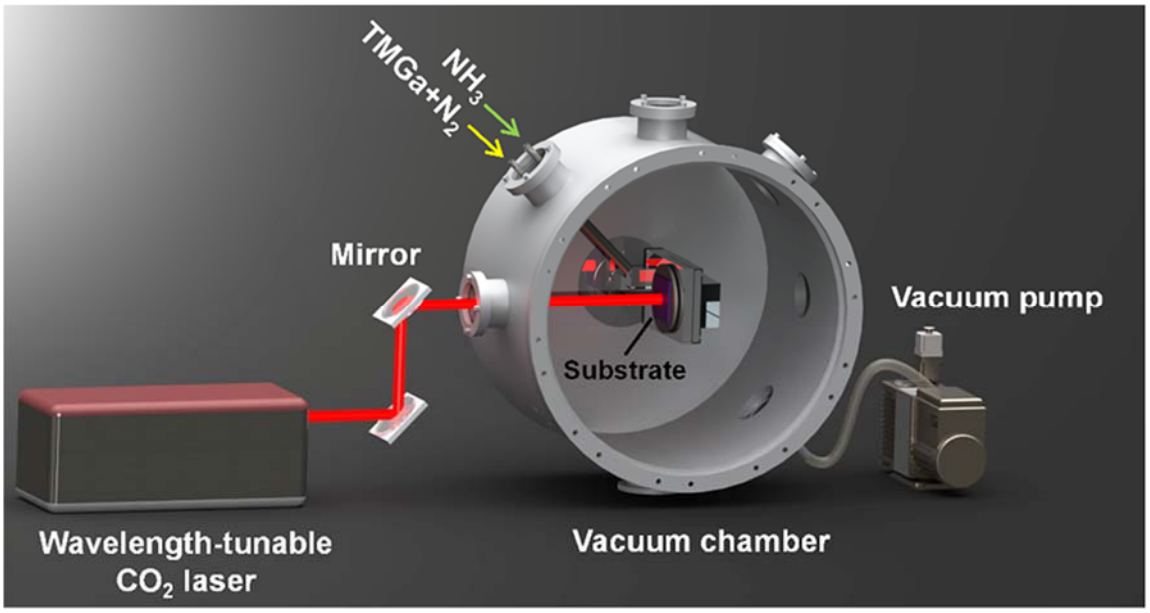

Figure 5.1 The schematic of the LMOCVD system.

5.2.2 NH_3 absorption spectrum and finding resonant vibrational excitation wavelengths

In order to find appropriate wavelengths achieving resonant vibrational excitation of NH_3 molecules, it is essential to found out available emission lines matching NH_3 molecular vibrational modes within the CO_2 laser wavelength range (9.2 - 10.8 μm). Due to the discrete emission lines of the CO_2 laser, effective NH_3 absorption spectrum within the CO_2 laser wavelength range was measured in a vacuum chamber with an absorption path length of 40.64 cm. The chamber was evacuated to a base pressure of 1×10^{-3} Torr. Gaseous NH_3 was subsequently introduced into the chamber and reach a pressure of 10 Torr. The incident laser power was kept at 220 W. A power meter was used to measure the laser power before and after passing through the chamber. The drop in laser power was calculated as the absorption percentage.

Three strong absorption peaks were observed at 9.219, 10.35, and 10.719 μm (resonant wavelengths), corresponding to the NH-wagging modes (v_2) at 1084.63,

968.32, and 932.51 cm^{-1}, respectively.[22,28] Among all six vibrational modes of NH_3 molecules, the NH-wagging mode is strongly infrared active. A NH_3 molecule in the NH-wagging mode vibrates in an umbrella inversion way.[29,30] Due to the barrier that the nitrogen atom encounters on its travel through the proton plane, the vibrational level is split into two components at 932.51 (v_{2+}) and 968.32 cm^{-1} (v_{2-}) which correspond to the observed absorption peaks at 10.719 and 10.35 μm, respectively.[28-32] The strongest absorption peak at 9.219 μm is ascribed to the NH rotational-vibrational transition at 1084.63 cm^{-1} [5(J) → 6(J'), K=0].

5.2.3 Characterization

The Surface morphologies of the GaN films were studied using a field-emission scanning electron microscope (FESEM, Hitachi S4700). The qualities of GaN films were examined using a Raman microscope (Renishaw inVia H 18415, Argon ion laser, λ = 514 nm) and X-ray diffractometer (Rigaku D/Max B diffractometer, Co Kα λ = 1.788 Å). The doping type, carrier concentration and mobility of the GaN films were obtained via the Van der Pauw method at room temperature. The optical emission spectra (OES) of laser irradiated NH_3 were taken in open air using a spectrometer (Shamrock SR-303i-A, Andor Technology) coupled with an intensified charged coupled device (ICCD) (iStar DH-712, Andor Technology). The IR laser beam was focused to a diameter around 1 mm using a ZnSe convex lens (f = 25.4 cm). A welding torch with a nozzle diameter of 1.5 mm was used to introduce the NH_3 gas at a flowrate of 50 sccm. The CO_2 laser beam was directed perpendicularly to the NH3 flow. The laser incident power density was fixed at 1.4×10^4 W/cm^2 for all laser wavelengths. All spectra were taken with a vertical collecting length of 0.5 mm along the emission, centred at the tip of the emission, and with a horizontal slit

width of 30 μm centered at the tip apex of the emission. A background spectrum captured before collecting the emission spectra was subtracted from all spectra.

5.3 Results and discussion

5.3.1 FESEM images of the GaN films

The morphologies and grain sizes of the GaN films deposited at different laser wavelengths are shown in Figs. 5.2(a) – 5.2(e), respectively. Crystalline GaN films containing highly oriented grains along the c-axis with hexagonal facets are observed, indicating the formation of wurtzite GaN films on the Si(100) substrates. Generally, a mixture of cubic and hexagonal GaN tends to grow on Si(100) substrates because the (001) plane of Si possesses a fourfold symmetry.[23-27] However, the nitridation process promotes the silicon nitride formation and prohibits cubic GaN nucleation. Therefore, hexagonal GaN dominates the GaN growth.[23-27]

It is generally accepted that grain boundaries impact negatively on the electrical and optical properties of GaN films.[33,34] Increasing grain sizes leads to reduced grain boundaries and results in a reduced amount of defects and stress. Therefore, the crystalline quality and optical properties of GaN films are improved accordingly.[33,34] Fig. 5.2(f) compares the average grain sizes of the GaN films grown at different laser wavelengths. As shown in Figs. 5.2(a) and 5.2(d), GaN grains with average grain sizes of 1.0 and 2.1 μm are obtained at nonresonant wavelengths of 9.201 and 10.591 μm, respectively. The average grain sizes increase to 4.0, 3.8, and 3.1 μm at resonant wavelengths 9.219, 10.350, and 10.719 μm, respectively, as shown in Figs. 5.2(b), 5.2(c), and 5.2(e).

The cross-sectional SEM images of the GaN films deposited at non- (9.201 μm) and resonant wavelengths (9.219 μm) for 5 minutes are exhibited in Figs 5.3(a) and 5.3(b), respectively. The resonant deposition, Fig. 5.3(b), results in a thicker GaN film (7 μm) than the nonresonant deposition, Fig. 5.3(a), indicating a higher growth rate (around 2.7 times higher) at the resonant deposition. Fig. 5.3(c) compares the deposition rates obtained at all five wavelengths. It is obvious that resonant depositions result in higher GaN growth rates than nonresonant depositions. The highest growth rate (84 μm/h) is achieved at 9.219 μm, which is ~ 42 times higher than that of conventional MOCVD (2 μm/h).[6,12,13] Although not as significant as those obtained under the resonant wavelengths, promoted GaN growth rates are also observed at nonresonant wavelengths, 9.201 and 10.591 μm, and are ascribed to the coupled energy via laser irradiation. However, the same amount of energy coupled at different wavelengths yields obviously divergent results as observed in Figs. 5.2(f) and 5.3(c).

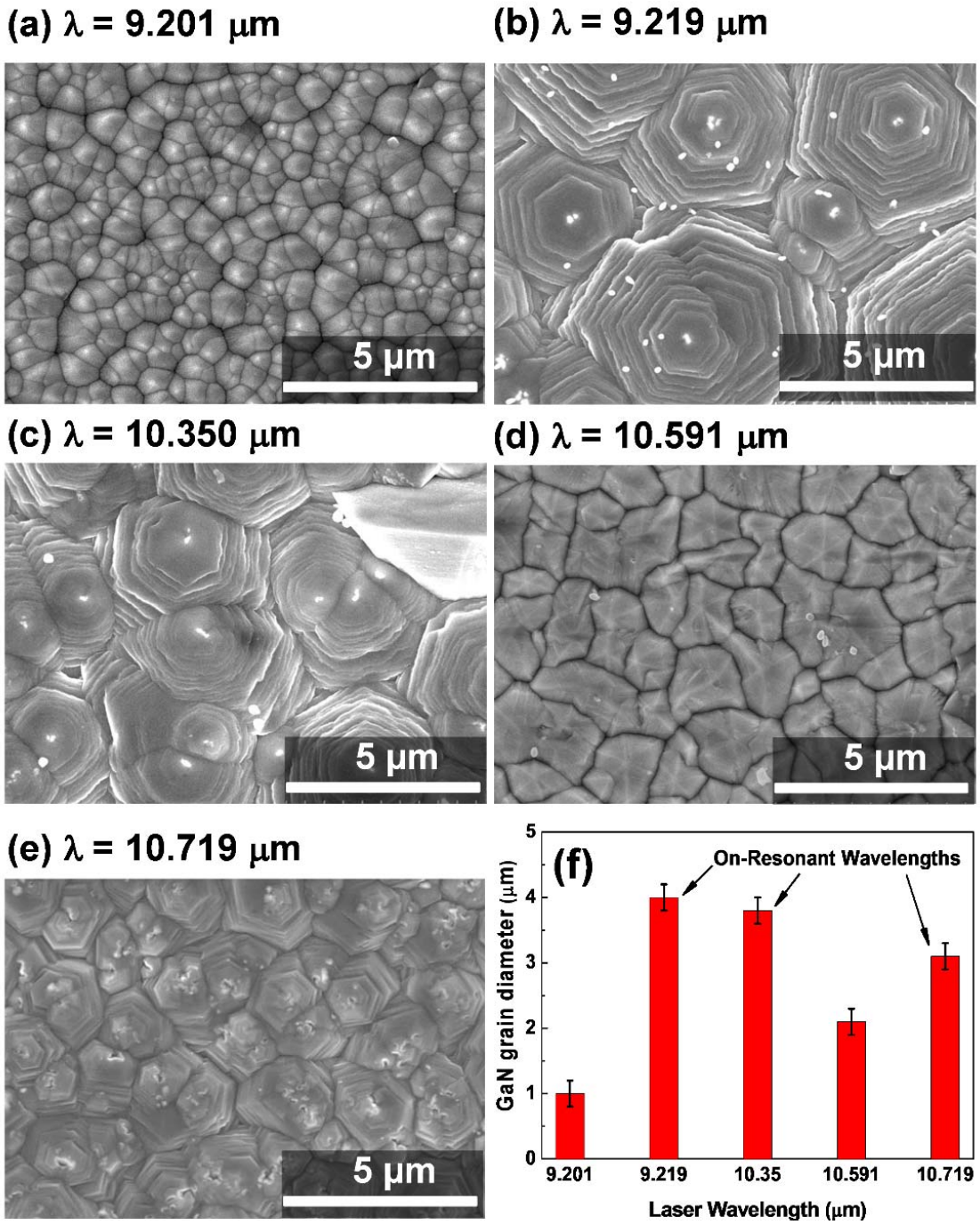

Figure 5.2 (a) SEM images of GaN films deposited on Si (100) at excitation laser wavelength of (a) 9.201 μm, (b) 9.219 μm, (c) 10.350 μm, (d) 10.591 μm, and (e) 10.719 μm, respectively. (f) A chart showing average GaN grain sizes obtained at different laser wavelengths.

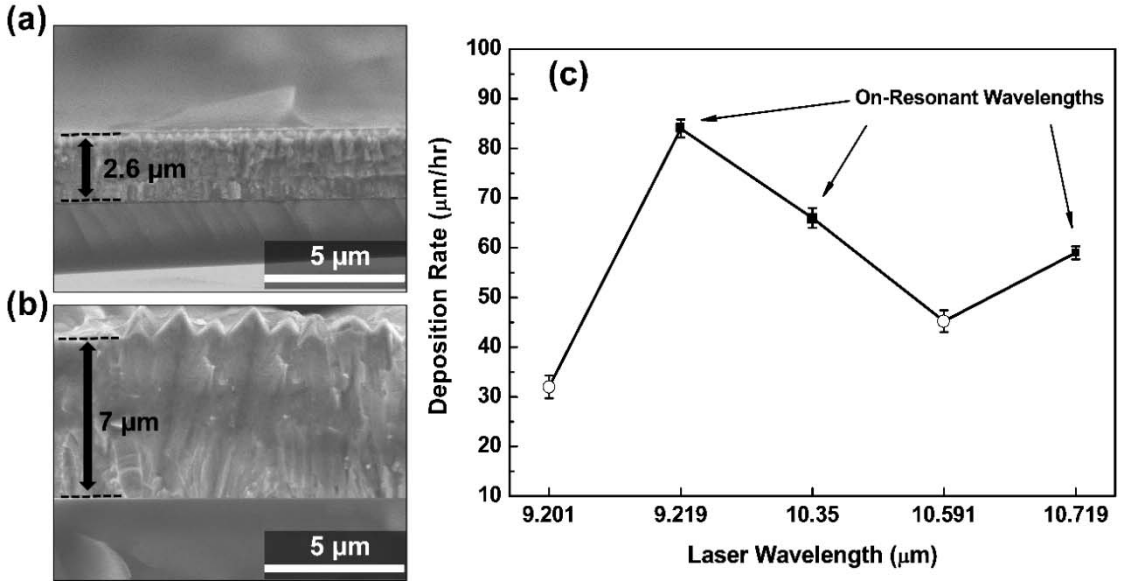

Figure 5.3 (a) SEM images of GaN films deposited on Si (100) at excitation laser wavelength of (a) 9.201 μm, (b) 9.219 μm, (c) 10.350 μm, (d) 10.591 μm, and (e) 10.719 μm, respectively. (f) A chart showing average GaN grain sizes obtained at different laser wavelengths.

5.3.2 Raman spectra of the GaN films

Raman spectroscopy is a powerful method evaluating the quality and residual stress of GaN films.[35] Raman spectroscopic studies were conducted under a $Z(X,X)\bar{Z}$ backscattering geometry, where Z and $\bar{Z}$ represent the projection direction of the incoming and scattered light, and X represents the polarization direction of the incoming and scattered light. Fig. 5.4(a) shows the Raman spectra of the GaN films grown at different laser wavelengths. Two prominent Raman shifts at around 567 and 733 cm^{-1} are observed from all samples, corresponding to the GaN E_{2H} and A_1(LO) phonon modes, respectively. These modes originate from allowed vibrational states in the wurtzite GaN epitaxial layer.[35] The exact positions of the GaN E_{2H} phonon peak of the samples were summarized in Table 5.1.

It is well known that the E_{2H} mode in the GaN Raman spectra reflects crystalline quality and stress of the crystals.[35] The E_{2H} peaks were shifted to lower wave-numbers (red-shift) compared with the standard frequency value of the E_{2H} phonon mode of strain-free GaN at 567.8 cm^{-1}. The peak positions of the E_{2H} were observed to have red-shifts of about 1.7, 1, 1.3, 1.3 and 1.2 cm^{-1} for the samples grown at laser wavelengths of 9.201, 9.219, 10.35, 10.591 and 10.719 μm, respectively. The red-shift in the position of E_{2H} indicated that the GaN films suffered from tensile stress. The stress levels of the GaN epilayer can be calculated using the following equation:[36] $\sigma = \Delta\omega / 4.3$ (cm^{-1}. GPa^{-1}), where σ is the biaxial stress and $\Delta\omega$ is the E_{2H} phonon peak shift. The estimated tensile stresses were calculated and summarized in Table 5.1. The Raman spectra indicated that the GaN films grown at laser wavelengths of 9.219 μm exhibited the lowest stress.

Moreover, as observed in Fig. 5.4(a), the E_{2H} peak is much stronger in the resonant samples (9.219, 10.35, and 10.719 μm) than in the nonresonant samples (9.201 and 10.591 μm), indicating better crystalline quality of the resonant samples. The strongest E_{2H} peak is observed when resonantly excited at 9.219 μm, denoting the highest GaN crystalline quality. The full-width-at-half-maximum (FWHM) values of the E_{2H} peaks of the GaN samples were summarized in Table 5.1. A narrow E_{2H} peak, i.e. a low FWHM value, indicates a better crystalline quality. According to Table 5.1., it is obvious that FWHMs of resonant samples are lower than those of nonresonant samples. The lowest FWHM, 9.3 cm^{-1}, is observed in the resonant sample excited at 9.219 μm, indicating the highest GaN crystalline quality.

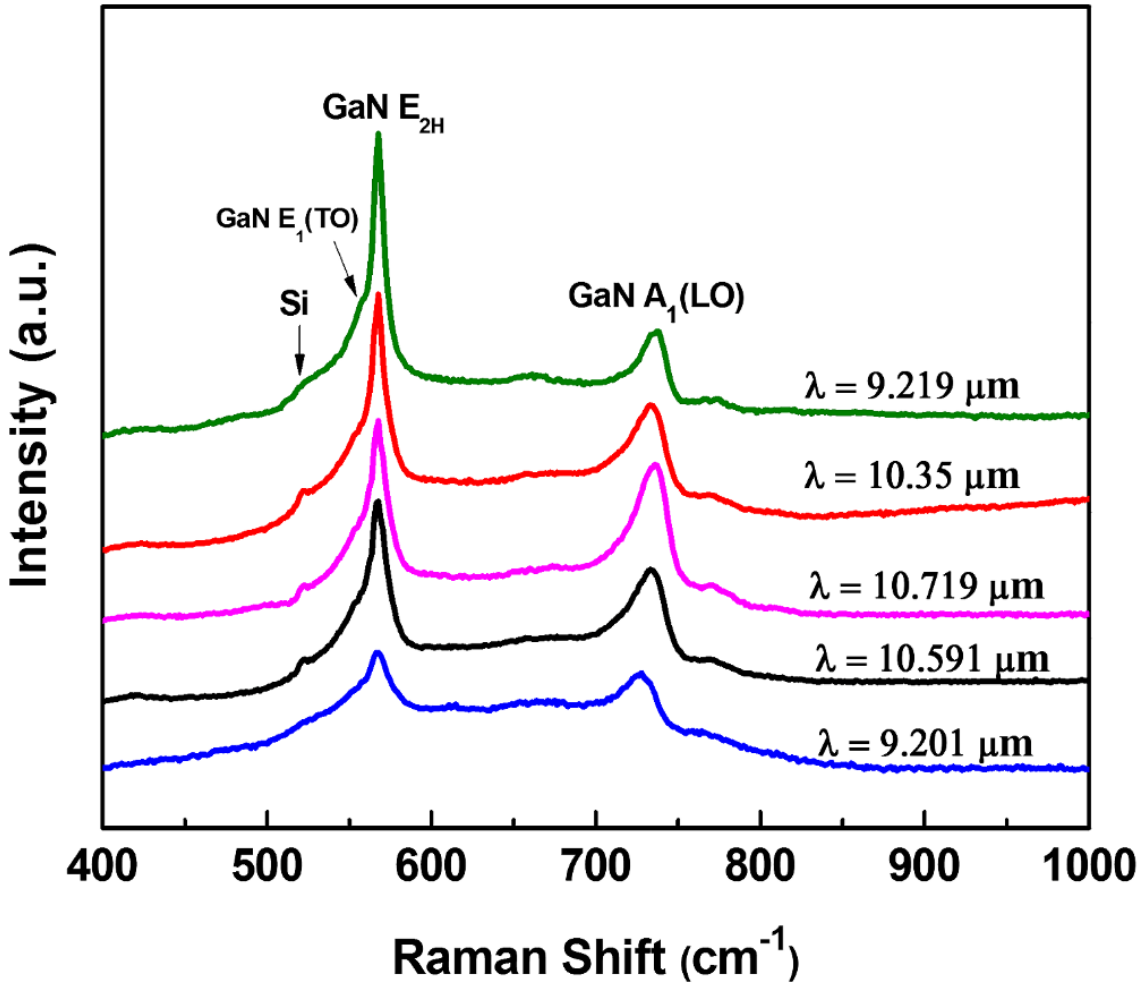

Figure 5.4 Raman spectra of the GaN films grown at resonant (9.219, 10.35, and 10.719 μm) and nonresonant (9.201 and 10.591 μm) wavelengths.

Table 5.1 Summary of GaN films characterization grown on Si (100) substrates at different laser wavelengths.

Sample	Laser wavelength (μm)	Average grain sizes (μm)	Growth rate (μm/hr)	GaN E_{2H} peak position (cm^{-1})	GaN E_{2H} peak FWHM (cm^{-1})	σ (GPa)
I	9.201	1	32	566.1	19	0.395
II	9.219	4	84	566.8	9.3	0.233
III	10.350	3.8	66	566.5	10.1	0.302
IV	10.590	2.1	45	566.5	11.9	0.302
V	10.719	3.1	59	566.6	11.2	0.280

5.3.3 XRD characterization of the GaN films

Figs. 5.5(a) and 5.5(b) exhibit the XRD diffraction curves of the GaN films obtained at 9.219 (resonant wavelength) and 9.201 μm (nonresonant wavelength), respectively. The XRD peaks at around 40.2° and 87.02° are observed in both curves and attributed to the GaN {0001} family planes. These peaks correspond to the (0002) and (0004) orientations of wurtzite GaN, respectively, indicating a high c-axis orientation of the GaN films deposited on the Si(100) substrates.[37]It is observed from Fig. 5.5(a) and 5.5(b) that the GaN XRD peaks are much stronger in the resonant sample than those in the nonresonant sample, which is attributed to the improved crystalline quality.

The GaN (0002) rocking curves of the GaN films deposited at the resonant (9.219 μm) and nonresonant (9.201 μm) wavelengths are exhibited in Figs. 5.5(c) and 5.5(d), respectively. FWHM values of the rocking curves of (0002) symmetric and (10-12) asymmetric diffraction peaks were summarized in Table 5.2. It is well known that the FWHM of XRD in the (0002) reflection reveals information about the out-of-plane misorientation of domains (tilt) while the FWHM of the GaN (10-12) peak is sensitive to both tilt and twist. Thus, the FWHM of the (0002) peak is usually used to evaluate the screw or mixed threading dislocations (TDs) density and the FWHM of XRD in the (10-12) reflection corresponds to the lattice distortion from all components of the TDs including edge, screw and mixed screw-edge dislocations.[37,38] Low FWHM values indicate low TDs density and better crystalline quality.

As shown in Table 5.2, (0002) FWHM values of 92 and 60 arcmin and (10-12) FWHM values of 99 and 67 arcmin are observed for the GaN samples deposited at the nonresonant wavelengths of 9.201 and 10.591 μm, respectively. For the GaN film deposited with resonant excitation, the FWHMs of (0002) are 39, 45, and 55 arcmin and

the FWHMs of (10-12) are 43, 53, and 61 arcmin at resonant wavelengths of 9.219, 10.350, and 10.719 μm, respectively. The distinctive FWHMs decrease in resonant samples compared to those with nonresonant samples indicates improved GaN crystalline quality and reduced TDs density by using resonant excitation. However, the crystalline quality of GaN films are inferior to that reported for conventional MOCVD,[6] which is attributed to the high growth rates of GaN, large crystal lattice mismatch (16.9%), and thermal coefficient of expansion mismatch (113%) between the GaN epilayer and the Si substrate.[6,8]

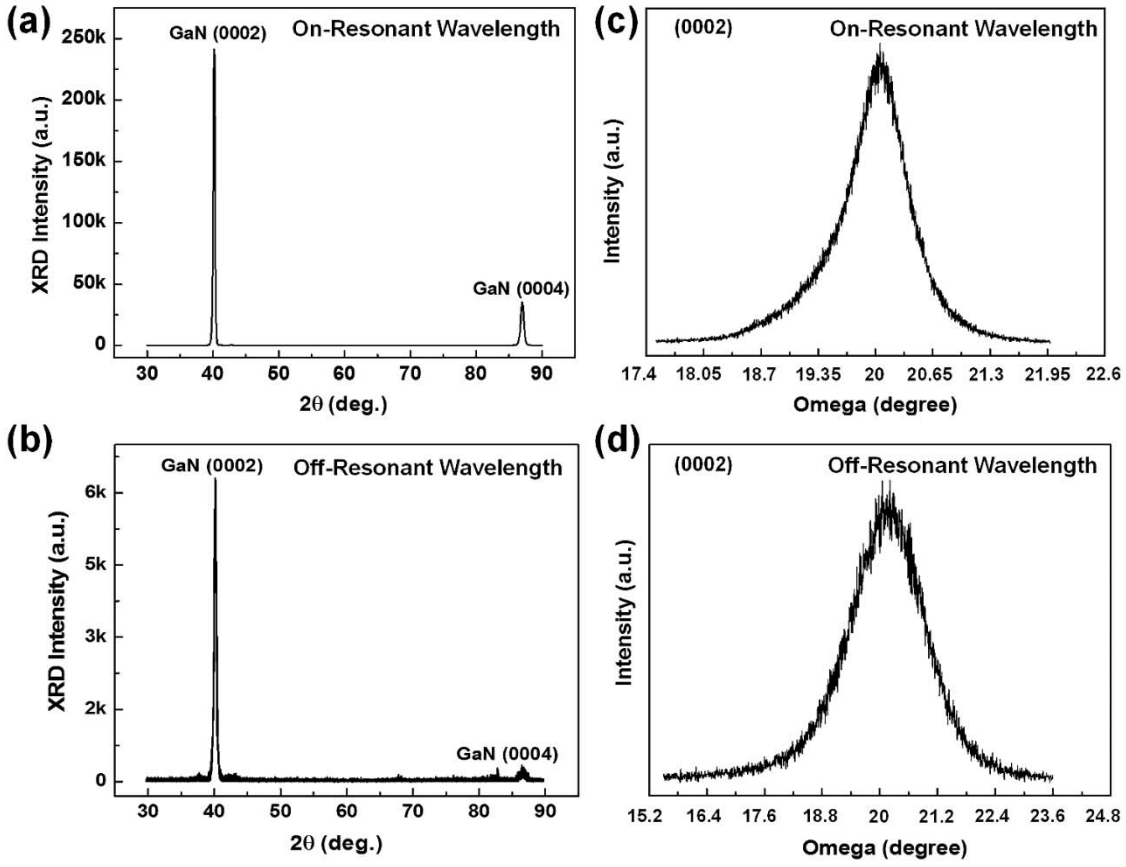

Figure 5.5 X-ray diffraction curves of GaN films deposited at (a) resonant wavelength of 9.219 μm and (b) nonresonant wavelength of 9.201 μm (x-ray diffractometer: Rigaku D/Max B diffractometer, Co Kα λ = 1.788 Å). Rocking curves of (0002) diffraction peaks of

GaN films deposited at (c) resonant wavelength of 9.219 μm and (d) nonresonant wavelength of 9.201 μm.

Table 5.2 Summary of GaN films characterization grown on Si (100) substrates at different laser wavelengths.

Sample	Laser wavelength (μm)	GaN (0002) peak ω-FWHM (arcmin)	GaN (10-12) peak ω-FWHM (arcmin)
I	9.201	92	99
II	9.219	39	43
III	10.350	45	53
IV	10.590	60	67
V	10.719	55	61

5.3.4 Hall measurement of the GaN films

Hall measurements using the Van der Pauw method were conducted to characterize carrier concentrations and mobilities of the GaN films deposited at resonant (9.219 μm) and nonresonant (9.201 μm) wavelengths. Both GaN films were demonstrated to be n-type semiconductors. Corresponding carrier concentrations and mobilities are 8.27×10^{17} cm^{-3} and 299.5 cm^2/Vs for the resonant sample, and 4.9×10^{18} cm^{-3} and 119.1 cm^2/Vs for the nonresonant sample. The relatively high carrier concentrations are indicative of high concentration of unintentionally doped impurities. However, the resonant sample possesses a lower carrier concentration but higher mobility, compared to nonresonant sample.

5.4 Mechanism of the Resonant Vibrational Excitation

According to above experimental results, two points are clearly demonstrated. The first is that resonant vibrational excitation can significantly promote GaN growth rates and improve GaN crystalline quality when comparing to conventional thermal heating and nonresonant laser irradiation. The second is that the same amount of energy coupled into different vibrational states lead to diverse results. In this study, the resonant

excitation of the NH rotational-vibrational transition at 1084.63 cm-1 [5(J) → 6(J'), K=0] leads to the highest GaN growth rate, best crystalline quality, and highest carrier mobility. To understand the reasons behind the difference, optical emission spectroscopic (OES) investigations were carried out to study the evolution of NH_3 molecules under laser irradiation at resonant and nonresonant wavelengths in open air. Fig. 5.6 shows optical images of the NH_3 flows under laser irradiation at different wavelengths. Stronger emissions are observed from NH_3 flows when irradiated at resonant wavelengths (i.e. 9.219, 10.350, and 10.719 μm) than those at nonresonant wavelengths (i.e. 10.591 and 9.201 μm). The shape and brightness of the laser-induced plasma reflect dissociation of NH_3 molecules under the laser irradiation. According to Fig. 5.6, resonant excitations lead to NH_3 flows of brighter colors and expanded diameters due to accelerated NH_3 dissociation, promoted chemical reactions, and increased reactive species concentrations.[39] The brightest and strongest NH_3 flow is observed under the resonant excitation at 9.219 μm.

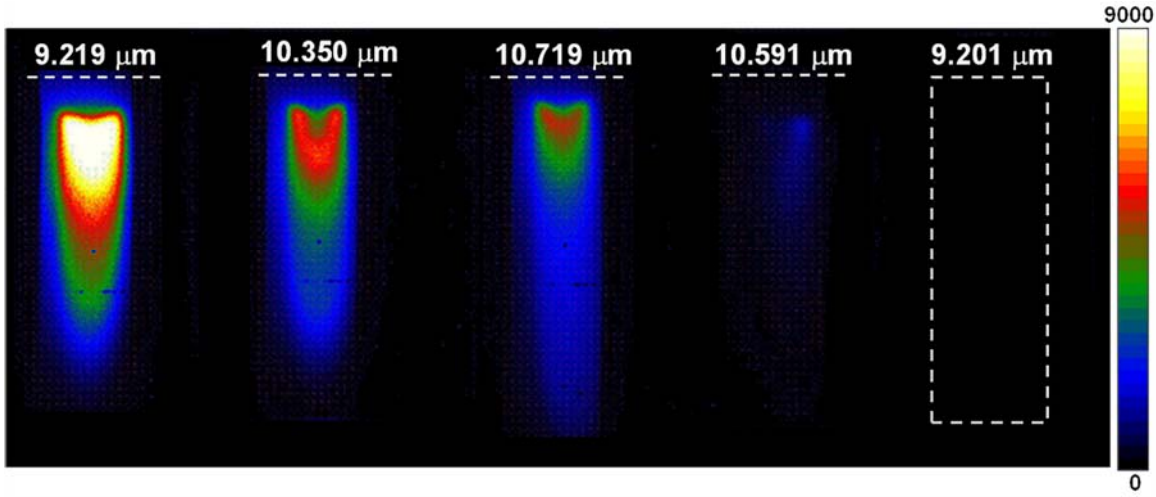

Figure 5.6 Optical images of NH^3 flows when irradiated at different laser wavelengths in open air.

OES spectra of the laser-irradiated NH_3 are shown in Fig. 5.7. Emissions from OH, NH, N^+, H_α, N, and H_β are observed at 309, 336, 463, 486, 496, and 656 nm, respectively. Strong emissions from NH_2 radicals are observed at 525, 543, 569, 603, 629, and 663 nm in all OES spectra from resonantly excited NH_3 flows, indicating effective dissociation of NH_3 molecules. Obviously increased emission intensities of OH, NH, NH_2, N, N^+, and H are observed at the resonant wavelength of 9.219 μm. However, only very weak emission intensities of NH and NH_2 radicals are identified when irradiated at the nonresonant wavelength of 10.591 μm. No emission peak is observed at the nonresonant wavelength of 9.201 μm.

N, NH, and NH_2 are active nitrogen species for growing GaN.[20,21,40] Growth of high-quality GaN films requires a sufficient supply of active nitrogen and gallium species by cracking NH_3 and TMGa molecules, respectively, and transporting atomic N and Ga to proper lattice sites. The dissociation energies for dissociating TMGa into active gallium species has been reported to be much lower than that of NH_3.[20,21] It is found that with the laser photons, the TMGa molecules undergo fragmentation with relative ease in analogy with their thermolytic instability.[20,21,41] However, effective decomposition of NH_3 molecules requires a high temperature around 1000 ^oC, which also leads to increased parasitic reactions, GaN decomposition and N escaping.[13] Therefore, decomposing NH_3 at an appropriate temperature is essential for growing high-quality GaN.

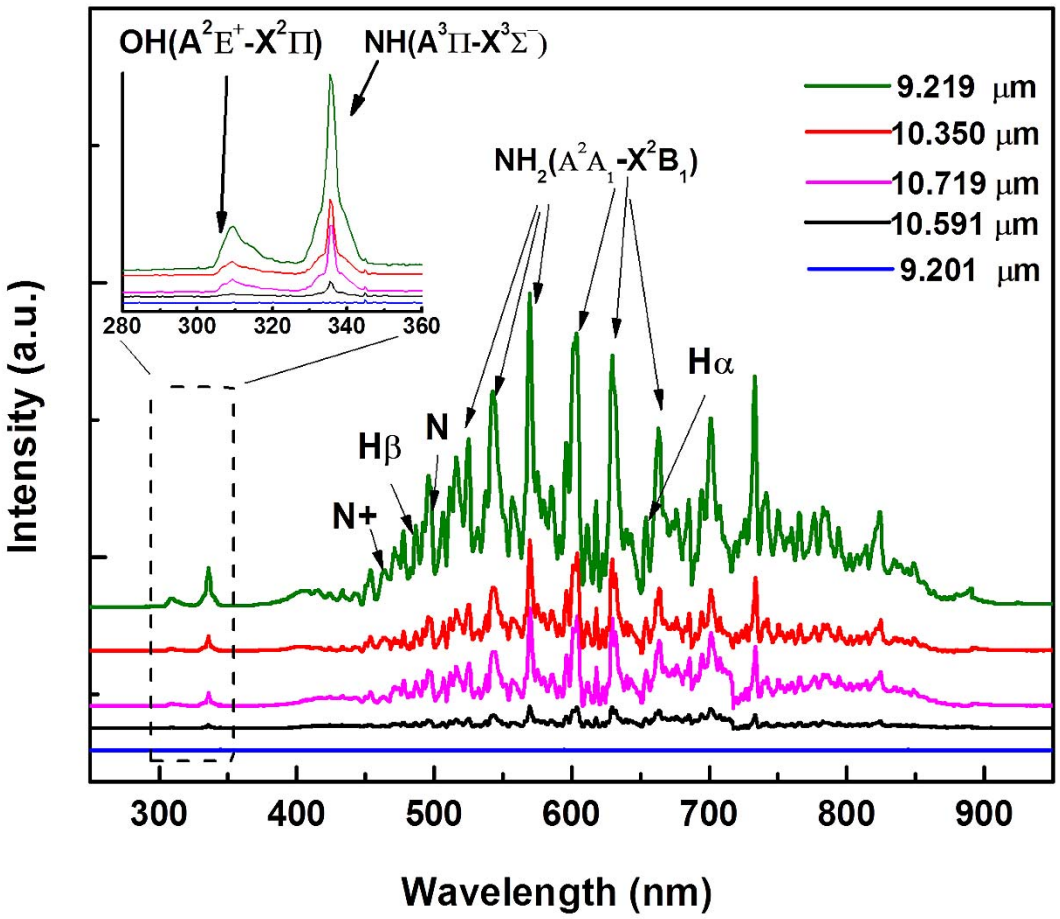

Figure 5.7 Optical emission spectra of the NH_3 under laser irradiation at different wavelengths in open air.

It is generally believed formation of GaN in MOCVD includes four key steps:[13,40] (i) TMGa:NH_3 adduct formation, (ii) amide formation and methane elimination, (iii) trimer formation, and (iv) decomposition reaction and creating N and Ga to form GaN. The first gas-phase reaction is a spontaneous reaction between TMGa and NH_3 to form a stable adduct [$(CH_3)_3Ga:NH_3$]. It is reported that the formation of the adduct as parasite reaction significantly degrades GaN film quality and growth rate at high temperatures.[13,21,40] The amide formation, trimer formation and decomposition reaction can be expressed by equations (5.2), (5.3) and (5.4), respectively:[13,40]

$(CH_3)_3Ga + NH_3 \rightarrow (CH_3)_3Ga:NH_3$ (5.1)

$(CH_3)_3Ga{:}NH_3 \rightarrow (CH_3)_2Ga{:}NH_2 + CH_4$ (5.2)

$3[(CH_3)_2Ga{:}NH_2] \rightarrow [(CH_3)_2Ga{:}NH_2]_3$ (5.3)

$[(CH_3)_2Ga{:}NH_2]_3 \rightarrow 3GaN + 6CH_4$ (5.4)

The OES results indicate that the resonant vibrational excitation effectively dissociates NH_3 molecules and increases the concentrations of the active nitrogen species, i.e. N, NH, and NH_2. Based on the reported 4-step mechanism, effective decomposition of NH_3 is suggested to reduce the formation of the $TMGa{:}NH_3$ adduct[21] in the first step and decrease the energy barriers for the rest of the steps, and therefore results in the increased GaN growth rate.

It is noteworthy that performance of a GaN-based device is limited by parasitic defect-induced emission, such as the yellow luminescence observed in GaN.[42,43] Unintentionally doped GaN is generally a n-type semiconductor due to a high concentration of shallow donor Si_{Ga} and O_N.[43] It is reported that H radicals can form neutral complexes with shallow donors and acceptor dopants. These reactions help eliminating oxygen impurities, reducing impurity density and increasing in carrier mobility and resistivity of gallium nitride films.[42] Considering the concentration of atomic hydrogen resulted from NH_3 decomposition, oxygen impurities in GaN are expected to be reduced. It is suggested that with the increments of H radicals, Fig. 5.7, the GaN crystalline quality and carrier mobility increase under resonant excitations, compared to those at nonresonant wavelengths.

Therefore, GaN films of better crystalline quality, lower impurity densities, and high deposition rates are obtained under resonant vibrational excitation. The results are in good accordance with the SEM, Raman, and XRD results.

5.5 Conclusions

In summary, vibrational excitations of NH_3 molecules were studied using a tunable CO_2 laser in growing crystalline GaN films on Si(100) substrates. The resonant vibrational excitation at 9.219, 10.350, and 10.719 μm were more efficient than nonresonant excitation in dissociating NH_3 molecules and enhancing the GaN deposition rate and quality. The OES results showed the resonant excitation of the NH-wagging modes modifies the synthesis process in a way that increases the supplies of NH, NH_2, N, N^+, and H. This leads to the enhancement in GaN deposition rates and improvement in crystalline quality. The extremely high GaN growth rate of ~ 84 μm/h with an improved crystalline quality was achieved under the resonant excitation at 9.219 μm. The red-shift in the position of E_{2H} of Raman spectra indicated that the GaN films grown on Si suffered from tensile stress and the films grown at laser wavelengths of 9.219 μm exhibited the lowest stress. The FWHM value of the XRD rocking curves of GaN (0002) and GaN (10-12) diffraction peaks decreased at resonant depositions and reached its minimum values at 9.219 μm, indicating reduced TDs density. XRD ω-FWHMs of 45 arcmin for the GaN(0002) and of 53 arcmin for the GaN(10-12) reflection were measured for samples grown at laser wavelength of 9.219 μm; the FWHMs of the GaN(0002) and GaN(10-12) planes are about 3-5 times broader than those of the best GaN epilayer samples reported in literature.[6] Further investigation are done in chapter 7 to improve the quality of the GaN films deposited via the LMOCVD techniques while maintaining high growth rates.

5.6 Reference

1. Khan, A.; Balakrishnan, K.; Katona, T., Ultraviolet light-emitting diodes based on group three nitrides. *Nature photonics* 2008, *2* (2), 77-84.

2. Avramescu, A.; Lermer, T.; Müller, J.; Eichler, C.; Bruederl, G.; Sabathil, M.; Lutgen, S.; Strauss, U., True green laser diodes at 524 nm with 50 mW continuous wave output power on c-plane GaN. *Applied physics express* **2010,** *3* (6), 061003.

3. Wu, Y.-F.; Kapolnek, D.; Ibbetson, J. P.; Parikh, P.; Keller, B. P.; Mishra, U. K., Very-high power density AlGaN/GaN HEMTs. *IEEE Transactions on Electron Devices* **2001,** *48* (3), 586-590.

4. Nakamura, S.; Pearton, S.; Fasol, G., The blue laser diode. the complete story. IOP Publishing: **2001**.

5. Ehrentraut, D.; Meissner, E.; Bockowski, M., *Technology of gallium nitride crystal growth*. Springer Science & Business Media: **2010**; Vol. 133.

6. Schenk, H.; Frayssinet, E.; Bavard, A.; Rondi, D.; Cordier, Y.; Kennard, M., Growth of thick, continuous GaN layers on 4-in. Si substrates by metalorganic chemical vapor deposition. *Journal of Crystal Growth* **2011,** *314* (1), 85-91.

7. Kizilyalli, I. C.; Edwards, A. P.; Aktas, O.; Prunty, T.; Bour, D., Vertical power pn diodes based on bulk GaN. *IEEE Transactions on Electron Devices* **2015,** *62* (2), 414-422.

8. Frayssinet, E.; Cordier, Y.; Schenk, H.; Bavard, A., Growth of thick GaN layers on 4-in. and 6-in. silicon (111) by metal-organic vapor phase epitaxy. *physica status solidi (c)* **2011,** *8* (5), 1479-1482.

9. Luo, W.; Wu, J.; Goldsmith, J.; Du, Y.; Yu, T.; Yang, Z.; Zhang, G., The growth of high-quality and self-separation GaN thick-films by hydride vapor phase epitaxy. *Journal of Crystal Growth* **2012,** *340* (1), 18-22.

10. Tomida, D.; Kagamitani, Y.; Bao, Q.; Hazu, K.; Sawayama, H.; Chichibu, S.; Yokoyama, C.; Fukuda, T.; Ishiguro, T., Enhanced growth rate for ammonothermal gallium nitride crystal growth using ammonium iodide mineralizer. *Journal of Crystal Growth* **2012,** *353* (1), 59-62.

11. Mori, Y.; Imade, M.; Maruyama, M.; Yoshimura, M., Growth of GaN crystals by Na flux method. *ECS Journal of Solid State Science and Technology* **2013,** *2* (8), N3068-N3071.

12. Collazo, R.; Mita, S.; Aleksov, A.; Schlesser, R.; Sitar, Z., Growth of Ga-and N-polar gallium nitride layers by metalorganic vapor phase epitaxy on sapphire wafers. *Journal of crystal growth* **2006,** *287* (2), 586-590.

13. Watson, I. M., Metal organic vapour phase epitaxy of AlN, GaN, InN and their alloys: A key chemical technology for advanced device applications. *Coordination Chemistry Reviews* **2013,** *257* (13), 2120-2141.

14. Creighton, J. R.; Wang, G. T.; Coltrin, M. E., Fundamental chemistry and modeling of group-III nitride MOVPE. *Journal of Crystal Growth* **2007,** *298*, 2-7.

15. Zhao, D.; Zhu, J.; Jiang, D.; Yang, H.; Liang, J.; Li, X.; Gong, H., Parasitic reaction and its effect on the growth rate of AlN by metalorganic chemical vapor deposition. *Journal of Crystal Growth* **2006,** *289* (1), 72-75.

16. Thon, A.; Kuech, T. F., High temperature adduct formation of trimethylgallium and ammonia. *Applied physics letters* **1996,** *69* (1), 55-57.

17. Choi, H.; Cheong, M.; Rana, M.; Chua, S.; Osipowicz, T.; Pan, J., Rutherford backscattering analysis of GaN decomposition. *Journal of Vacuum Science & Technology B: Microelectronics and Nanometer Structures Processing, Measurement, and Phenomena* **2003,** *21* (3), 1080-1083.

18. Koleske, D.; Wickenden, A.; Henry, R.; Culbertson, J.; Twigg, M., GaN decomposition in H 2 and N 2 at MOVPE temperatures and pressures. *Journal of crystal growth* **2001,** *223* (4), 466-483.

19. Lin, Y.; Zhou, S.; Wang, W.; Yang, W.; Qian, H.; Wang, H.; Lin, Z.; Liu, Z.; Zhu, Y.; Li, G., Performance improvement of GaN-based light-emitting diodes grown on Si (111) substrates by controlling the reactor pressure for the GaN nucleation layer growth. *Journal of Materials Chemistry C* **2015,** *3* (7), 1484-1490.

20. Rabiee Golgir, H.; Gao, Y.; Zhou, Y. S.; Fan, L.; Thirugnanam, P.; Keramatnejad, K.; Jiang, L.; Silvain, J.-F. o.; Lu, Y. F., Low-Temperature Growth of Crystalline Gallium Nitride Films Using Vibrational Excitation of Ammonia Molecules in Laser-Assisted Metalorganic Chemical Vapor Deposition. *Crystal Growth & Design* **2014,** *14* (12), 6248-6253.

21. Bhat, T. N.; Rajpalke, M. K.; Roul, B.; Kumar, M.; Krupanidhi, S., Substrate nitridation induced modulations in transport properties of wurtzite GaN/p-Si (100) heterojunctions grown by molecular beam epitaxy. *Journal of Applied Physics* **2011,** *110* (9), 093718.

22. Nakada, Y.; Aksenov, I.; Okumura, H., GaN heteroepitaxial growth on silicon nitride buffer layers formed on Si (111) surfaces by plasma-assisted molecular beam epitaxy. *Applied physics letters* **1998,** *73* (6), 827-829.

23. Shen, K.-C.; Jiang, M.-C.; Liu, H.-R.; Hsueh, H.-H.; Kao, Y.-C.; Horng, R.-H.; Wuu, D.-S., Pulsed laser deposition of hexagonal GaN-on-Si (100) template for MOCVD applications. *Optics express* **2013,** *21* (22), 26468-26474.

24. Fan, L.; Xie, Z. Q.; Park, J.; He, X. N.; Zhou, Y.; Jiang, L.; Lu, Y., Synthesis of nitrogen-doped diamond films using vibrational excitation of ammonia molecules in laser-assisted combustion flames. *Journal of Laser Applications* **2012,** *24* (2), 022001.

25. David, C. W., IR vibration-rotation spectra of the ammonia molecule. *J. Chem. Educ* **1996,** *73* (1), 46.

26. McBride, J.; Nicholls, R., The vibration-rotation spectrum of ammonia gas. I. *Journal of Physics B: Atomic and Molecular Physics* **1972,** *5* (2), 408.

27. Ghosh, D.; Hussain, S.; Ghosh, B.; Bhar, R.; Pal, A., Stress and grain boundary properties of GaN films prepared by pulsed laser deposition technique. *ISRN Materials Science* **2014,** *2014*.

28. Chowdhury, M. P.; Roy, R.; Chakraborty, B.; Pal, A., Beryllium-doped polycrystalline GaN films: Optical and grain boundary properties. *Thin solid films* **2005,** *491* (1), 29-37.

29. Kuball, M., Raman spectroscopy of GaN, AlGaN and AlN for process and growth monitoring/control. *Surface and Interface Analysis* **2001,** *31* (10), 987-999.

30. Moram, M.; Vickers, M., X-ray diffraction of III-nitrides. *Reports on progress in physics* **2009,** *72* (3), 036502.

31. Arslan, E.; Ozturk, M. K.; Teke, A.; Ozcelik, S.; Ozbay, E., Buffer optimization for crack-free GaN epitaxial layers grown on Si (1 1 1) substrate by MOCVD. *Journal of Physics D: Applied Physics* **2008,** *41* (15), 155317.

32. Xie, Z. Q.; He, X. N.; Hu, W.; Guillemet, T.; Park, J. B.; Zhou, Y. S.; Bai, J.; Gao, Y.; Zeng, X. C.; Jiang, L., Excitations of precursor molecules by different laser powers in laser-assisted growth of diamond films. *Crystal Growth & Design* **2010,** *10* (11), 4928-4933.

33. Parikh, R. P.; Adomaitis, R. A., An overview of gallium nitride growth chemistry and its effect on reactor design: Application to a planetary radial-flow CVD system. *Journal of crystal growth* **2006,** *286* (2), 259-278.

34. Pearton, S.; Zolper, J.; Shul, R.; Ren, F., GaN: Processing, defects, and devices. *Journal of applied physics* **1999,** *86* (1), 1-78.

35. Reshchikov, M. A.; Morkoç, H., Luminescence properties of defects in GaN. *Journal of applied physics* **2005,** *97* (6), 5-19.

CHAPTER 6 LOW-TEMPERATURE GROWTH OF CRYSTALLINE GALLIUM NITRIDE FILMS USING VIBRATIONAL EXCITATION OF AMMONIA MOLECULES

6.1 Introduction

Gallium nitride (GaN), a III-V compound semiconductor with a wide, direct band gap of ~3.4 eV, has been utilized in widespread applications, such as optoelectronics and high-power electronic devices.[1-3] High-quality crystalline GaN films are in demand for their ability to enhance the performance and reliability of GaN-based devices.[4-7] However, growth of high-quality crystalline GaN films requires growth techniques using high temperatures, such as metalorganic chemical vapor deposition (MOCVD, ~950-1100 ^{o}C), molecular beam epitaxy (MBE, ~800 ^{o}C), and hydride vapor phase epitaxy (HVPE, ~750 ^{o}C).[6-8] A sufficiently high temperature is necessary to overcome the activation barriers to precursor chemisorption and adatom surface diffusion. However, high substrate temperatures can also cause adverse effects, such as biaxial stress within GaN films, nitrogen loss, and GaN decomposition, which degrade the efficiency of GaN-based devices.[9-10] The biaxial stress is caused by the difference between thermal expansion coefficients of the GaN epitaxial layer and substrates (e.g., sapphire and silicon (Si)), and results in a poor light extraction in GaN-based light-emitting diodes (LEDs).[10] To reduce the thermal stress in GaN films, substrates with a matching lattice, including lithium aluminate ($LiAlO_2$), lithium gallate ($LiGaO_2$), and silicon carbide (SiC), are preferred.[11-13] However, such lattice-matching substrates are too expensive to be commercialized. A high growth temperature will also lead to nitrogen reevaporation and GaN decomposition, which limits the growth rate of GaN films.[14] So far, the growth rates of GaN films synthesized by MOCVD and MBE were reported to be 4 and 1 μm/h, respectively.[15-16] Therefore, a low-temperature synthetic technique is highly desired in growing crystalline GaN films.

In conventional GaN synthetic methods, energy is added into the gas precursors in the form of thermal heating. Energy is first deposited to kinetic energy of the reactant molecules and eventually makes its way into the internal modes (electronic, vibrational, and rotational) via collisions.[6-8] However, universal thermal heating is short of selectivity in chemical reactions. Attempts at promotion of material synthesis have been investigated by exploring infrared (IR)-laser-assisted vibrational excitations of precursor molecules, in which energy is directly coupled into specific molecules towards selective reaction pathways.[17-18] Highly efficient energy coupling through vibrational excitation provides reactant molecules with sufficient energy to surmount reaction barriers and influence reaction pathways.[19-20] In our previous studies, substantial enhancement in diamond growth was observed with resonant vibrational excitation of ethylene molecules in IR-laser-assisted combustion CVD process.[21-22]

In this study, low-temperature growth of highly c-oriented GaN films was achieved at a growth rate of up to 12 μm/h using laser-assisted metalorganic chemical vapor deposition (LMOCVD). Resonant excitation of the NH-wagging mode (v_2) in NH_3 molecules was realized using a wavelength-tunable carbon dioxide (CO_2) laser at a matching wavelength of 9.219 μm. GaN films were successfully deposited on sapphire at a substrate temperature as low as 250 ^oC. A GaN growth rate of up to 12 μm/h was achieved at 600 ^oC using the LMOCVD method, which is 4.6 times faster than that of conventional MOCVD (2.6 μm/h). The influence of laser resonant vibrational excitation of NH_3 on the GaN film growth was investigated.

6.2 Experimental Section

6.2.1 Measurement of laser power absorption by NH_3 molecules

The absorption spectra of CO_2 laser power by gaseous NH_3 were measured in a vacuum chamber with an absorption path length of 40.64 cm (Fig. 6.1). Absorption measurement of laser power at different laser wavelengths (9.2-10.9 μm) was performed at three different gas pressures of 1, 10, and 100 torr, respectively. In the experiments, the chamber was evacuated to a base pressure of 1×10^{-2} torr. NH_3 gas was subsequently introduced into the chamber. The incident laser power was kept at 80 W. A power meter was used to measure the laser power before and after passing through the chamber. The drop in laser power was calculated as the absorption percentage.

6.2.2 Growth of GaN films

Fig. 6.1 shows the experimental setup of the LMOCVD system for the growth of crystalline GaN films at low temperatures. GaN films were grown on c-plane sapphire substrates at different temperatures (250-600 ^oC). The sapphire substrates, with a dimension of 10×10 mm^2, were ultrasonically cleaned with organic solvents (acetone and methanol) and deionized water, dried, and loaded into the LMOCVD chamber, sequentially. Then, the chamber was evacuated to a base pressure of 1×10^{-2} torr using a mechanical pump. Trimethylgallium (TMGa) and ammonia (NH_3) precursors were used as gallium (Ga) and nitrogen (N) precursors, respectively. The gas flow rate of NH_3 was 1200 standard cubic centimeters per minute (sccm), and TMGa was carried into the reaction chamber using nitrogen as the carrying gas at a flow rate of 16 sccm. The growth pressure was maintained at 100 torr during the growth process. A wavelength-tunable CO_2 laser (PRC, wavelength range from 9.2 to 10.9 μm) was used to achieve resonant

vibrational excitation of the NH_3 molecules. The laser was tuned at a wavelength of 9.219 μm with a power of 80 W to resonantly excite the rotational-vibrational transition of the NH-wagging mode (ν_2, 1084.63 cm^{-1}) of NH_3 molecules and couple the laser energy into the molecules. The laser beam, with a diameter of around 6-9 mm, was irradiated in parallel to the substrate surface inside the chamber through a zinc selenide (ZnSe) window, as shown in Fig. 6.1. The distance between the laser beam and substrate surface was maintained at about 20 mm. The substrate temperature was maintained at a constant temperature of 150, 250, 350, 450, and 600 ^oC, respectively. The deposition time was kept at 1 hr. To understand the effects of laser-induced energy coupling, GaN films were also synthesized by the conventional MOCVD technique under the same growth conditions (deposition temperature, deposition time, gas flow rate, and growth pressure) without laser irradiation.

6.2.3 Characterization of GaN films

The crystallinity of the GaN films was examined using a powder X-ray diffractometer (Rigaku D/Max B diffractometer, Co $K_{\alpha 1}$ λ= 1.788 Å). Surface morphologies and dimensions of the GaN films were studied using a field emission scanning electron microscope (FESEM, S4700). An energy dispersive X-ray spectrometer (EDX, Oxford X-max 20 mm^2) was applied to analyze the composition of the GaN films. The optical properties of GaN films were studied using a photoluminescence spectrometer (iHR320 photoluminescence spectrometer with Si detector and indium gallium arsenide (InGaAs) detector).

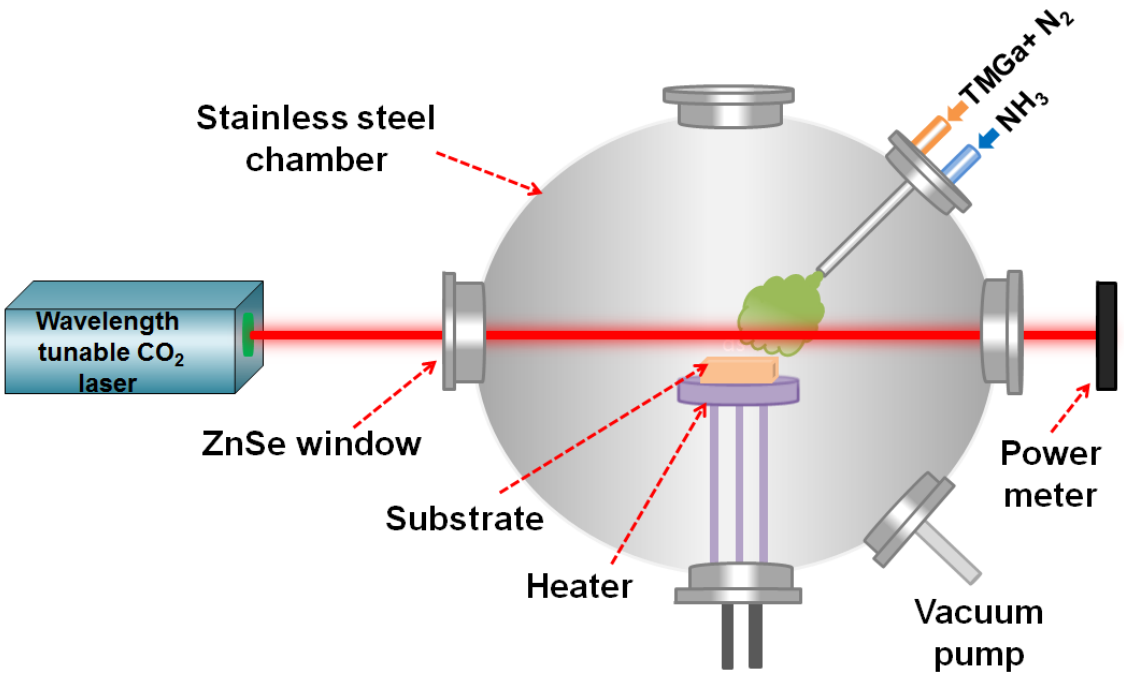

Figure 6.1 Illustration of the experimental setup for the CO_2 laser-assisted MOCVD growth of GaN films at low temperatures.

6.3 Results and discussion

6.3.1 The roles of resonant vibrational excitation of NH_3 in GaN growth

NH_3 is a dominant nitrogen source in GaN synthesis. However, NH_3 has low decomposition efficiency due to a high NH bond energy (93-105 kcal/mol).[23] A sufficient amount of active N species are required for GaN growth. The growth rate of GaN depends on the molecular flux of active N and Ga species that transport to substrates.[24] The dissociation energies for dissociating TMGa into active gallium species has been reported to be much lower than that of NH_3.[23] It is found that with the laser photons, the TMGa molecules undergo fragmentation with relative ease in analogy with their thermolytic instability. However, it is difficult to grow GaN films at temperatures lower than 500 ^oC using a conventional MOCVD method due to the low dissociation efficiency of NH_3.[23] To increase the reactivity of NH_3 is, therefore, critical in low-temperature

growth of GaN. Through resonant vibrational excitation of the NH-wagging mode in NH_3 molecules, the reactivity of NH_3 is selectively enhanced; and the dissociation efficiency of NH_3 at low temperature is promoted.[25-26]

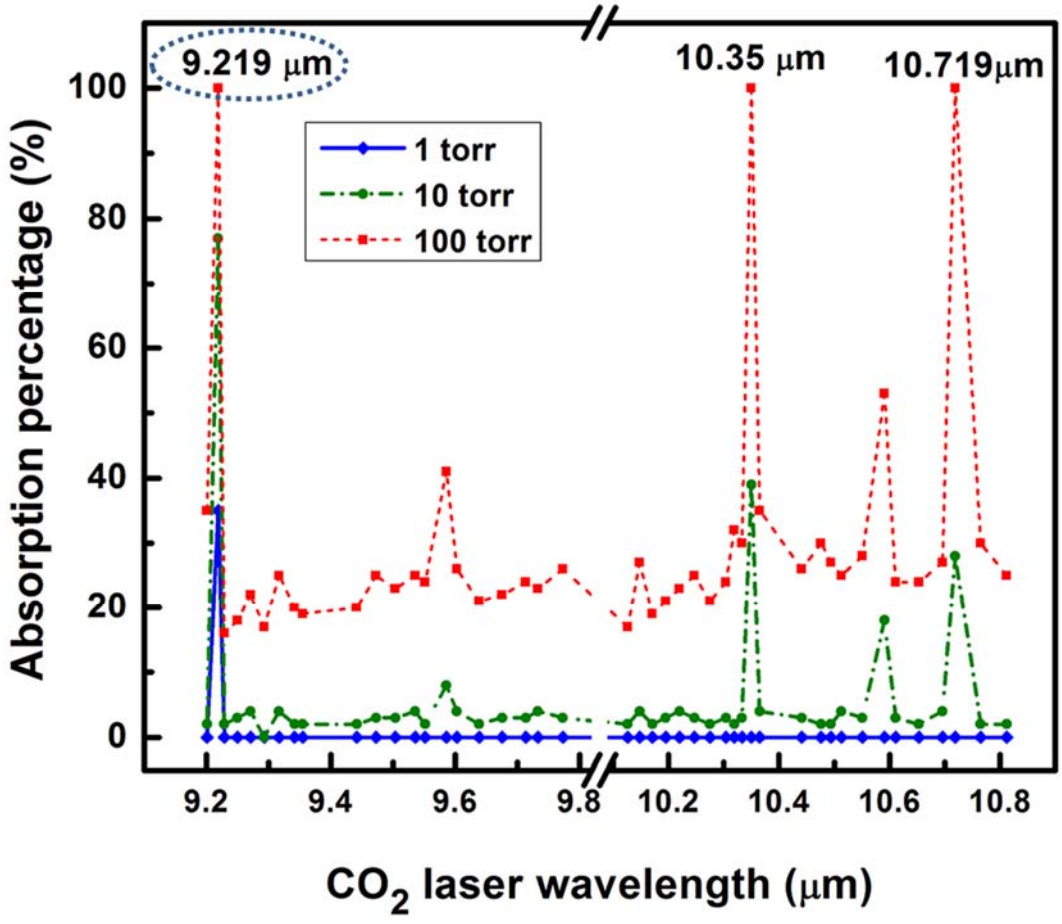

Figure 6.2 Illustration of the experimental setup for the CO_2 laser-assisted MOCVD growth of GaN films at low temperatures.

The absorption spectra of the CO_2 laser power by NH_3 gas at different gas pressures of 1, 10, and 100 torr are shown in Fig. 6.2. Three strong absorption peaks were observed at 9.219, 10.35, and 10.719 μm, respectively, at the NH_3 pressure of 10 and 100 torr. At a pressure of 100 torr, the laser energy at these three wavelengths was completely absorbed by NH_3 gas, while only one absorption peak at 9.219 μm was observed at a

pressure of 1 torr. The absorptions at these wavelengths were attributed to the resonant vibrational excitation of the NH-wagging mode (ν_2) of the NH_3 molecules.[25-26] NH_3 has a pyramidal shape with three hydrogen atoms forming the base and a nitrogen atom at the top. The NH-wagging mode vibrates in an umbrella inversion way. There is a barrier to umbrella inversion that the nitrogen atom faces on its travels through the hydrogen plane.[25] The existence of the barrier results in a splitting of a fundamental vibrational level of the NH-wagging mode into two components at 932.51 (ν_2+) and 968.32 cm^{-1} (ν_2-), giving rise to the observed absorption peaks at laser wavelengths of 10.719 (932.92 cm^{-1}) and 10.35 μm (966.18 cm^{-1}), respectively.[25-26] The strongest absorption peak at 9.219 μm is attributed to a rotational-vibrational transition (J=5 → J'=6, K=0) of the ν_2 mode at 1084.63 cm^{-1}. The perfect match between the CO_2 laser wavelength at 9.219 μm (1084.71 cm^{-1}) and the rotational-vibrational transition line of the NH_3 (1084.63 cm^{-1}) makes a stronger absorption at 9.219 μm than that at 10.35 and 10.719 μm. The rotational-vibrational excitation of NH_3 molecules at 9.219 μm contributes to dissociating of NH_3 molecules at low temperatures.

OES spectrum of the laser-irradiated NH_3 under laser irradiation at wavelength of 9.219 μm in open air are shown in Fig. 6.3. Emissions from OH, NH, N^+, H_α, N, and H_β are observed at 309, 336, 463, 486, 496, and 656 nm, respectively. Strong emissions from NH_2 radicals are observed at 525, 543, 569, 603, 629, and 663 nm in all OES spectrum from resonantly excited NH_3 flows, indicating effective dissociation of NH_3 molecules in room temperature. It worthy to note the N, NH, and NH_2 are active nitrogen species for growing GaN. Therefore, OES results indicate that the resonant vibrational excitation effectively dissociates NH_3 molecules.

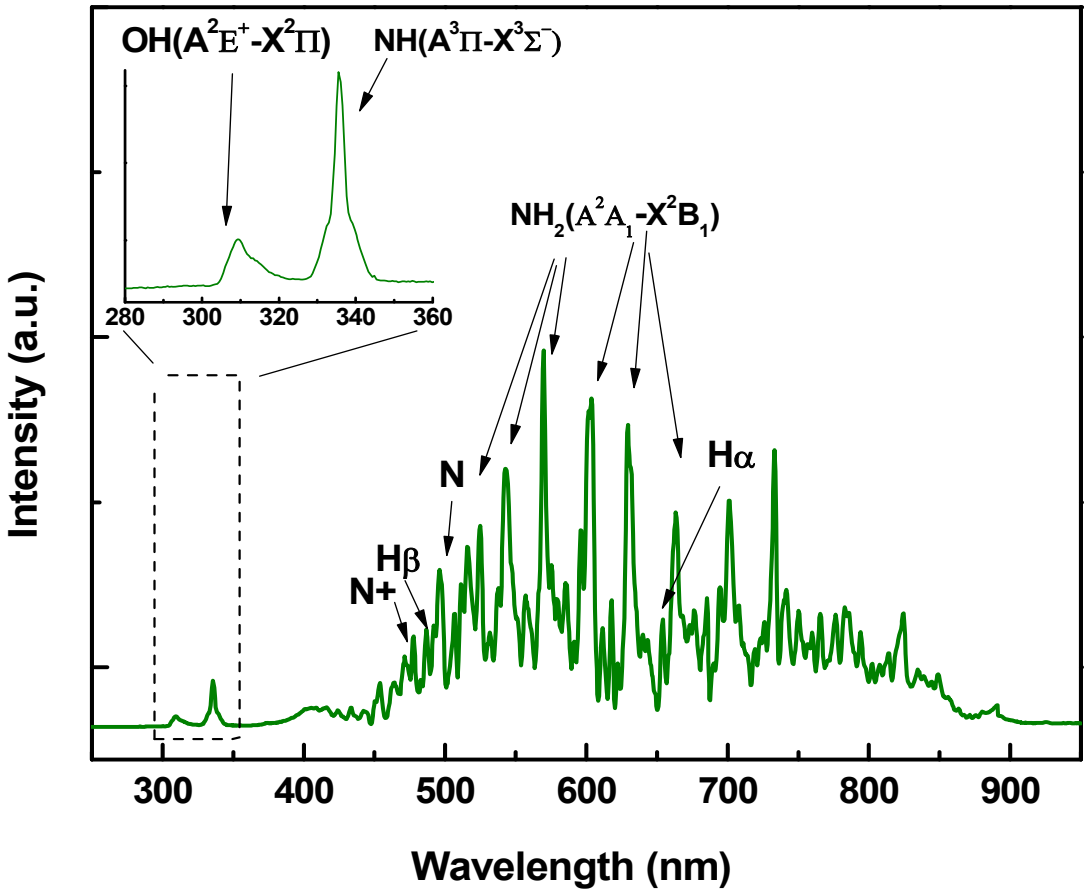

Figure 6.3 Optical emission spectra of the NH_3 under laser irradiation at wavelength of 9.219 μm in open air.

6.3.2 Characterization of GaN films

X-ray diffraction (XRD) 2θ spectra of the GaN films grown at different temperatures (i.e., 150, 250, 350, 450, and 600 ^{o}C) are shown in Fig. 6.4. Figs. 6.4(a) and 6.4(b) compare the XRD 2θ patterns of the GaN films grown by LMOCVD and MOCVD, respectively. A XRD peak attributed to the (0002) plane of GaN is observed in the GaN samples grown by LMOCVD at temperatures from 250 to 600 ^{o}C. This peak is indexed to wurtzite GaN with a hexagonal structure,[27] indicating the high c-plane orientation of the GaN films. Therefore, it can be confirmed that the synthesis of GaN

films was achieved at a temperature as low as ~250 ºC by the LMOCVD technique with the laser resonant vibrational excitation of NH_3. In contrast, the (0002) diffraction peak was only found for the sample grown by MOCVD at a temperature of 600 ºC, suggesting that a much higher substrate temperature is required for the growth of GaN using conventional MOCVD (Fig. 6.4(b)). As shown in Fig. 6.4(a), the intensity of the (0002) peak increases as the substrate temperature increases from 250 to 600 ºC. The intensity increase can be attributed to the improved crystalline quality of the GaN films due to the substrate temperature increase.[28] Additionally, a 2θ signal at 86º was observed for the GaN film grown at 600 ºC with LMOCVD (Fig. 6.4(a)). This (0004) GaN peak also refers to c-axis-oriented GaN films.

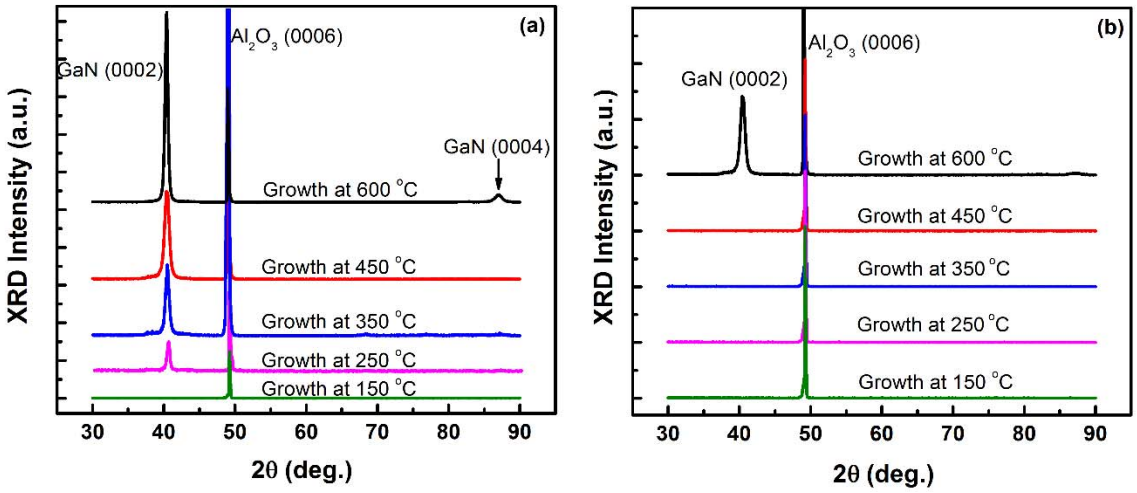

Figure 6.4 X-ray diffraction spectra of the GaN films grown on sapphire substrates at different temperatures (250-600 ºC) by (a) LMOCVD and (b) MOCVD.

The XRD φ-scan determined the degree of in-plane alignment of GaN films grown at different temperatures (250-600 ºC) by LMOCVD relative to the sapphire substrate, as shown in Fig. 6.5. The scanning planes used for φ-scan were (11-20) for sapphire and hexagonal (10–11) and cubic (200) for GaN films. The diffraction peaks from (10–11) plane of GaN film were observed at intervals of 60º for all samples grown

at temperatures from 250 to 600 ºC, which confirmed the hexagonal structure of the epitaxial GaN films. It is also observed that there is a ~30º rotation of the GaN unit cell with respect to sapphire substrate due to the large lattice mismatch between GaN and sapphire substrate (Fig. 6.5). However, no diffraction peaks from the (200) plane of cubic GaN film were observed for all samples grown at different temperatures (250-600 ºC) by LMOCVD (Fig. 6.6).

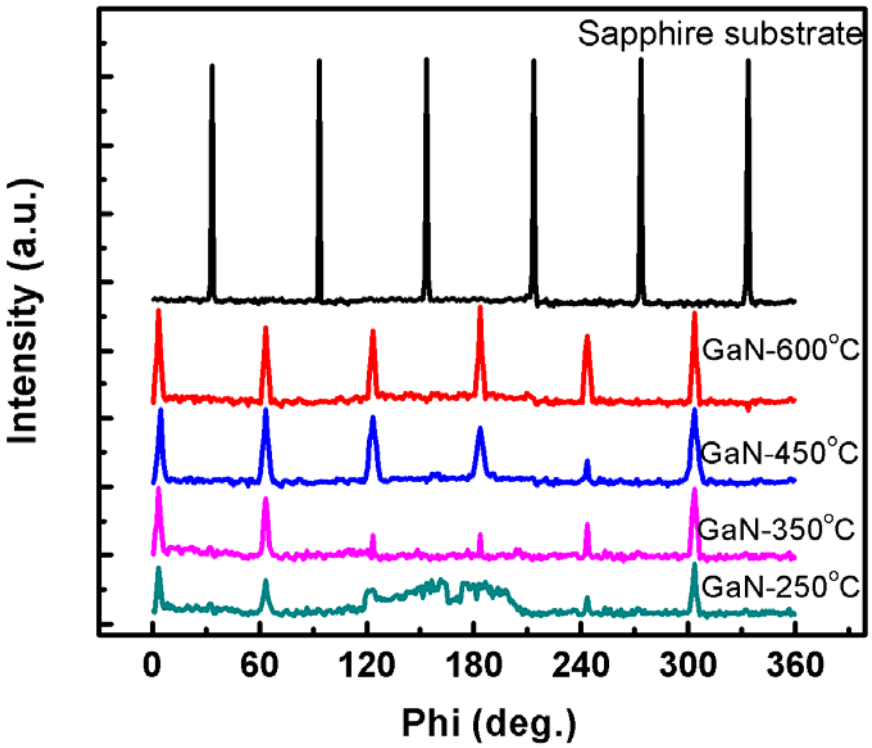

Figure 6.5 XRD φ-scan of (11-20) plane of sapphire substrate and (10–11) plane of GaN films grown on sapphire at different temperatures (250-600 ºC) by LMOCVD.

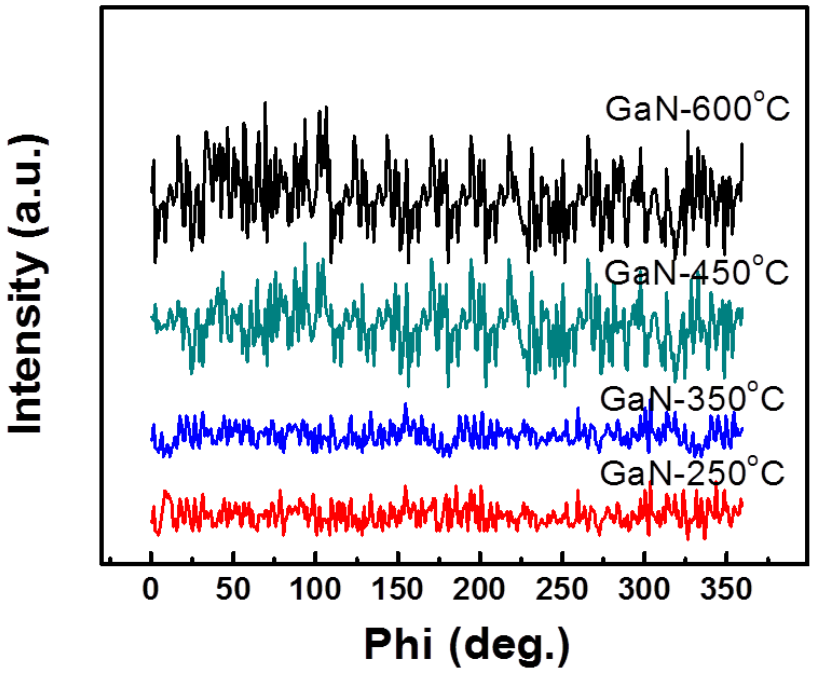

Figure 6.6 XRD phi-scan of (200) plane of GaN films grown by LMOCVD.

The 2θ position and full width at half maximum (FWHM) of (0002) diffraction peaks obtained from XRD are shown in Table 6.1. The FWHM of the (0002) plane reflects lattice distortion from screw dislocations and mixed dislocations.[28] As shown in Table 6.1, a small FWHM value of 0.18° was obtained for the GaN sample grown by LMOCVD at 600 °C. For the GaN film grown by MOCVD at 600 °C, the FWHM of (0002) was 0.20°. The distinctive reduction in the FWHM of GaN films deposited by LMOCVD indicates that the laser resonant vibrational excitation of NH_3 leads to a decrease in lattice distortion and improvement in the quality of the GaN films. For the GaN films grown by LMOCVD, the FWHM of the (0002) plane decreased monotonically with the increase in the substrate temperature from 250 to 600 °C (Table 6.1). This means that the crystalline quality of GaN films improves continuously with the increase in the growth temperature, which is explained by the reduction in diffusion

barriers and increase in diffusion rates of Ga and N species as the substrate temperature increases.[28]

Table 6.1 The GaN (0002) diffraction peak position, FWHM of GaN (0002) peak, GaN growth rates, and the grain size of GaN films grown at different temperatures (250-600 °C).

Sample	Substrate temperature (°C)	2θ (°)	FWHM of (0002) (°)	Growth rate (μm/h)
LMOCVD	250	40.55	0.27	0.15
LMOCVD	350	40.60	0.25	0.60
LMOCVD	450	40.42	0.21	1.60
LMOCVD	600	40.40	0.18	12
MOCVD	600	40.47	0.20	2.60

The effectiveness of laser resonant vibrational excitation of NH_3 on the uniformity and surface morphology of GaN films is clearly shown by the FESEM images shown in Fig 6.7. For the GaN film grown with LMOCVD at 250 °C (Fig. 6.7(a)), small domains of about ~30 ± 5 nm with hexagonal facets were obtained. The average domain sizes were ~65 ± 10 and ~100 ± 10 nm for the GaN films grown by LMOCVD at 350 and 450 °C, respectively (Figs. 6.7(b) and 6.7(c)). With a further increase in the substrate temperature to 600 °C, the lateral size of the islands with hexagonal facets increased. With a coalescence of crystallite islands, GaN structures with flat facets were obtained by LMOCVD at 600 °C, as shown in Fig. 6.7(d). In contrast, the surface of the GaN sample grown at 600 °C by MOCVD was rough with obvious hexagonal hillocks (Fig. 6.7(f)). Additionally, the threshold temperature to grow GaN films by MOCVD is 600 °C. Below this temperature, no GaN deposition is observed on substrate surfaces (Fig. 6.7(e)) that agree with the XRD results.

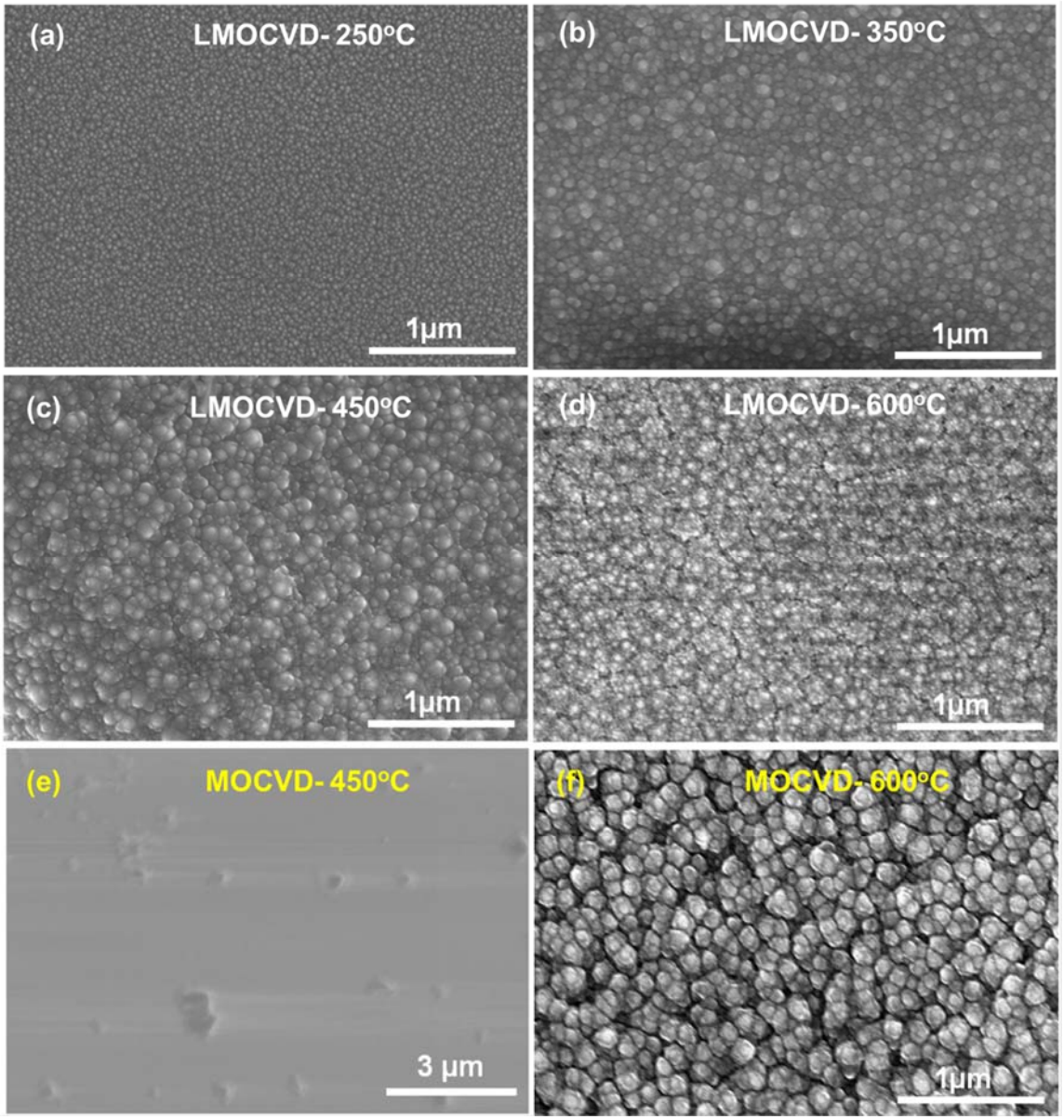

Figure 6.7 SEM images of GaN films grown by LMOCVD at temperatures of (a) 250, (b) 350, (c) 450, and (d) 600 °C; and SEM images of GaN films grown by MOCVD at temperatures of (e) 450, and (f) 600 °C.

The cross-sectional SEM images of the GaN films were obtained to explore the effect of laser resonant vibrational excitation of NH_3 on the growth rate. Figs. 6.8(a) and 6.8(b) show the cross-sectional SEM images of the GaN films grown at 600 °C by LMOCVD and MOCVD, respectively. A growth rate of 12 μm/h was achieved by

LMOCVD, which is ~4.6 times faster than that of MOCVD (this work, ~2.6 µm/h). Moreover, compared with the growth rate of GaN synthesized by other studies (MBE: ~1 µm/h; and MOCVD: ~4 µm/h),[15-16] laser resonant vibrational excitation contributes to a drastic enhancement in the GaN growth rate. Table 6.1 shows the GaN growth rates by LMOCVD at different temperatures from 250 to 600 °C. As the substrate temperature increased, the thickness of the GaN films increased.

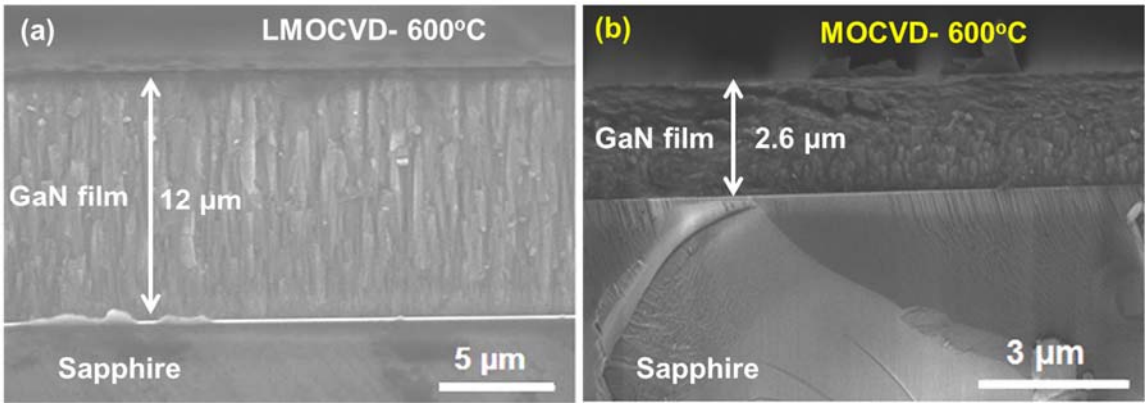

Figure 6.8 Cross-sectional SEM images of GaN films grown at 600 oC by (a) LMOCVD (b) MOCVD.

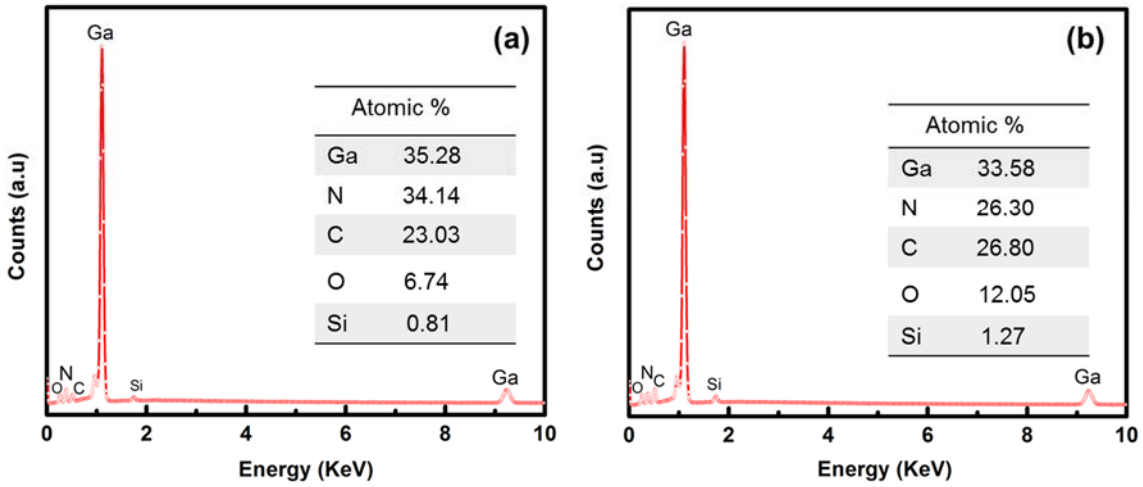

Figure 6.9 EDX spectra of GaN films grown at 600 °C by (a) LMOCVD (b) MOCVD.

The EDX results in Fig. 6.9 confirm the presence of Ga and N elements in the GaN films, as well as carbon (C), oxygen (O), and silicon (Si) as impurities. According to the EDX spectra obtained from GaN films grown at 600 ºC by LMOCVD and MOCVD, obvious increases of 7.84% in N concentration and 1.7% in Ga concentration were observed in the sample grown with LMOCVD. The resonant vibrational excitation of the NH bond vibration in NH_3 molecules plays an important role in the dissociation of NH_3 and the increase of N species in the reaction. The increase in N content in the deposited films explains why the GaN growth rate was highly improved using LMOCVD, which is in agreement with other studies.[29] Furthermore, it is worthy to note that the impurity content (C, O, and Si) in the GaN film grown with LMOCVD decreased considerably (Fig. 6.9). In MOCVD growth, Ga reacts with impurity elements in the absence of sufficient active N atoms or N-related intermediates. However, laser resonant vibrational excitation of NH_3 in LMOCVD increased the production of active N-related intermediates, eliminating the impurity content incorporated into the film during GaN growth. With the reduction in impurities, the GaN crystal islands grow larger in size, leading to higher crystallinity, a full coalescence, and a smooth surface morphology of GaN films. It is also worthy to note that EDX measurements here just express a semi-quantitative analysis and the values do not reflect actual composition of the GaN films.[30] Large concentration of oxygen and carbon in the films is just an artifact resulting from the very low detection efficiency of EDX for light elements.

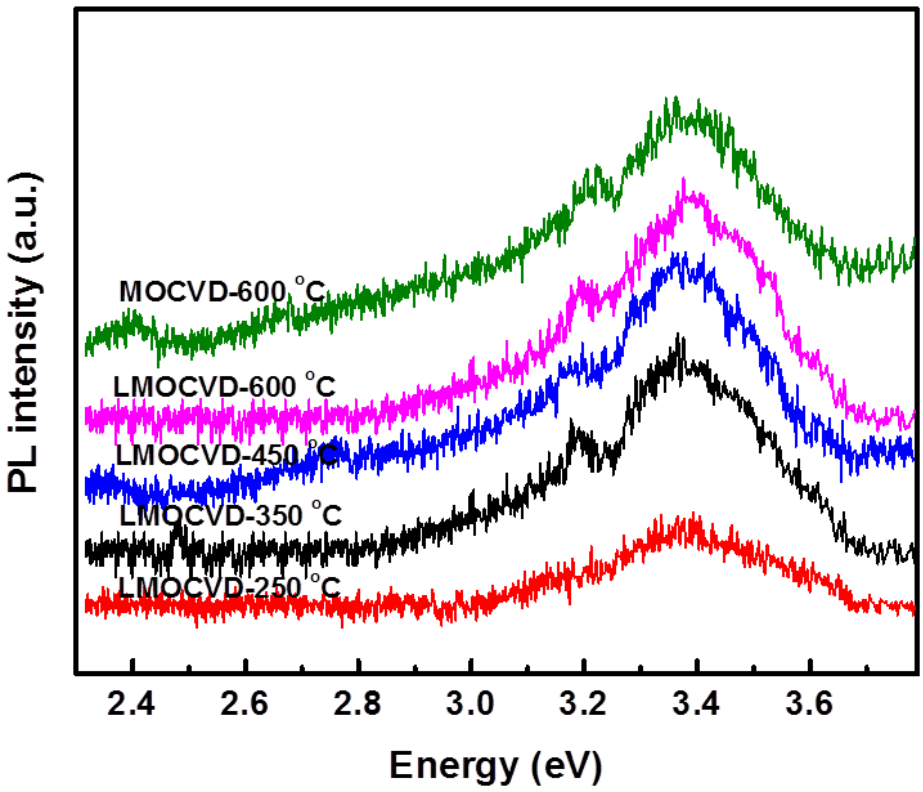

Figure 6.10 PL spectra of GaN films acquired with a 325 nm laser.

The PL spectra of GaN films have been acquired using a laser with a wavelength of 325 nm. As shown in Fig. 6.10, two peaks located at ~3.4 and ~3.2 eV are observed in the PL spectra of the samples grown at different temperatures from 250 to 600 ºC by LMOCVD. The strong peak at ~3.4 eV is the near band edge (NBE) transition peak, while the weak peak at ~3.2 eV can be attributed to radiative recombination between a shallow donor and the valence band.[31] Another possible reason for the peak at ~3.2 eV can be associated with the formation of small amount of cubic GaN at low temperatures growth. The PL spectra further confirmed the hexagonal structure of the GaN films grown on sapphire substrates at different temperatures from 250 to 600 ºC by LMOCVD. The GaN film grown at 600 ºC by LMOCVD showed a near-band-edge (NBE) emission at about ~3.398 eV which was closer to the NBE emission of bulk GaN (3.47 eV),[31]

compared to that of MOCVD with ~3.394 eV. The NBE peaks of GaN films grown by LMOCVD at 250, 350, and 450 ^{o}C are ~3.388, ~3.391, and ~3.392 eV, respectively.

It is valuable to note that there are several studies of using the polycrystalline GaN films with columnar structures for photonic and electronic devices.[32-33] In this study, the quality of the polycrystalline GaN films grown at low temperatures by LMOCVD are comparable to those reported values,[32-33] suggesting a potential of heteroepitaxial GaN film grown by LMOCVD for electronic and photonic applications.

6.4 Conclusions

The LMOCVD technique was developed for low-temperature growth of GaN films on sapphire substrates through laser resonant vibrational excitation of NH_3 molecules. The highly c-oriented GaN films were successfully grown at temperatures as low as 250 ^{o}C. Low-temperature growth of GaN films is ascribed to the enhanced decomposition efficiency of NH_3 with resonant excitation of rotational-vibrational transition (1084.71 cm^{-1}) of the NH-wagging mode at the laser wavelength of 9.219 μm. The FWHM of (0002) diffraction peaks obtained from XRD for GaN films grown at 600 ^{o}C decreased from 0.20^{o} (MOCVD) to 0.18^{o} (LMOCVD), indicating an improvement in crystalline quality by LMOCVD. SEM images showed that the laser resonant vibrational excitation of NH_3 helped to grow GaN films with smooth and uniform surface morphology. A high GaN growth rate of up to 12 μm/h was achieved at 600 ^{o}C by LMOCVD, which is ~4.6 times faster than that of conventional MOCVD with 2.6 μm/h. This approach suggests that the laser resonant vibrational excitation of precursors is promising in increasing NH_3 reactivity and promoting GaN synthesis, which could be extended to synthesis of other nitride semiconductors.

6.5 References

1. Avramescu, A.; Lermer, T.; Müller, J.; Eichler, C.; Bruederl, G.; Sabathil, M.; Lutgen, S.; Strauss, U., True green laser diodes at 524 nm with 50 mW continuous wave output power on c-plane GaN. Applied physics express 2010, 3 (6), 061003.

2. Biju, K. P.; Subrahmanyam, A.; Jain, M. K., Low-temperature growth of polycrystalline GaN films using modified activated reactive evaporation. Journal of Crystal Growth 2009, 311 (8), 2275-2280.

3. Bour, D.; Nickel, N.; Van de Walle, C.; Kneissl, M.; Krusor, B.; Mei, P.; Johnson, N., Polycrystalline nitride semiconductor light-emitting diodes fabricated on quartz substrates. Applied Physics Letters 2000, 76 (16), 2182-2184.

4. Brandt, O.; Waltereit, P.; Ploog, K. H., Determination of strain state and composition of highly mismatched group-III nitride heterostructures by x-ray diffraction. Journal of Physics D: Applied Physics 2002, 35 (7), 577.

5. Cheng, K.; Leys, M.; Degroote, S.; Germain, M.; Borghs, G., High quality GaN grown on silicon (111) using a Si x N y interlayer by metal-organic vapor phase epitaxy. Applied Physics Letters 2008, 92 (19), 192111.

6. Chin, A. H.; Ahn, T. S.; Li, H.; Vaddiraju, S.; Bardeen, C. J.; Ning, C.-Z.; Sunkara, M. K., Photoluminescence of GaN nanowires of different crystallographic orientations. Nano letters 2007, 7 (3), 626-631.

7. Crim, F. F., Making energy count. Science 2007, 316 (5832), 1707-1708.

8. David, C. W., IR vibration-rotation spectra of the ammonia molecule. J. Chem. Educ 1996, 73 (1), 46.

9. Fan, L.; Xie, Z. Q.; Park, J.; He, X. N.; Zhou, Y.; Jiang, L.; Lu, Y., Synthesis of nitrogen-doped diamond films using vibrational excitation of ammonia molecules in laser-assisted combustion flames. Journal of Laser Applications 2012, 24 (2), 022001.

10. Gao, Y.; Zhou, Y.; Park, J.; Wang, H.; He, X. N.; Luo, H.; Jiang, L.; Lu, Y., Resonant excitation of precursor molecules in improving the particle crystallinity, growth rate and optical limiting performance of carbon nano-onions. Nanotechnology 2011, 22 (16), 165604.

11. Gibart, P., Metal organic vapour phase epitaxy of GaN and lateral overgrowth. Reports on Progress in Physics 2004, 67 (5), 667.

12. Gogova, D.; Kasic, A.; Larsson, H.; Hemmingsson, C.; Monemar, B.; Tuomisto, F.; Saarinen, K.; Dobos, L.; Pecz, B.; Gibart, P., Strain-free bulk-like GaN grown by hydride-vapor-phase-epitaxy on two-step epitaxial lateral overgrown GaN template. Journal of applied physics 2004, 96 (1), 799-806.

13. Hashimoto, T.; Wu, F.; Speck, J. S.; Nakamura, S., A GaN bulk crystal with improved structural quality grown by the ammonothermal method. Nature materials 2007, 6 (8), 568-571.

14. Iliopoulos, E.; Adikimenakis, A.; Dimakis, E.; Tsagaraki, K.; Konstantinidis, G.; Georgakilas, A., Active nitrogen species dependence on radiofrequency plasma source

operating parameters and their role in GaN growth. Journal of crystal growth 2005, 278 (1), 426-430.

15. Ke, X.; Jun, X.; Peizhen, D.; Yongzong, Z.; Guoqing, Z.; Rongsheng, Q.; Zujie, F., γ-LiAlO 2 single crystal: a novel substrate for GaN epitaxy. Journal of crystal growth 1998, 193 (1), 127-132.

16. Khan, A.; Balakrishnan, K.; Katona, T., Ultraviolet light-emitting diodes based on group three nitrides. Nature photonics 2008, 2 (2), 77-84.

17. Killelea, D. R.; Campbell, V. L.; Shuman, N. S.; Utz, A. L., Bond-selective control of a heterogeneously catalyzed reaction. Science 2008, 319 (5864), 790-793.

18. Kim, M.; Oshima, M.; Kinoshita, H.; Shirakura, Y.; Miyamura, K.; Ohta, J.; Kobayashi, A.; Fujioka, H., Investigation of the initial stage of GaN epitaxial growth on 6 H-Si C (0001) at room temperature. Applied physics letters 2006, 89 (3), 031916.

19. Koleske, D.; Wickenden, A.; Henry, R.; Culbertson, J.; Twigg, M., GaN decomposition in H 2 and N 2 at MOVPE temperatures and pressures. Journal of crystal growth 2001, 223 (4), 466-483.

20. Kushvaha, S.; Kumar, M. S.; Yadav, B.; Tyagi, P. K.; Ojha, S.; Maurya, K.; Singh, B., Influence of laser repetition rate on the structural and optical properties of GaN layers grown on sapphire (0001) by laser molecular beam epitaxy. CrystEngComm 2016, 18 (5), 744-753.

21. Mesrine, M.; Grandjean, N.; Massies, J., Efficiency of NH 3 as nitrogen source for GaN molecular beam epitaxy. Applied physics letters 1998, 72 (3), 350-352.

22. Nakamura, S., The roles of structural imperfections in InGaN-based blue light-emitting diodes and laser diodes. Science 1998, 281 (5379), 956-961.

23. Nakamura, S.; Harada, Y.; Seno, M., Novel metalorganic chemical vapor deposition system for GaN growth. Applied Physics Letters 1991, 58 (18), 2021-2023.

24. Sakurada, K.; Kobayashi, A.; Kawaguchi, Y.; Ohta, J.; Fujioka, H., Low temperature epitaxial growth of GaN films on LiGa O 2 substrates. Applied physics letters 2007, 90 (21), 211913.

25. Shen, Y.; Zhou, Z.; Chen, P. C., R. Zhang, Y. Shi, and YD Zheng, W. Tong, and W. Park. Appl. Phys. A: Mater. Sci. Process 1999, 68, 593.

26. Vézian, S.; Natali, F.; Semond, F.; Massies, J., From spiral growth to kinetic roughening in molecular-beam epitaxy of GaN (0001). Physical Review B 2004, 69 (12), 125329.

27. Waltereit, P.; Brandt, O.; Trampert, A.; Grahn, H.; Menniger, J.; Ramsteiner, M.; Reiche, M.; Ploog, K., Nitride semiconductors free of electrostatic fields for efficient white light-emitting diodes. Nature 2000, 406 (6798), 865-868.

28. Wu, Y.-F.; Kapolnek, D.; Ibbetson, J. P.; Parikh, P.; Keller, B. P.; Mishra, U. K., Very-high power density AlGaN/GaN HEMTs. IEEE Transactions on Electron Devices 2001, 48 (3), 586-590.

29. Xie, Z.; Zhou, Y.; He, X.; Gao, Y.; Park, J.; Ling, H.; Jiang, L.; Lu, Y., Fast growth of diamond crystals in open air by combustion synthesis with resonant laser energy coupling. Crystal Growth & Design 2010, 10 (4), 1762-1766.

30. Xie, Z. Q.; He, X. N.; Hu, W.; Guillemet, T.; Park, J. B.; Zhou, Y. S.; Bai, J.; Gao, Y.; Zeng, X. C.; Jiang, L., Excitations of precursor molecules by different laser powers in laser-assisted growth of diamond films. Crystal Growth & Design 2010, 10 (11), 4928-4933.

31. Yagi, S., Highly sensitive ultraviolet photodetectors based on Mg-doped hydrogenated GaN films grown at 380 C. Applied Physics Letters 2000, 76 (3), 345-347.

32. Yang, Z.; Li, L.; Wang, W., GaN grown by molecular beam epitaxy at high growth rates using ammonia as the nitrogen source. Applied physics letters 1995, 67 (12), 1686-1688.

33. Zare, R. N., Laser control of chemical reactions. science 1998, 279 (5358), 1875-

CHAPTER 7 LMOCVD GROWTH OF HIGH QUALITY GAN EPILAYER

7.1 Introduction

Gallium nitride (GaN) with excellent physical properties, such as wide direct bandgap, high electron mobility and high thermal stability, has been extensively studied and attracted attentions for applications in light-emitting diodes (LEDs), high-power electronic devices and short wavelength optoelectronics.[1-3] Current commercial GaN-based devices are fabricated by epitaxy onto foreign substrates because the GaN bulk and freestanding substrate technology is still immature.[4] High-quality GaN are routinely grown by hydride vapor phase epitaxy (HVPE), ammonothermal, molecular beam epitaxy (MBE), and metal-organic chemical vapor deposition (MOCVD).[5-11] Although HVPE and ammonothermal methods with the advantage of high growth rates have emerged to obtain bulk GaN,[5-7] they lack the precise control and heterojunction layer growth required for device structures. The overwhelming majority of GaN epilayers and GaN-based devices are grown by MOCVD and MBE.[8-12] The MOCVD growth rate of GaN epilayers commonly exceeds 1–3 μm/h, while MBE is typically performed with a growth rate up to 1 μm/h.[8-12] The relatively slow growth rates limit these traditional methods for many device structures that require thick GaN layers. Therefore, synthetic techniques with high growth rates are highly in demand for the scalable production of high-quality GaN epilayers to satisfy the steadily increasing requirement, since it can help reducing the cycle time in device fabrication.

Laser-assisted MOCVD (LMOCVD) is an ideal method for various material growth with advantages of low growth temperature, fast growth rate, and the capability to deposit patterned materials.[13-17] Several semiconductor materials, including silicon, gallium arsenide, indium phosphide, and aluminum nitride, have been successfully grown

using the LMOCVD.[13-17] For instance, Zhou *et al*.[18] reported ultraviolet laser LMOCVD growth of GaN at low temperatures, leading to films having (0002) preferential orientation with a broad XRD peak. However, the photolysis of the precursors with UV laser resulted in the low density of the reactive radicals and a low GaN growth rate. On the other hand, CO_2 laser LMOCVD has been successfully used to prepare various kinds of thin films at high growth rates.[16,19-25] For example, Iwanaga *et al*.[19] reported the deposition of large-area amorphous silicon films using CO_2 laser LMOCVD with a high growth rate of > 60 μm/h in a relatively low laser power and low substrate temperatures. In chapter 6, we have demonstrated the fast growth of GaN films with (0002) preferential orientation using CO_2 laser LMOCVD with a growth rate up to 84 μm/h at low temperatures,[23] where the experiments were designed to elucidate the GaN growth mechanism via CO_2 laser LMOCVD rather than to optimize the material crystalline quality. The high GaN growth rate is due to the mixed photolysis/pyrolysis reactions of the precursors and the photo-induced effects, as has been evidenced by wavelength dependence of GaN growth rates.[22-24] However, the low-temperature deposition resulted in films with broad XRD peaks and low crystalline quality.[19,22] It has been reported that the deposition of high-quality GaN films, which is preferred for device applications, requires high growth temperatures.[26-29]

In this chapter, we successfully demonstrated the fast growth of high-quality GaN epilayers on sapphire substrates with a high growth rate of 25.8 μm/h using an optimized CO_2 laser LMOCVD method. The growth of GaN epilayers followed previously documented two-step growth steps,[30] including a thin three dimensional (3D) GaN layer growth, lateral growth and coalescence of the 3D layer and, finally, quasi-two

dimensional (2D) growth at high temperatures. The growth rate of 25.8 μm/h is 8.6 times higher than that has been used in GaN epliayers by traditional MOCVD.[11,12] This work provides a simple and cost-effective way to realize fast and high-quality GaN epilayer growth with high potential in GaN-based optoelectronic applications.

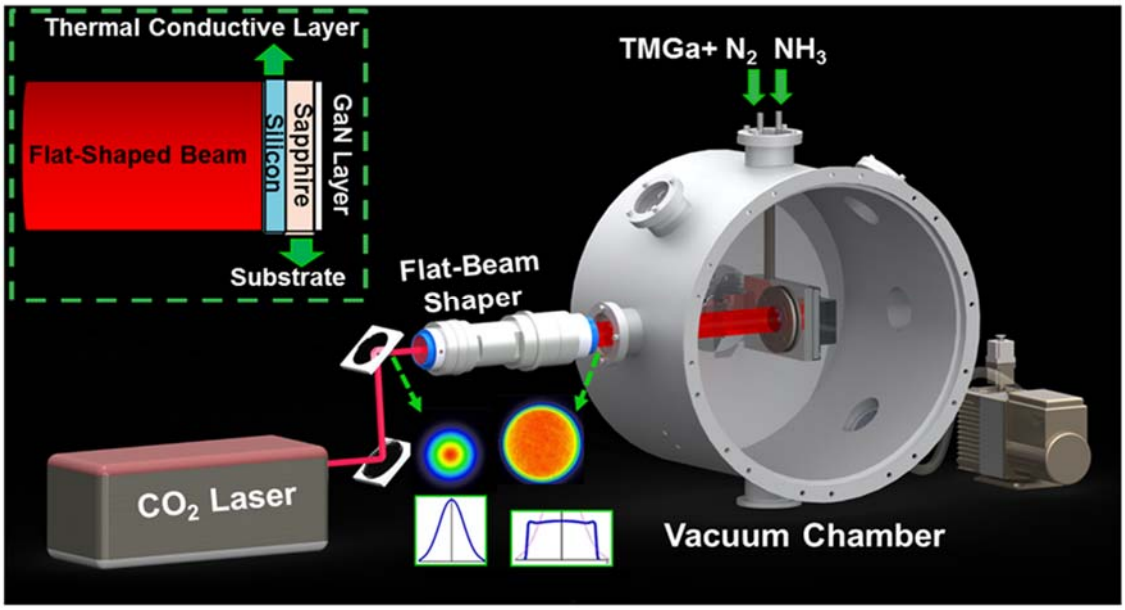

Figure 7.1 Schematic of the experimental setup of CO_2 laser LMOCVD system.

7.2 Methods

7.2.1 Growth of GaN layers

The growth of GaN layers on c-plane (0001) orientation sapphire substrates was performed in a home-made vertical LMOCVD system. The schematic experimental setup of the LMOCVD system is shown in Fig. 7.1. Trimethylgallium (TMGa) and ammonia (NH_3) were used as the Ga and N precursors, respectively. Prior to the GaN growth, a thin Si layer was coated on sapphire as thermal conductive layer to absorb laser energy. Then, 1 × 1 cm^2 sapphire substrates were successively cleaned in piranha and 15% HCl solution, and then loaded into the LMOCVD reactor. A continuous-wave (CW) and wavelength-tunable CO_2 laser (PRC Inc., $\lambda = 9.201$ μm) was used for substrate heating. A

flat-top laser beam shaper (Edmund Optics) was used to generate a beam with a uniform power distribution (output beam diameter ~ 20 mm) from a Gaussian CO_2 laser beam (Fig. 1a), in order to realize a uniform substrate temperature for material growth with controlled crystal orientations. The chamber pressure during the growth process was kept at ~ 10 Torr. A two-step growth process was used for growing high-quality and smooth GaN layers without using AlN buffer layers.[30] NH_3 (26 mmol/min) and TMGa (20 μmol/min) were introduced simultaneously into the reactor chamber after the substrate temperature was stable under laser irradiation. The growth process started with deposition of a very thin 3D GaN layer for 10 second at 700 ^oC (laser power ~ 95 W). The growth was then interrupted and the 3D GaN layer was annealed at 990 ^oC for 5 min (laser power ~ 160 W) under NH_3 with a flow rate of 26 mmol/min. The subsequent growth of unintentionally doped GaN epilayer was carried out for 10 min at substrate temperatures ranging from 930 to 990 °C by adjusting the laser power. The substrate temperature during the growth was monitored using a pyrometer (Omega, OS3752).

7.2.2 Characterization

The morphology of GaN layers was examined by scanning electron microscopy (SEM, S4700) and atomic force microscopy (AFM, Bruker Dimension ICON SPM). The structural properties of GaN layers were investigated using transmission electron microscopy (TEM, FEI Tecnai OsirisTM), high-resolution X-Ray diffraction (HR-XRD), and Raman spectroscopy. High-resolution TEM (HRTEM) was performed in a FEI Tecnai OsirisTM instrument operated at 200 kV. Cross-sectional TEM samples were prepared using a FEI Helios NanoLab 660 FIB/SEM. To minimize ion beam damage to the surface of the top layer (GaN), a 20 nm-thick Ti coating was deposited on the GaN

surface prior to FIB processing. Bulk milling of the sample was performed using a 30 keV Ga+ beam and polishing step was done using a 10 keV Ga+ beam. The approximate thickness of the final lamellae, mounted on Cu grids, was 60-100 nm. HR-XRD measurements were performed using Rigaku Smart Lab Diffractometer with Cu Ka1 radiation (l = 1.5406 Å). Raman spectra were recorded using a Raman microscopy (Renishaw inVia H 18415, Argon ion laser, λ = 514.5 nm). Hall effect measurements were carried out via the Van der Pauw method at room temperature. Optical transmission data were collected using a Perkin-Elmer LAMBDA 1050 UV/Vis/NIR spectrophotometer.

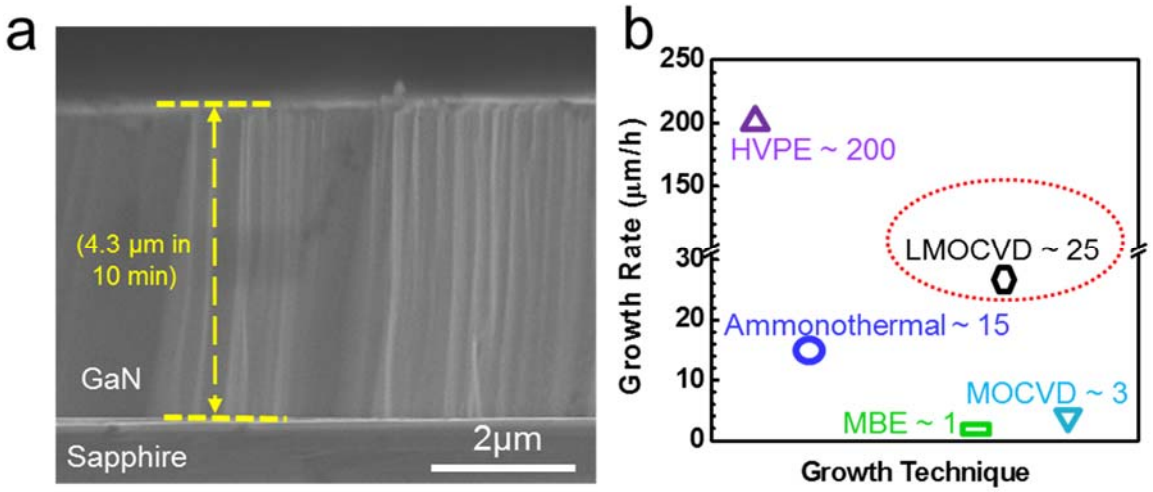

Figure 7.2 (a) Cross-sectional SEM image of the ~ 4.3 µm thick GaN epilayer grown on a sapphire (0001) substrate at 990 ºC for 10 min. (b) A comparison of growth rate between different techniques used for growth of high-quality GaN.

7.3 Results and discussion

The cross-sectional SEM image in Fig. 7.2 is a typical LMOCVD GaN sample grown at 990 °C for 10 min, which shows a very sharp interface between GaN and sapphire substrate. The thickness of GaN epilayers was measured to be ~ 4.3 µm, corresponding to a growth rate of ~ 25.8 µm/h which was much higher compared to the

conventional MBE (~ 1 μm/h) and MOCVD (~ 3 μm/h) techniques for GaN epilayer growth (Fig. 1c).[18-12] In addition, the overall processing time for LMOCVD was less than 20 min, but not several hours as required for the HVPE, ammonothermal, MOCVD, and MBE techniques.[5-12]

Morphological evolution of GaN during the growth process was investigated, as shown in Fig. 7.3. In step 1, very thin GaN 3D islands were grown at 700 °C. With annealing at 990 ºC for 5 min under NH_3 flow, the GaN islands grew up laterally, and started to coalesce gradually. In step 2, with increasing of growth time at high temperature (HT), the GaN islands increased in sizes and grew into a continuous and smooth film followed by a rapid coalescence.[31] Figs. 7.3a and 7.3b show the top view of GaN islands after 30 and 90 s HT growth, respectively. It is notable that the size and height distribution of the GaN islands are rather uniform after 90 s. The coalescence of GaN islands with a smooth surface was completed after ~ 120 s HT growth, and inverted hexagonal pyramid pits were formed, diminishing and disappearing eventually (not shown here). Fig. 7.3c shows the SEM image of the GaN epilayers after 10 min HT growth. It is clear that very smooth GaN surface is obtained and 2D step growth mode is dominant over the entire substrate.

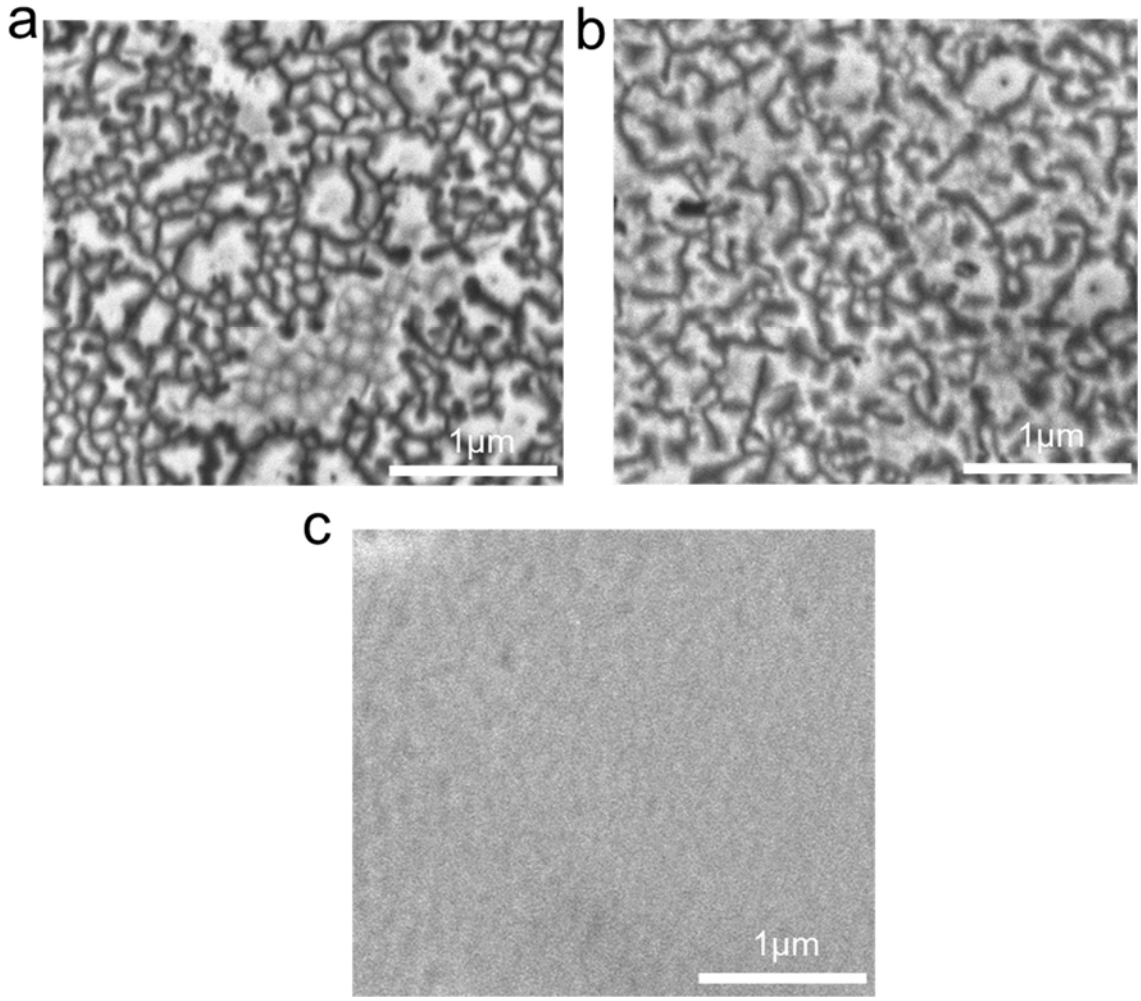

Figure 7.3 Morphological characterization of GaN epilayers grown on sapphire substrates. SEM plan views of GaN during growth process: (a) GaN islands after 30 s HT growth, (b) GaN islands after 90 s HT growth, and (c) GaN epilayers after 10 min HT growth.

The AFM images of 2×2 μm^2 surface area of fully coalesced GaN epilayers in Fig. 7.4 shows excellent dislocation-mediated step-flow morphology with spiral hillocks, which is similar to that of high-quality GaN grown by MOCVD and MBE methods at much lower growth rates.[9, 32] AFM measurement further reveals that the surface root-mean square (RMS) roughness for GaN layers grown at 990 ^oC is as small as 1.892 nm, slightly higher than that of reported works with much lower growth rates.[9, 32-33] This flat GaN surface is of paramount importance for the fabrication of high-performance GaN-based optical and optoelectronic devices. The RMS roughness for GaN layers grown at

930 and 960 °C with identical growth conditions was calculated to be 1.103 and 1.253 nm (Figs. 7.4a and 7.4b), respectively, revealing a smoother GaN growth at relatively lower temperatures in this work.

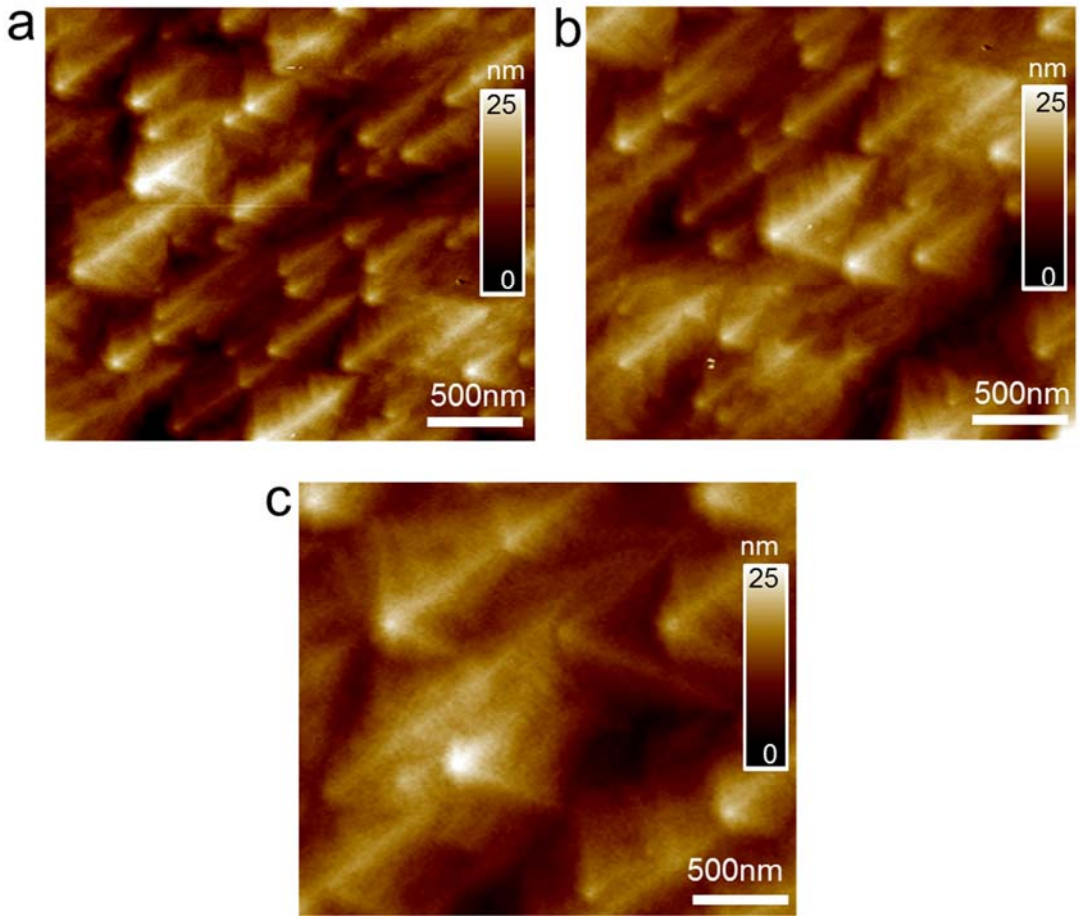

Figure 7.4 AFM images of GaN epilayers grown on sapphire substrates at (a) 930 °C, (b) 960 °C and (c) 990 °C for 10 min.

The cross-sectional TEM image of the GaN layers grown at 990 °C, sapphire substrate and GaN/sapphire hetero-interface are shown in Fig. 7.5a to c, respectively. It is observed that the as-grown GaN layer has a single-crystalline structure with an epitaxial layer even at the GaN/sapphire hetero-interfaces. The lattice fringes with a spacing of ~ 0.517 nm correspond to the GaN c-plane interplanar distance, indicating that the epitaxial layer is c-plane oriented. All the (0002) lattice fringes appear parallel to the substrate

surface. Fig. 7.5d shows the selected-area electron diffraction (SAED) pattern for GaN epitaxial layer, further revealing the single crystal array of spots indexed to the (0002) of wurtzite GaN. The regularity of the atomic arrangement and the absence of a diffuse streak from the SAED pattern indicate the high quality of the crystalline phase.[34]

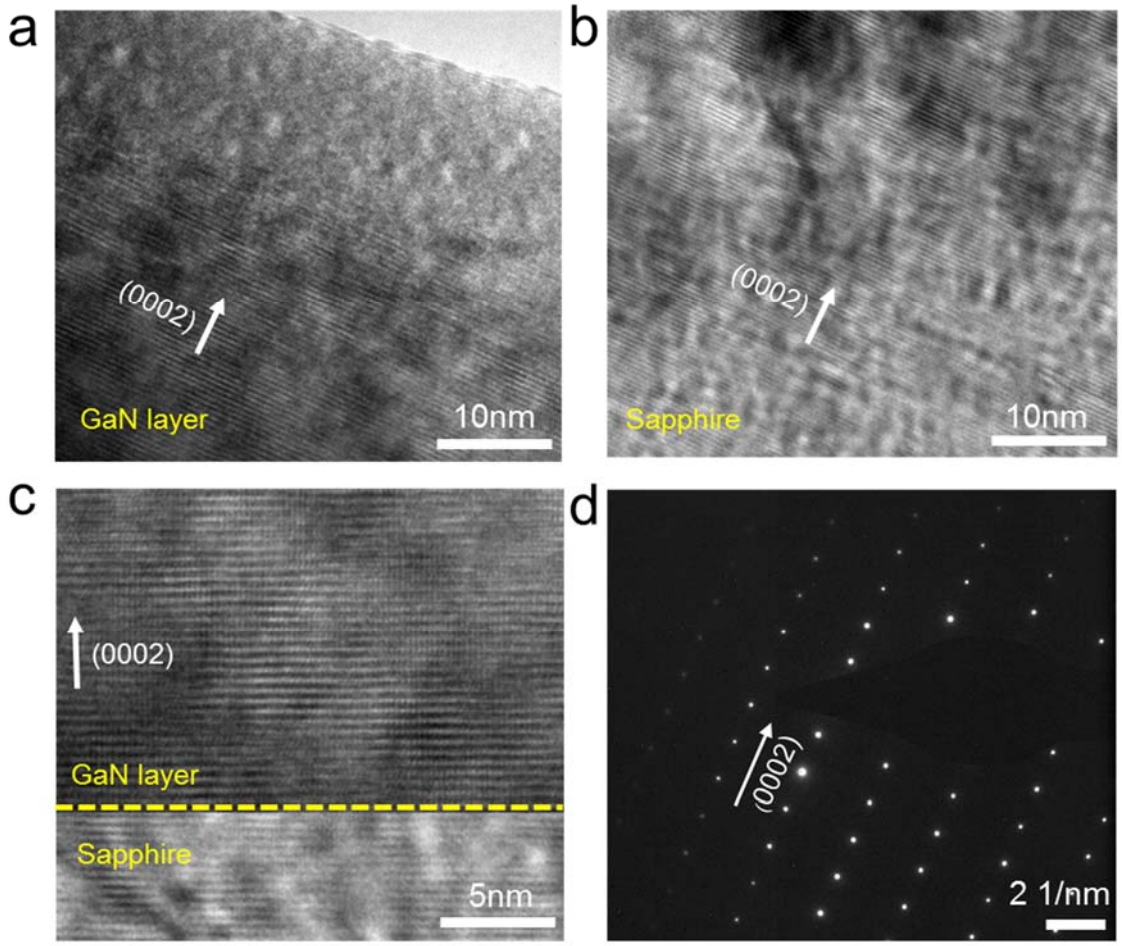

Figure 7.5 Structural characterization of GaN epilayers grown on sapphire substrates at 990 °C. High-resolution cross-sectional TEM image of (a) GaN epilayer, (b) sapphire substrate and (c) the GaN/sapphire hetero-interface. (d) Selected-area diffraction pattern for the GaN epilayer.

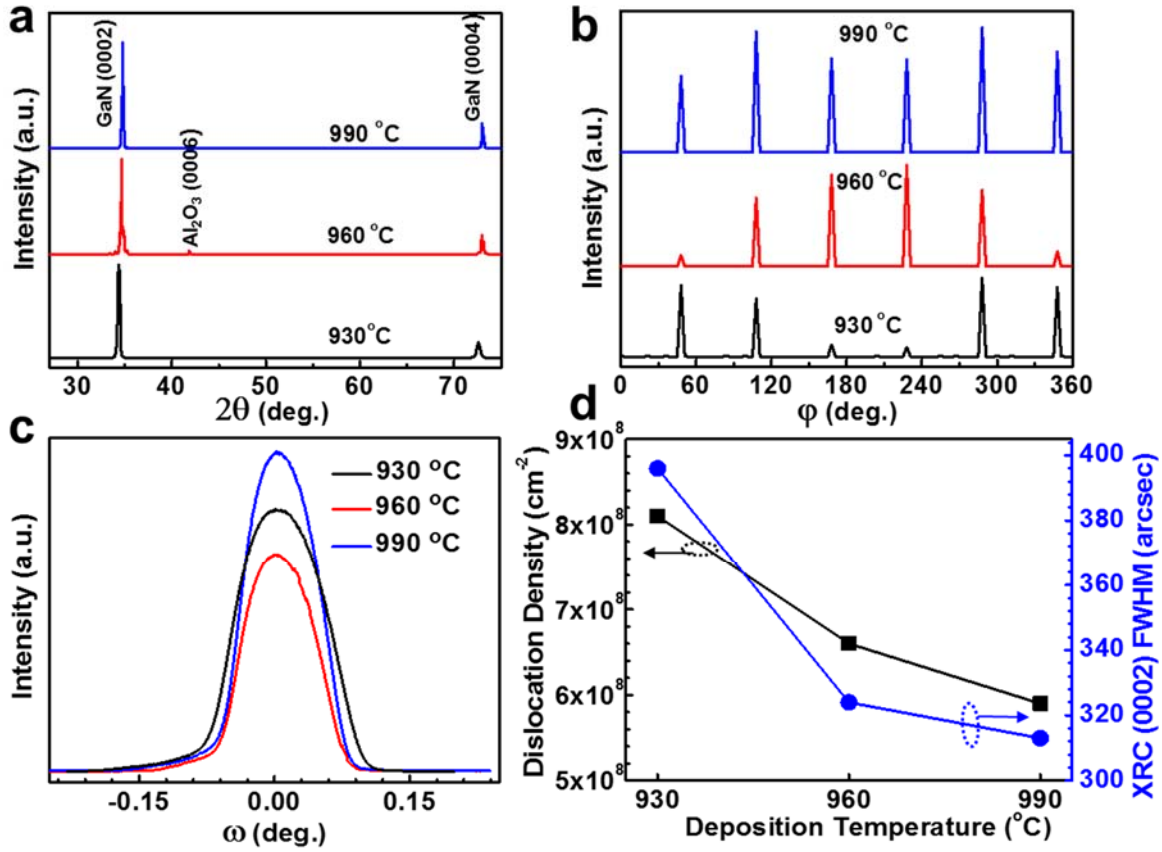

Figure 7.6. Crystallographic characterization of GaN epilayers grown on sapphire with respect to growth temperatures ranging from 930 to 990 °C. (a) X-ray 2θ scan. (b) X-ray φ scan. (c) XRC curves of the GaN (0002) peak. (d) Temperature dependence of the dislocation density (■) and XRC (0002) FWHM (●) for the GaN epilayers grown on sapphire.

XRD was performed to study the structural properties of the GaN epilayers grown on sapphire. Fig. 7.6a is a typical XRD 2θ scan for the GaN films on sapphire grown at different temperatures. Two peaks at around 34.51 and 72.64 were observed in each spectrum, which correspond to the wurtzite GaN (0002) and (0004) reflections, respectively. Therefore, the out-of-plane epitaxial relationship of GaN (0001)/sapphire can be determined for these samples. Furthermore, it can be seen that the intensity of GaN (0002) and (0004) is gradually increased and the peaks become sharper as the GaN

growth temperature increases from 930 to 990 °C, revealing the improved crystalline quality of the GaN films at higher temperatures.

To evaluate the in-plane epitaxial relationship between the GaN films and the sapphire substrates, XRD ϕ scan was conducted while 2θ was kept constant at the peak position and the sample was rotated 360º around the surface normal. Fig. 7.6b shows the normalized φ scans of GaN (10-12), where six-fold rotational peaks with an interval of 60° can been clearly identified for all samples. The variation in the peak intensity versus φ is obvious for each diffraction due to the noncoplanarity of the beam vector and the surface normal, which is very common in practice.[35] A quantitative comparison of the peak intensity among samples grown at different temperatures was not undertaken, because in thin films with strong preferential orientation, the diffraction intensity of the planes parallel to the surface is extremely sensitive to the sample orientation.[35] Both the XRD 2θ and φ scan results clearly confirm that single-crystalline hexagonal GaN epilayers have been grown on the sapphire substrates at temperatures ranging from 930 to 990 ºC.

X-ray rocking curve (XRC) is a valid method to determine the crystalline quality of GaN films. The full-width at half-maximum (FWHM) of XRC for the (0002) peak is usually used to evaluate the screw treading dislocations density (TDD), while the FWHM of XRC for (10-12) peak corresponds to the lattice distortion from all components of the TDDs, including edge and screw dislocations.[36] Fig. 7.6c compares the GaN (0002) XRCs for the GaN epilayers grown on the sapphire substrates at different temperatures. The FWHM values of the GaN (0002) and (10-12) planes were summarized in Table 7.1. For the sample grown at 930 ºC, the FWHMs of the GaN (0002) and (10-12) planes were

measured to be 396 and 471 arcsec, respectivelly. Both values monotonously decreased to 324 and 443 arcsec for the sample grown at 960 °C, and further decreased to 313 and 390 arcsec for the sample grown at 990 °C, indicating that the GaN layers grown at higher temperature correspond to higher purity and crystalline quality. Note that the low FWHM values obtained at 990 °C are also comparable to those of GaN layers grown on sapphire using the conventional MOCVD and MBE technique.[37] We have estimated the dislocation density existing in the GaN layers grown on sapphire at various growth temperatures using the following equation:[36]

$$D_{screw} = \frac{\beta_{(0002)}{}^2}{9\, b_{screw}{}^2}, \tag{7.1}$$

$$D_{edge} = \frac{\beta_{(10-12)}{}^2}{9\, b_{edge}{}^2}, \tag{7.2}$$

$$D_{Total} = D_{screw} + D_{edge}, \tag{7.3}$$

where D_{screw} and D_{edge} are the screw dislocation and edge dislocation density, respectively. β is the FWHM value measured from XRC (0002) and (10-12) planes in degrees and b is the Burgers vector length (b_{screw} = 0.5185 nm, b_{edge} = 0.3189 nm) for GaN. Fig. 7.6d shows the temperature dependence of dislocation density in the as-grown GaN epilayers. The estimated total dislocation densities D_{Total} for the samples grown at 930, 960 and 990 °C are 8.1×10^8, 6.6×10^8 and 5.9×10^8 cm^{-2}, respectively. These findings further indicate that the LMOCVD GaN layers grown at higher temperatures have relatively lower crystalline defects.

Raman spectroscopy has been widely used to evaluate the quality and residual stress of nitride films.[35] Fig. 7.7a shows the room-temperature Raman spectra of GaN films grown at different temperatures. Two prominent phonon modes which are Raman

active, E_2 (high) and A1 (LO) modes, are observed in each spectrum, where E_2 (high) phonon is used to characterize the in-plane stress state of the GaN films. The stress can be calculated by

$$\sigma = \frac{\Delta\omega}{4.3\ (cm^{-1}\ Gpa^{-1})} \tag{7.4}$$

where σ is the biaxial stress and Δω is the E_2 (high) phonon peak shift. The E_2 (high) phonon of stress-free GaN is around 567.6 cm-1.[36] The E_2 (high) phonon modes obtained from GaN films grown at 930, 960 and 990 ^oC are located at 568.7, 571.5 and 570 cm^{-1}, respectively. The E_2 (high) mode peaks for all the samples blue-shift compared to that of stress-free GaN, which indicates that all the GaN films are under compressive stress, as predicted for the GaN grown on sapphire substrates.[37] It is known most of the film stresses arise during sample cooling-down after growth.

Fig. 7.7b compares the measured compressive stresses in the GaN films grown at different temperatures. The GaN sample grown at 930 ^oC shows less in-plane compressive stress compared with the samples grown at higher temperatures of 960 and 990 ^oC. Additionally, the FWHM values of the E_2 (high) peak for GaN epilayers decreased with the increase in the growth temperature, further indicating of high crystalline quality of GaN epilayers obtained at higher growth temperatures.

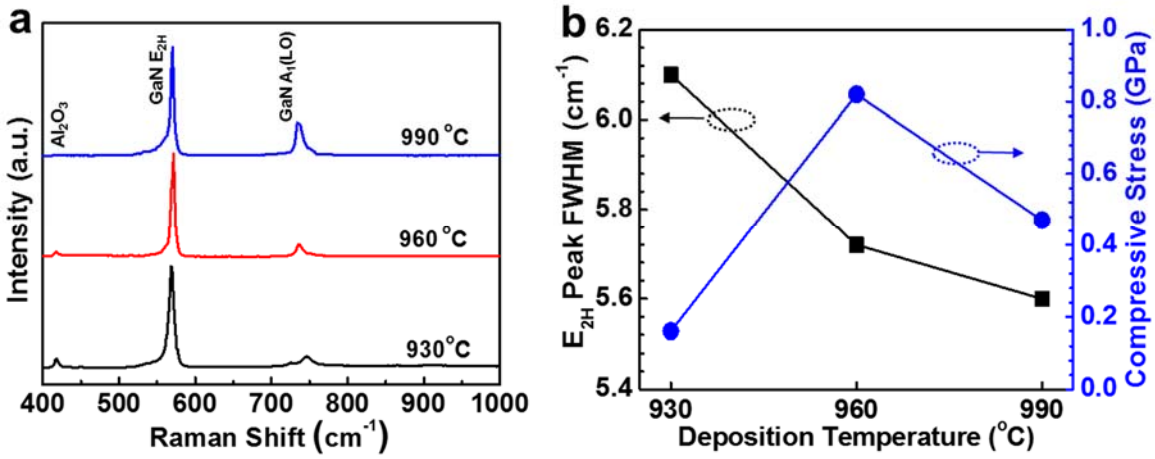

Figure 7.7 Residual stress evaluation of the GaN epilayers grown on sapphire. (a) Typical Raman spectra of GaN epilayers grown on sapphire at different temperatures. (b) The temperature dependence of FWHM of GaN E_2 (high) peak (■) and film stresses (●).

Electrical and optoelectronic properties of the GaN epilayers were also investigated (Fig. 7.8). Room-temperature Hall effect measurements were performed to study the electrical property of the GaN epilayers, as shown in Fig. 7.8a and Table I. We found that as the growth temperature increases from 930 to 960 and 990 ºC, the mobility increases from 226 to 293 and 369 $cm^2\ V^{-1}\ s^{-1}$ and the carrier concentration decreases from 8.4×10^{16} to 5.3×10^{16} and $3.1 \times 10^{16}\ cm^{-3}$, respectively. The mobility measured in our study is comparable to those reported in several studies for high-quality GaN films deposited using MOCVD and MBE at high temperatures.[41-45] The observed mobility increase with the increased temperature was also reported in the MOCVD GaN films. This can be attributed to the increased film thickness and the improved crystallinity, namely, the crystal defects in the GaN films affect their mobility by scattering the charge carriers.[41-45]

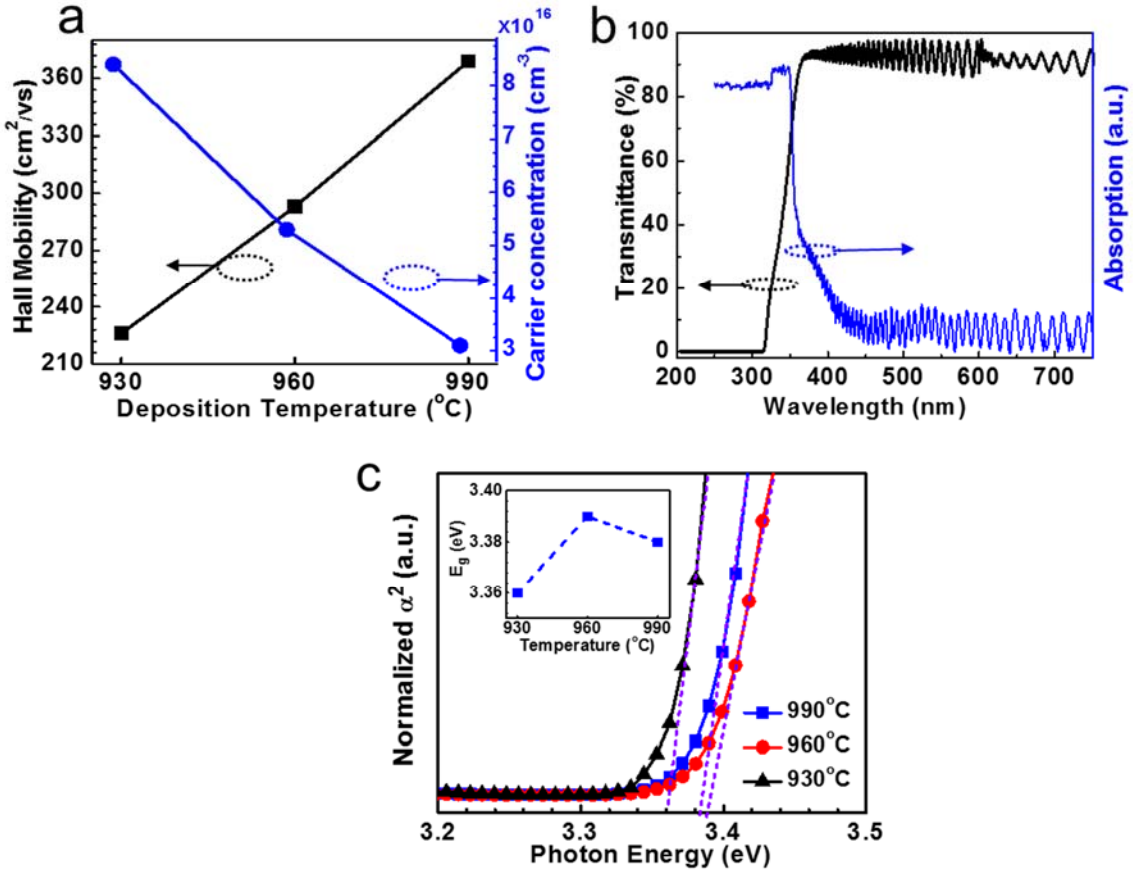

Figure 7.8 Electrical and optical properties of the LMOCVD GaN epilayers grown on sapphire. (a) Temperature dependence of Hall mobility (■) and resistivity (●) of the GaN layers. (b) Transmission and absorption spectra of the GaN layers grown at 990 °C. (c) The optical band gap extracted from (b).

The optical transmission and absorption spectra of GaN epliayers grown at 990 °C are shown in Fig. 7.8b. The absorption coefficient was derived from spectrophotometry in transmission mode (Fig. 7.8c). The band gap, E_g, of semiconductors with direct band gaps can be estimated using the following equation:[46]

$$\alpha^2 \sim (h\upsilon - E_g), \quad (3)$$

where α is the absorption coefficient, h is the Plank's constant, υ is the frequency, and E_g is the semiconductor band gap.[46] The value of optical band gap can be

approximated from a linear extrapolation of square absorption, α^2, to the point of interception with the photon energy axis (Fig. 5c). As shown in the inset of Fig. 5c, the extracted band gaps, E_g, for GaN epilayers grown at 930, 960 and 990 °C are 3.36, 3.39 and 3.38 eV, respectively. These values are slightly smaller than that of bulk GaN.

Although high crystalline quality GaN epilayers have been realized based on CO_2 LMOCVD, there are still some issues to address for the industrialization of GaN epilayer growth via LMOCVD technique. For instance, when compared with MOCVD and MBE techniques, the size of GaN samples grown by LMOCVD are relatively small due to the relatively small beam size (20 mm in diameter). By adding a beam expander, laser beams could be extended to cover the whole wafers as well as maintain the required laser fluence for GaN growth, based on which LMOCVD technique is feasible for wafer-scale GaN growth. However, further optimization and design improvement are still required to achieve GaN epi-structures with a homogeneous thickness and quality over the whole wafers. Overall, the CO_2 LMOCVD proposed in this work is a simple and low-cost method for fast and high-quality GaN epilayer growth, and might bring up a broad application in future electronics and optoelectronics.

Table 7.1 Summary of characteristics of the LMOCVD GaN epilayers grown on sapphire at different temperatures

No.	Temp. (°C)	RMS (nm)	Bandgap (eV)	E_{2H} (cm^{-1})	σ (Gpa)	(0002) FWHM (arcsec)	(10-12) FWHM (arcsec)	Dislocation density (cm^{-2})	Mobility (cm^2/vs)	Carrier concentration (cm^{-3})
I	930	1.103	3.36	568.7	0.26	396	471	8.1E8	226	8.4×10^{16}
II	960	1.253	3.39	571.5	0.82	324	443	6.6E8	293	5.3×10^{16}
III	990	1.892	3.38	570	0.47	313	390	5.9E8	369	3.1×10^{16}

7.4 Conclusions

In conclusion, we have demonstrated the rapid growth of high-quality GaN epilayers with an extremely high growth rate of ~ 25.8 μm/h via a CO_2 laser-assisted MOCVD method. It is found that the substrate temperature plays an important role in different aspects of GaN film growth, including morphology, structural evolution, electrical and optical properties. The surface morphology of LMOCVD GaN films demonstrates no degradation of the growth mode, maintaining a dislocation-mediated step-flow growth with RMS roughness of ~ 1.9 nm. For the GaN sample grown at 990 °C with high growth rates, the FWHM in rocking curve ω-scan for GaN (0002) line and (10-12) line are, 313 and 390 arcsec, respectively, suggesting its high purity and high crystalline quality. Raman measurement shows the presence of biaxial compressive stress in the as-grown GaN layers. These results demonstrate that LMOCVD technique can produce high-quality GaN epilayers with fast growth rates, opening a new pathway for nitride related materials fabrication used for next-generation electronics and optoelectronics.

7.5 References

1. Akasaki, I.; Amano, H., Breakthroughs in improving crystal quality of GaN and invention of the p–n junction blue-light-emitting diode. Japanese journal of applied physics 2006, 45 (12R), 9001.

2. Asif Khan, M.; Bhattarai, A.; Kuznia, J.; Olson, D., High electron mobility transistor based on a GaN‐Al x Ga1− x N heterojunction. Applied Physics Letters 1993, 63 (9), 1214-1215.

3. Ponce, F.; Bour, D., Nitride-based semiconductors for blue and green light-emitting devices. Nature 1997, 386 (6623), 351.

4. Liu, L.; Edgar, J. H., Substrates for gallium nitride epitaxy. Materials Science and Engineering: R: Reports 2002, 37 (3), 61-127.

5. Fujito, K.; Kubo, S.; Nagaoka, H.; Mochizuki, T.; Namita, H.; Nagao, S., Bulk GaN crystals grown by HVPE. Journal of Crystal Growth 2009, 311 (10), 3011-3014.

6. Hashimoto, T.; Wu, F.; Speck, J. S.; Nakamura, S., A GaN bulk crystal with improved structural quality grown by the ammonothermal method. Nature materials 2007, 6 (8), 568-571.

7. Yamane, H.; Shimada, M.; Clarke, S. J.; DiSalvo, F. J., Preparation of GaN single crystals using a Na flux. Chemistry of Materials 1997, 9 (2), 413-416.

8. Tarsa, E.; Heying, B.; Wu, X.; Fini, P.; DenBaars, S.; Speck, J., Homoepitaxial growth of GaN under Ga-stable and N-stable conditions by plasma-assisted molecular

beam epitaxy. Journal of Applied Physics 1997, 82 (11), 5472-5479.

9. Heying, B.; Averbeck, R.; Chen, L.; Haus, E.; Riechert, H.; Speck, J., Control of GaN surface morphologies using plasma-assisted molecular beam epitaxy. Journal of Applied Physics 2000, 88 (4), 1855-1860.

10. Boyd, A. R.; Degroote, S.; Leys, M.; Schulte, F.; Rockenfeller, O.; Luenenbuerger, M.; Germain, M.; Kaeppeler, J.; Heuken, M., Growth of GaN/AlGaN on 200 mm diameter silicon (111) wafers by MOCVD. physica status solidi (c) 2009, 6 (S2).

11. Nakamura, S.; Harada, Y.; Seno, M., Novel metalorganic chemical vapor deposition system for GaN growth. Applied Physics Letters 1991, 58 (18), 2021-2023.

12. Heikman, S.; Keller, S.; DenBaars, S. P.; Mishra, U. K., Growth of Fe doped semi-insulating GaN by metalorganic chemical vapor deposition. Applied Physics Letters 2002, 81 (3), 439-441.

13. Iga, R.; Sugiura, H.; Yamada, T., Selective growth of III-V semiconductor compounds by laser-assisted epitaxy. Semiconductor science and technology 1993, 8 (6), 1101.

14. Shinn, G. B.; Gillespie, P.; Wilson Jr, W.; Duncan, W. M., Laser‐assisted metalorganic chemical vapor deposition of zinc selenide epitaxial films. Applied Physics Letters 1989, 54 (24), 2440-2442.

15. Allen, S., Laser chemical vapor deposition: A technique for selective area deposition. Journal of Applied Physics 1981, 52 (11), 6501-6505.

16. Herman, I. P., Laser-assisted deposition of thin films from gas-phase and surface-adsorbed molecules. Chemical Reviews 1989, 89 (6), 1323-1357.

17. Duty, C.; Jean, D.; Lackey, W., Laser chemical vapour deposition: materials, modelling, and process control. International Materials Reviews 2001, 46 (6), 271-287.

18. Zhou, B.; Li, Z.; Tansley, T.; Butcher, K., Growth mechanisms in excimer laser photolytic deposition of gallium nitride at 500° C. Journal of crystal growth 1996, 160 (3-4), 201-206.

19. Iwanaga, T.; Hanabusa, M., CO2 laser CVD of disilane. Japanese Journal of Applied Physics 1984, 23 (7A), L473.

20. Thirugnanam, P.; Xiong, W.; Mahjouri-Samani, M.; Fan, L.; Raju, R.; Mitchell, M.; Gao, Y.; Krishnan, B.; Zhou, Y.; Jiang, L., Rapid growth of m-plane oriented gallium nitride nanoplates on silicon substrate using laser-assisted metal organic chemical vapor deposition. Crystal Growth & Design 2013, 13 (7), 3171-3176.

21. Besling, W.; Goossens, A.; Meester, B.; Schoonman, J., Laser-induced chemical vapor deposition of nanostructured silicon carbonitride thin films. Journal of applied physics 1998, 83 (1), 544-553.

22. Rabiee Golgir, H.; Gao, Y.; Zhou, Y. S.; Fan, L.; Thirugnanam, P.; Keramatnejad, K.; Jiang, L.; Silvain, J.-F. o.; Lu, Y. F., Low-Temperature Growth of Crystalline Gallium Nitride Films Using Vibrational Excitation of Ammonia Molecules in Laser-Assisted Metalorganic Chemical Vapor Deposition. Crystal Growth & Design 2014, 14 (12), 6248-6253.

23. Golgir, H. R.; Zhou, Y. S.; Li, D.; Keramatnejad, K.; Xiong, W.; Wang, M.; Jiang, L. J.; Huang, X.; Jiang, L.; Silvain, J. F., Resonant and nonresonant vibrational excitation of ammonia molecules in the growth of gallium nitride using laser-assisted metal organic chemical vapour deposition. Journal of Applied Physics 2016, 120 (10), 105303.

24. Lu, Y.; Golgir, H. R.; Zhou, Y., GROWTH OF NITRIDE FILMS. US Patent 20,160,340,783: 2016.

25. Meunier, M.; Flint, J.; Haggerty, J.; Adler, D., Laser‐induced chemical vapor deposition of hydrogenated amorphous silicon. I. Gas‐phase process model. Journal of applied physics 1987, 62 (7), 2812-2821.

26. Park, M.; Maria, J.-P.; Cuomo, J.; Chang, Y.; Muth, J.; Kolbas, R.; Nemanich, R.; Carlson, E.; Bumgarner, J., X-ray and Raman analyses of GaN produced by ultrahigh-rate magnetron sputter epitaxy. Applied physics letters 2002, 81 (10), 1797-1799.

27. Schiaber, Z. S.; Leite, D. M.; Bortoleto, J. R.; Lisboa-Filho, P. N.; da Silva, J. H., Effects of substrate temperature, substrate orientation, and energetic atomic collisions on the structure of GaN films grown by reactive sputtering. Journal of Applied Physics 2013, 114 (18), 183515.

28. Hao, M.; Ishikawa, H.; Egawa, T., Formation chemistry of high-density nanocraters on the surface of sapphire substrates with an in situ etching and growth mechanism of device-quality GaN films on the etched substrates. Applied physics letters 2004, 84 (20), 4041-4043.

29. Yadav, B. S.; Major, S.; Srinivasa, R., Growth and structure of sputtered gallium nitride films. Journal of Applied Physics 2007, 102 (7), 073516.

30. Lahreche, H.; Leroux, M.; Laügt, M.; Vaille, M.; Beaumont, B.; Gibart, P., Buffer free direct growth of GaN on 6H–SiC by metalorganic vapor phase epitaxy. Journal of Applied Physics 2000, 87 (1), 577-583.

31. Li, J.; Chen, Z.; Jiao, Q.; Feng, Y.; Jiang, S.; Chen, Y.; Yu, T.; Li, S.; Zhang, G., Silane controlled three dimensional GaN growth and recovery stages on a cone-shape nanoscale patterned sapphire substrate by MOCVD. CrystEngComm 2015, 17 (24), 4469-4474.

32. Gunning, B. P.; Clinton, E. A.; Merola, J. J.; Doolittle, W. A.; Bresnahan, R. C., Control of ion content and nitrogen species using a mixed chemistry plasma for GaN grown at extremely high growth rates> 9 μ m/h by plasma-assisted molecular beam epitaxy. Journal of Applied Physics 2015, 118 (15), 155302.

33. Gibart, P., Metal organic vapour phase epitaxy of GaN and lateral overgrowth. Reports on Progress in Physics 2004, 67 (5), 667.

34. Kim, J.; Bayram, C.; Park, H.; Cheng, C.-W.; Dimitrakopoulos, C.; Ott, J. A.; Reuter, K. B.; Bedell, S. W.; Sadana, D. K., Principle of direct van der Waals epitaxy of single-crystalline films on epitaxial graphene. Nature communications 2014, 5.

35. Motamedi, P.; Cadien, K., Structure–property relationship and interfacial phenomena in GaN grown on C-plane sapphire via plasma-enhanced atomic layer deposition. RSC Advances 2015, 5 (71), 57865-57874.

36. Moram, M.; Vickers, M., X-ray diffraction of III-nitrides. Reports on progress in physics 2009, 72 (3), 036502.

37. Collazo, R.; Mita, S.; Aleksov, A.; Schlesser, R.; Sitar, Z., Growth of Ga-and N-polar gallium nitride layers by metalorganic vapor phase epitaxy on sapphire wafers. Journal of crystal growth 2006, 287 (2), 586-590.

38. Kuball, M., Raman spectroscopy of GaN, AlGaN and AlN for process and growth monitoring/control. Surface and Interface Analysis 2001, 31 (10), 987-999.

39. Tripathy, S.; Chua, S.; Chen, P.; Miao, Z., Micro-Raman investigation of strain in GaN and Al x Ga 1− x N/GaN heterostructures grown on Si (111). Journal of Applied Physics 2002, 92 (7), 3503-3510.

40. Goni, A.; Siegle, H.; Syassen, K.; Thomsen, C.; Wagner, J.-M., Effect of pressure on optical phonon modes and transverse effective charges in GaN and AlN. Physical Review B 2001, 64 (3), 035205.

41. Ko, C.-H.; Chang, S.-J.; Su, Y.-K.; Lan, W.-H.; Chen, J. F.; Kuan, T.-M.; Huang, Y.-C.; Chiang, C.-I.; Webb, J.; Lin, W.-J., On the carrier concentration and Hall mobility in GaN epilayers. Japanese journal of applied physics 2002, 41 (3A), L226.

42. Meister, D.; Böhm, M.; Topf, M.; Kriegseis, W.; Burkhardt, W.; Dirnstorfer, I.; Rösel, S.; Farangis, B.; Meyer, B.; Hoffmann, A., A comparison of the Hall-effect and secondary ion mass spectroscopy on the shallow oxygen donor in unintentionally doped GaN films. Journal of Applied Physics 2000, 88 (4), 1811-1817.

43. Hwang, C.; Schurman, M.; Mayo, W.; Lu, Y.; Stall, R.; Salagaj, T., Effect of structural defects and chemical impurities on hall mobilities in low pressure MOCVD grown GaN. Journal of electronic materials 1997, 26 (3), 243-251.

44. Wang, T.; Shirahama, T.; Sun, H.; Wang, H.; Bai, J.; Sakai, S.; Misawa, H., Influence of buffer layer and growth temperature on the properties of an undoped GaN layer grown on sapphire substrate by metalorganic chemical vapor deposition. Applied Physics Letters 2000, 76 (16), 2220-2222.

45. Kordoš, P.; Javorka, P.; Morvic, M.; Betko, J.; Van Hove, J.; Wowchak, A.; Chow, P., Conductivity and Hall-effect in highly resistive GaN layers. Applied Physics Letters 2000, 76 (25), 3762-3764.

46. Klingshirn, C. F., Semiconductor optics. Springer Science & Business Media: 2012.

CHAPTER 8 BACK-TO-BACK SCHOTTKY METAL-SEMICONDUCTOR-METAL (MSM) PHOTODETECTOR ON LMOCVD-GROWN GAN FILMS

8.1 Introduction

In this chapter, the optical quality of as-grown GaN layers by CO_2 laser LMOCVD in chapter 7 are further evaluated by fabricating ultraviolet (UV) photodetector. The performance of GaN-based UV detectors is highly dependent on the crystallinity of GaN films.[1-4] It has been reported that threading dislocation has an adverse effect on the performance of GaN photodetectors, including dark current and responsivity.[1-4]

The GaN-based material system is appropriate for photodetection applications operated in the 200–365 nm wavelength range because of its tunable wide direct bandgap. In addition, nitride-based photodetectors also have the advantages of being solid-state and small in size, with good chemical and thermal stability, and having long lifetimes. GaN UV photodetectors have obtained increasing interest with various applications, such as flame monitoring, biomedicine, and UV astronomy.[5-7] These photodetectors are suitable for harsh environments with chemically inert properties.

GaN-based detectors with a variety of device structures, including Schottky-type [8-10], metal-semiconductor-metal (MSM)-type[1,2,11-13], and p–i–n type.[14–16] With a high response speed and low dark current characteristics, GaN MSM photodetector has attracted more attentions for UV photodetection applications as compared to GaN photodetectors with other device structures. Additionally, with no n- and p-type doped layers, GaN MSM device has simple fabrication processes (inset in Fig. 8.1).[17,18] Normally, MSM structures can use either back-to-back Schottky contacts or back-to-back ohmic contacts during photoconductive operation and cannot operate under 0 V bias.[1-3] Schottky contact photodetector is appropriate for applications with fast response speeds

and low dark current, while the ohmic contact photoconductor is suitable for high photosensitivity applications. Our devices in this chapter are Schottky-contact MSM-type detectors.

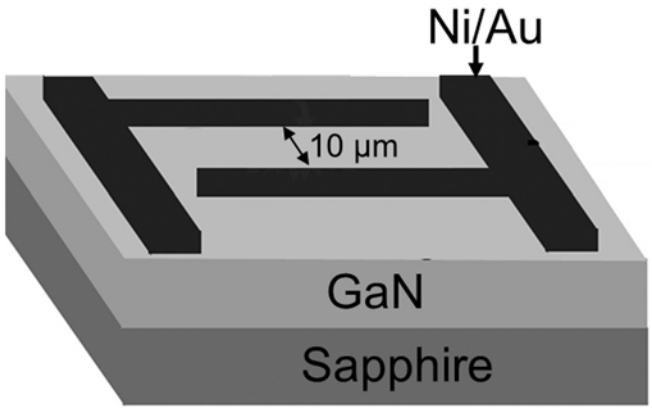

Figure 8.1. Schematic device structure of GaN MSM detector with Ni/Au contacts.

8.2 Experimental details: device fabrication and characterization

The undoped GaN epilayer used in our devices was grown on c-plane sapphire substrates at different temperatures 930, 960 and 990 °C by CO_2 laser MOCVD. The details of the crystal growth process have been reported in chapter 7. The sample was prepared before processing by first using standard solvent clean, then dipping in boiling aqua regia (3HCl : 1HCl) then buffered oxide etch (BOE) to remove any native oxide. GaN devices were fabricated using a standard photolithography: 1) patterning of photoresist, 2) deposition of Ni/Au (100 nm/20 nm) Schottky contact via magnetron sputtering, and 3) liftoff to form Schottky contacts (50 μm long, 10 μm wide with a spacing of 10 μm) on the GaN. Before electrical measurement, annealing treatment of GaN MSM devices was performed at 500 °C for 5 min in rapid thermal processing (RTP) furnace. The current-voltage (*I-V*) measurements of the GaN UV photodetectors were carried out using a Keithley 237 electrometer. Photoresponse measurements were

realized by using a Xe arc lamp with power of 150 W as UV light source. External quantum efficiency (EQE) measurement was performed by using an incident monochromatic light beam directed onto the photodetector and the data was collected via a Newport QE measurement kit. Transient response measurements were taken using a 337 nm, 4 ns pulsed laser as light source, and voltage variations were collected using an oscilloscope (LeCroy WaveRunner). All measurements were conducted at room temperature.

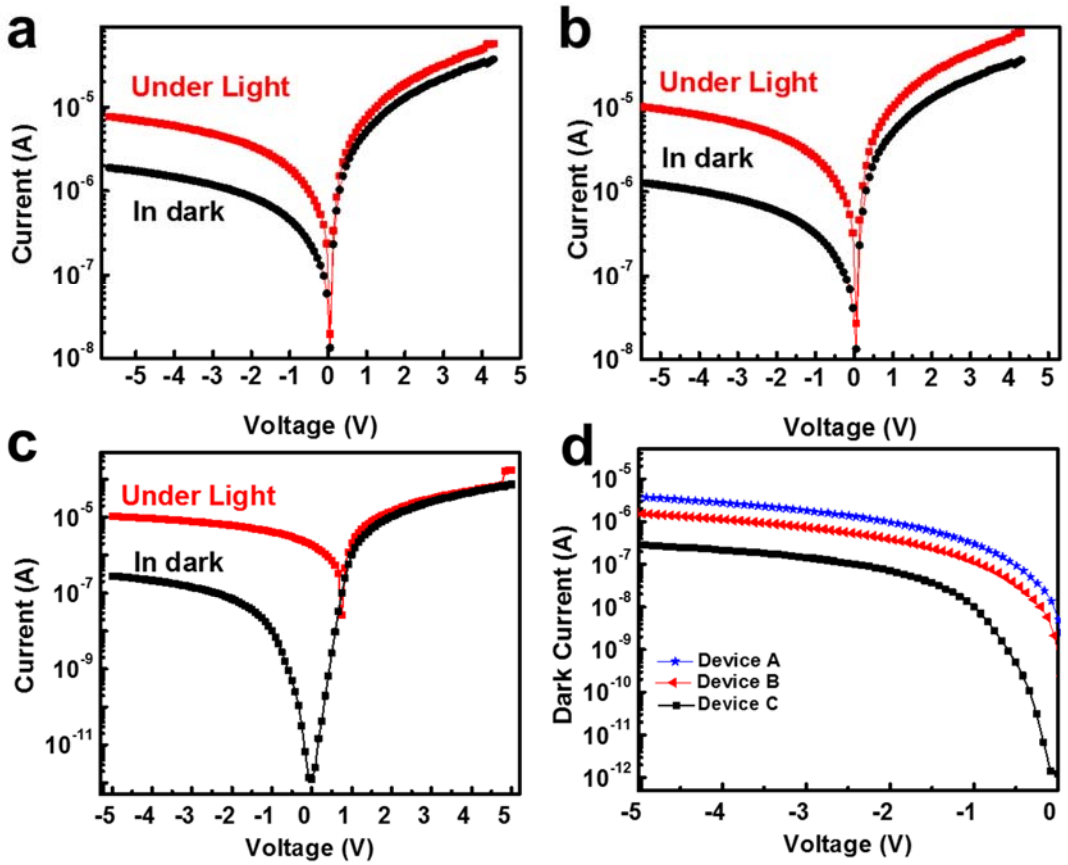

Figure 8.2. I-V curves of GaN MSM photodetectors fabricated on CO_2 laser LMOCVD GaN epilayers grown at (a) 930 (b) 960 and (c) 990 ^oC under light intensity of 0.1 mW cm^{-2} (red) and in dark (black). (d) Dark I-V characteristics of GaN detectors fabricated on GaN epilayers grown at different temperatures of 930 (device A), 960 (device B) and 990 ^oC (device C).

8.3 Results and discussion

Fig. 8.2 compares the current-voltage (I-V) characteristics of the MSM photodetector fabricated on CO_2 laser LMOCVD GaN epilayers grown at different substrate temperatures under light and in dark (light intensity ~ 0.1 mW cm^{-2}). The device dark currents were 1.96×10^{-6}, 1.3×10^{-6}, and 2×10^{-7} A at a bias voltage of -5 V and increased to 7.7×10^{-6}, 1.05×10^{-5}, and 1.2×10^{-5} A under light irradiation for GaN samples grown at 930, 960 and 990 ^{o}C, respectively, indicating a highly UV-sensitive photoconduction. The dark currents of devices are quite low like that of best GaN UV detectors reported previously with the same device structures.[1-4]

The dark current of MSM photodetectors was investigated, where they showing nearly symmetrical characteristics and for forward biases the dark current was almost the same, indicating that a good Schottky contact have been formed between the GaN epilayer and Ni/Au metal contact. However, the dark current values of the MSM photodetectors were different from one to another at given reverse biases. Fig. 8.2d displays the dark current of the three typical GaN-based MSM UV photodetector samples, A, B and C fabricated on LMOCVD GaN epilayers grown at different temperatures of 930, 960 and 990 ^{o}C, respectively. The dark current values of the three samples follows a sequence of C < B < A, which the lowest one is for the GaN sample grown at higher temperatures. Comparing the main parameters of the three samples as listed in Table 8.1, they have almost the same carrier concentrations but different dislocation densities, and both screw and edge dislocation densities of the samples are consistent with C < B < A. These results suggest that the lower dislocation densities are, then the lower the dark current is in the GaN MSM photodetectors. It has been reported that the dislocations are the paths of carrier

transportation and has a strong influence on the dark current of the GaN detectors.[3,4]

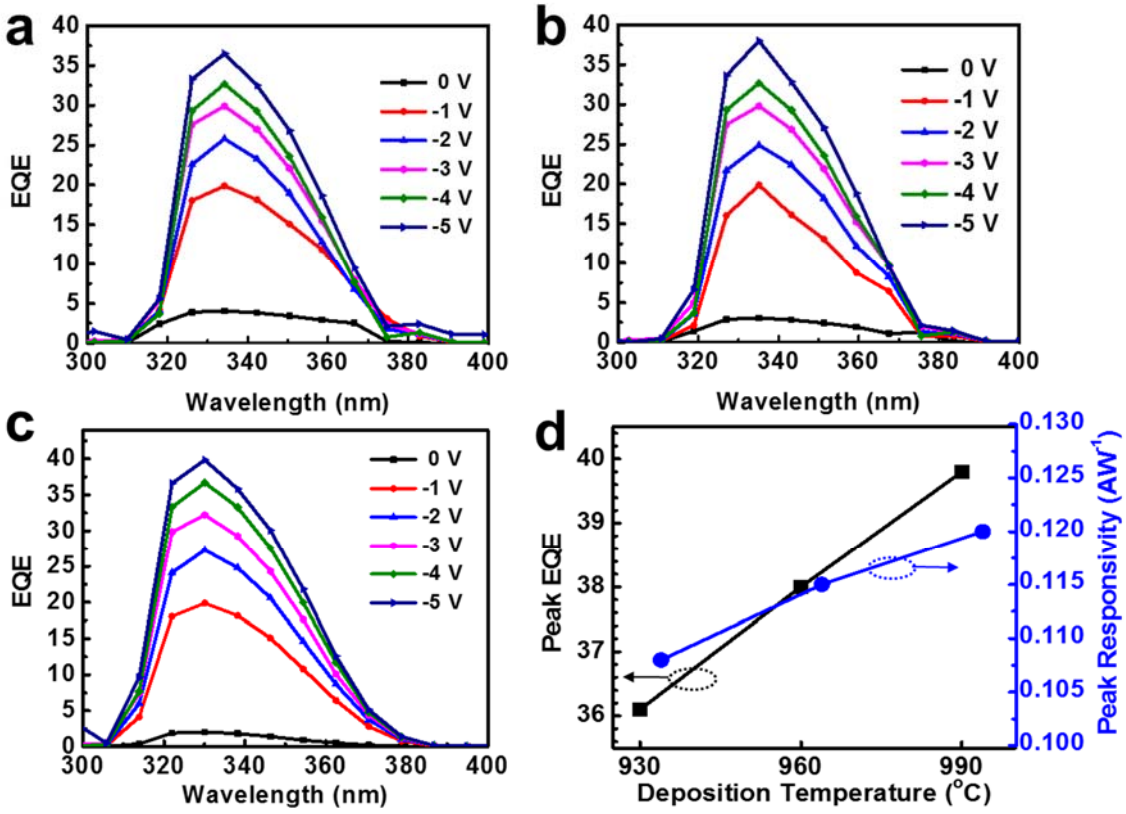

Figure 8.3. EQE spectra of GaN MSM photodetectors fabricated on CO_2 laser LMOCVD GaN epilayers grown at (a) 930 (b) 960 and (c) 990 ^{o}C under reverse bias from -5 to 0 V. (d) A comparison between peak EQE and responsivity of the detectors fabricated on GaN epilayers grown at different temperatures.

Fig. 8.3 shows the EQE of UV detectors measured at different reverse biases. The devices show a high sensitivity and high responsivity in the UV range that is near the band edge of GaN. However, EQE is quickly reduced with either decreasing or increasing wavelength, which is attributed to the increased electron-hole recombination and the reduced photo-penetration depth.[1-4] The EQEs are lower than 5 % at zero bias, and increase sharply with the increase in reverse bias and reach to 36, 38 and 40 % at a bias voltage of -5 V for photodetectors fabricated on LMOCVD GaN epilayers grown at 930,

960 and 990 ºC, respectively. The sharp increase of EQE versus reverse bias voltage corresponds to the rapid increase in photocurrent. The responsivity (R) of the device can be measured according to the following equation:[19]

$$R = \frac{EQE}{hc/\lambda}, \tag{8.1}$$

where h is the Planck's constant, c is the speed of light, and λ is the wavelength of light. The responsivity peak values of 0.108, 0.115, and 0.12 AW^{-1} were obtained at reverse bias voltage of 5 V for photodetectors fabricated on LMOCVD GaN epilayers grown at 930, 960 and 990 ºC, respectively. These values are comparable to that of commercial GaN UV photodetectors with value in the range of 0.1 to 0.2 AW^{-1}.[20,21] It is found the responsivity of the photodetectors decreases with increasing dislocation densities. The maximum responsivity is for the device fabricated on GaN epilayers grown at 990 ºC with lowest dislocation densities and highest crystalline quality.

According to the results in Table 8.1, the electron mobility of the three GaN samples grown at different temperatures are very different. The electron mobility of the undoped GaN epilayer decreases with the increase of the dislocation densities. Among the three undoped samples, the dislocation densities of sample C is the lowest and correspondingly the electron mobility is the highest. This phenomenon can be interpreted that the dislocation acts as charge defect traps in the GaN and these charge defect traps can increase the recombination probability of photogenerated electron-hole pairs and thus reduce the responsivity of GaN-based MSM photodetectors.[4] Additionally, since the photocurrent in these MSM photodetectors primarily comes from the drift current, the negatively charged scattering center may have a strong influence on the photogenerated

holes.[4] This may be another reason why the responsivity of the GaN-based MSM photodetectors becomes lower as dislocation density increases.

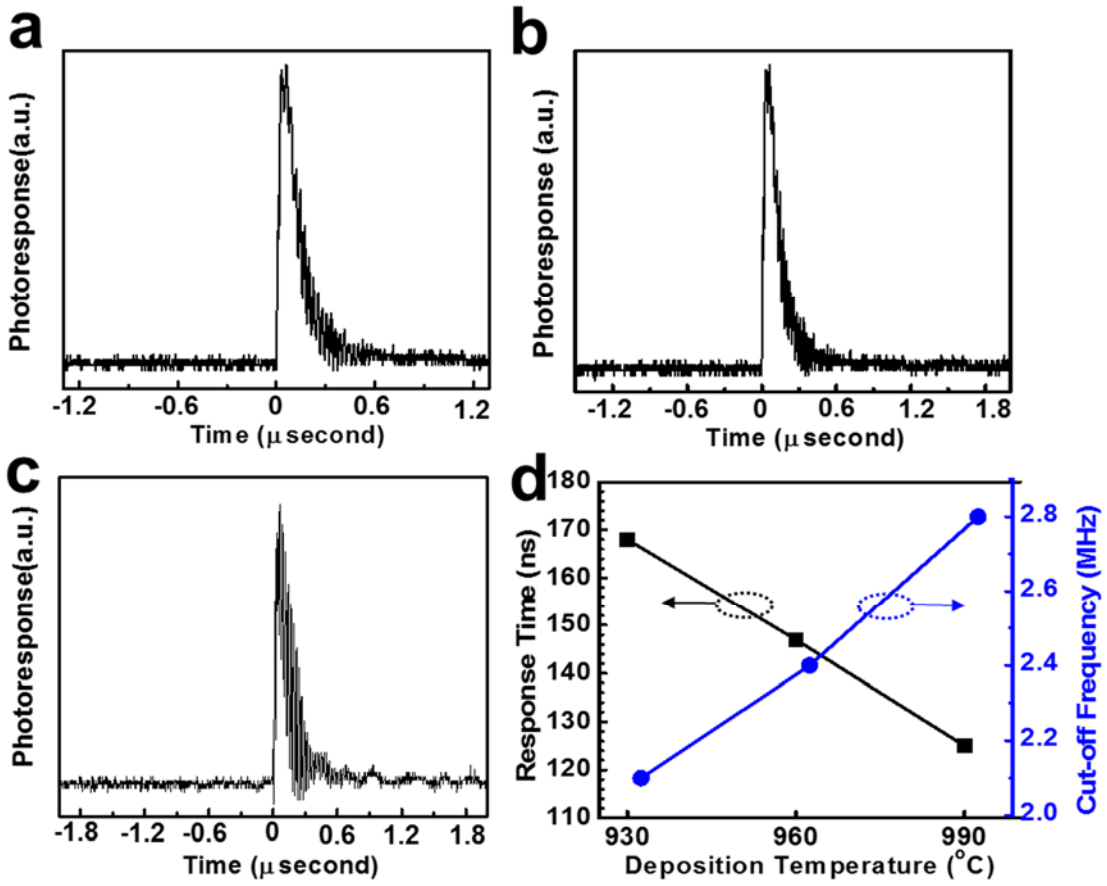

Figure 8.4 Typical transient photocurrent curve of GaN MSM photodetectors fabricated on CO_2 laser LMOCVD GaN epilayers grown at (a) 930 (b) 960 and (c) 990 ºC under reverse bias of -5 V measured with a 337 nm 4 ns-pulse laser as the light source. (d) A comparison between response time and cut-off frequency of the detectors fabricated on GaN epilayers grown at different temperatures.

Table 8.1 Summary of characteristics of MSM photodetectors fabricated on the LMOCVD GaN epilayers grown on sapphire at different temperatures.

Sample No	GaN Grown Temp. (ºC)	Bandgap (eV)	Dislocation density (cm^{-2})	Mobility (cm^2/vs)	Carrier concentration (cm^{-3})	Resistivity (mΩ-cm)	Dark Current (A)	Peak Responsivity (AW^{-1})	Response Time (ns)
A	930	3.36	8.1E8	220	8.4×10^{16}	19	1.96E-6	0.108	168
B	960	3.39	6.6E8	299	5.3×10^{16}	11	1.30E-6	0.115	147
C	990	3.38	5.9E8	365	3.1×10^{16}	9	0.20E-6	0.12	125

Finally, the response speed of the GaN UV photodetectors was measured by transient photocurrent method using a 337 nm pulsed laser with the pulse width less than 4 ns as the light source. Fig. 8.4 shows the response curves of the GaN photodetectors under a reverse bias voltage of -5 V. By fitting the photocurrent decay curve with the single exponential decay function, the response time of the devices was derived to be 168, 147 and 125 ns for photodetectors fabricated on LMOCVD GaN epilayers grown at 930, 960 and 990 ^{o}C, respectively, revealing a fast response speeds. It has been reported that the response time of the device should be limited by the resistor-capacitor time constant but not the GaN crystallinity or carrier mobility. Therefore, the theoretical charge transit time of the UV photodetector was evaluated using the equation below:[22,23]

$$t_e = \frac{L^2}{\mu_e V} \tag{8.2}$$

where μ_e is the carrier mobility, t_e is the charge transit time, L is the electrode gap spacing, and V is the applied bias. Based on the above equation, an increase in V leads to reduction of t_e, and thus the gain subsequently increases linearly. Using electron mobility measured for the GaN epilayers, L = 10 μm, and the applied voltage 5 V, the t_e was calculated to be 0.183, 0.134 and 0.11 ns, which was much lower than the measured response times of 168, 147 and 125 ns, respectively. The fastest response speed is for device fabricated on LMOCVD GaN epilayers grown 990 ^{o}C with highest crystalline quality and carrier mobility. Based on the measured response time of 125 ns, its 3-dB cut-off frequency (f_{3dB}) can be calculated by

$$f_{3dB} = \frac{0.35}{t_r}, \tag{8.3}$$ [22,23]

where t_r is the response time of the device. The 3-dB cut-off frequency of the UV GaN detectors were calculated to be 2.1, 2.4 and 2.8 MHz. Overall, the responsivity of 0.12 AW^{-1}, fast response time of 125 ns and 3-dB cut-off frequency of 2.8 MHz for the GaN UV detector are comparable to those of previously reported,[1-4] indicating the excellent optical properties of LMOCVD GaN layers grown with high growth rates.

8.4 Conclusions

In conclusion, we have reported the growth and characterization of back-to-back Schottky MSM UV photodetectors on LMOCVD-grown GaN films. The dark current, responsivity and, response speed of GaN UV detectors are comparable to those of commercial devices, indicating the excellent optical properties of LMOCVD GaN layers. We have also investigated the effect of GaN crystallinity and TDs on the property of GaN-based MSM photodetectors. It is found that the dark current of the GaN photodetectors increases with increasing TDs and the responsivity of the photodetectors decreases with increasing TDs. The best performance was obtained for device fabricated on LMOCVD GaN epilayers grown at 990 ^oC with highest crystalline quality and carrier mobility. Low dark current as low as 2×10^{-7} A and peak quantum efficiency as high as 40% was achieved at -5 V bias. The quantum efficiency showed a bias dependence, which are postulated to be due to the bias dependence of the depletion region width and corresponding electric field inside the space gap. Initial time-domain pulse response measurements show a 3-dB cut-off frequency of 2.8 MHz. These results demonstrate that LMOCVD technique can produce high-quality GaN epilayers with fast growth rates, opening a new pathway for nitride related materials fabrication used for next-generation electronics and optoelectronics.

8.5 References

1. Li, D.; Sun, X.; Song, H.; Li, Z.; Chen, Y.; Miao, G.; Jiang, H., Influence of threading dislocations on GaN-based metal-semiconductor-metal ultraviolet photodetectors. Applied Physics Letters 2011, 98 (1), 011108.

2. Sun, X.; Li, D.; Jiang, H.; Li, Z.; Song, H.; Chen, Y.; Miao, G., Improved performance of GaN metal-semiconductor-metal ultraviolet detectors by depositing SiO 2 nanoparticles on a GaN surface. Applied Physics Letters 2011, 98 (12), 121117.

3. Sun, X.; Li, D.; Li, Z.; Song, H.; Jiang, H.; Chen, Y.; Miao, G.; Zhang, Z., High spectral response of self-driven GaN-based detectors by controlling the contact barrier height. Scientific reports 2015, 5.

4. Wang, S.; Li, T.; Reifsnider, J.; Yang, B.; Collins, C.; Holmes, A.; Campbell, J., Schottky metal-semiconductor-metal photodetectors on GaN films grown on sapphire by molecular beam epitaxy. IEEE journal of quantum electronics 2000, 36 (11), 1262-1266.

5. Razeghi, M.; Rogalski, A., Semiconductor ultraviolet detectors. Journal of Applied Physics 1996, 79 (10), 7433-7473.

6. Ozbay, E.; Biyikli, N.; Kimukin, I.; Kartaloglu, T.; Tut, T.; Aytur, O., High-performance solar-blind photodetectors based on Al/sub x/Ga/sub 1-x/N heterostructures. IEEE Journal of selected topics in quantum electronics 2004, 10 (4), 742-751.

7. Pearton, S.; Zolper, J.; Shul, R.; Ren, F., GaN: Processing, defects, and devices. Journal of applied physics 1999, 86 (1), 1-78.

8. Chen, Q.; Yang, J.; Osinsky, A.; Gangopadhyay, S.; Lim, B.; Anwar, M.; Asif Khan, M.; Kuksenkov, D.; Temkin, H., Schottky barrier detectors on GaN for visible–blind ultraviolet detection. Applied Physics Letters 1997, 70 (17), 2277-2279.

9. Katz, O.; Garber, V.; Meyler, B.; Bahir, G.; Salzman, J., Anisotropy in detectivity of GaN Schottky ultraviolet detectors: Comparing lateral and vertical geometry. Applied physics letters 2002, 80 (3), 347-349.

10. Chang, P.-C.; Yu, C.; Chang, S.-J.; Lin, Y.; Wu, S., Low-noise and high-detectivity GaN UV photodiodes with a low-temperature AlN cap layer. IEEE Sensors Journal 2007, 7 (9), 1289-1292.

11. Li, J.; Xu, Y.; Hsiang, T.; Donaldson, W., Picosecond response of gallium-nitride metal–semiconductor–metal photodetectors. Applied physics letters 2004, 84 (12), 2091-2093.

12. Mosca, M.; Reverchon, J.-L.; Omnès, F.; Duboz, J.-Y., Effects of the buffer layers on the performance of (Al, Ga) N ultraviolet photodetectors. Journal of applied physics 2004, 95 (8), 4367-4370.

13. Pau, J.; Rivera, C.; Munoz, E.; Calleja, E.; Schühle, U.; Frayssinet, E.; Beaumont, B.; Faurie, J.; Gibart, P., Response of ultra-low dislocation density GaN photodetectors in the near-and vacuum-ultraviolet. Journal of applied physics 2004, 95 (12), 8275-8279.

14. Chen, M.; Sheu, J.-K.; Lee, M.-L.; Kao, C.; Chi, G.-C., Planar GaN p-i-n photodiodes with n+-conductive channel formed by Si implantation. Applied physics letters 2006, 88 (20), 203508.

15. Butun, B.; Tut, T.; Ulker, E.; Yelboga, T.; Ozbay, E., High-performance visible-blind GaN-based p-i-n photodetectors. Applied Physics Letters 2008, 92 (3), 033507.

16. Wang, X.; Hu, W.; Pan, M.; Hou, L.; Xie, W.; Xu, J.; Li, X.; Chen, X.; Lu, W., Study of gain and photoresponse characteristics for back-illuminated separate absorption and multiplication GaN avalanche photodiodes. Journal of Applied Physics 2014, 115 (1), 013103.

17. Carrano, J.; Grudowski, P.; Eiting, C.; Dupuis, R.; Campbell, J., Very low dark current metal–semiconductor–metal ultraviolet photodetectors fabricated on single-crystal GaN epitaxial layers. Applied physics letters 1997, 70 (15), 1992-1994.

18. Walker, D.; Monroy, E.; Kung, P.; Wu, J.; Hamilton, M.; Sanchez, F.; Diaz, J.; Razeghi, M., High-speed, low-noise metal–semiconductor–metal ultraviolet photodetectors based on GaN. Applied physics letters 1999, 74 (5), 762-764.

19. Guo, F.; Xiao, Z.; Huang, J., Fullerene Photodetectors with a Linear Dynamic Range of 90 dB Enabled by a Cross‐Linkable Buffer Layer. Advanced Optical Materials 2013, 1 (4), 289-294.

20. Monroy, E.; Omnès, F.; Calle, F., Wide-bandgap semiconductor ultraviolet photodetectors. Semiconductor Science and Technology 2003, 18 (4), R33.

21. Guo, F.; Yang, B.; Yuan, Y.; Xiao, Z.; Dong, Q.; Bi, Y.; Huang, J., A nanocomposite ultraviolet photodetector based on interfacial trap-controlled charge injection. Nature nanotechnology 2012, 7 (12), 798-802.

22. Fang, Y.; Huang, J., Resolving Weak Light of Sub‐picowatt per Square Centimeter by Hybrid Perovskite Photodetectors Enabled by Noise Reduction. Advanced Materials 2015, 27 (17), 2804-2810.

23. Marks, R.; Halls, J.; Bradley, D.; Friend, R.; Holmes, A., The photovoltaic response in poly (p-phenylene vinylene) thin-film devices. Journal of Physics: Condensed Matter 1994, 6 (7), 1379.

CHAPTER 9 SUMMARY AND FUTURE DIRECTIONS

9.1 Summary

This dissertation mainly focused on laser incorporation in metal organic chemical vapor deposition of gallium nitride films, which led to: 1) rapid growth of m-plane gallium nitride nanoplates 2) promotion of energy coupling efficiency and enhancement of gallium nitride deposition; 3) low-temperature growth of gallium nitride films; 4) fast growth of gallium nitride epilayers; and 5) realization of ultraviolet photodetectors based on the as-grown gallium nitride layers. Infrared-laser excitations of precursor molecules were used to assist the conventional MOCVD for promoting the GaN growth. In this dissertation, the different irradiation geometries were employed in LMOCVD growth of GaN. With a perpendicular laser-beam irradiation, the gas was excited and the substrate surface was heated up. While, with a parallel incidence related to the substrate surface, lasers permit pure gas-phase excitations, leaving the substrate cold.

The interlinked m-plane-oriented GaN nanoplates were rapidly grown on Si substrates using the LMOCVD method in perpendicular irradiation geometries. The FESEM and HRTEM images confirmed the formation of m-plane GaN nanoplates. The growth direction of GaN nanoplates was found to be the direction <10-10>. The A_1 (TO) mode of Raman further confirmed the m-plane orientation of the GaN nanoplates. The high deposition rate, low-growth temperature, and repeated growth on the different facets of the nanoplates resulted in the formation of m-plane-oriented interlinked GaN nanoplates. Therefore, the L-MOCVD is a suitable technique for the rapid growth of m-plane-oriented GaN nanoplates on Si substrate at low-growth temperatures.

Vibrational excitations of NH_3 molecules were studied using a tunable CO_2 laser in growing crystalline GaN films on Si (100) substrates. The resonant vibrational

excitation at 9.219, 10.350, and 10.719 μm were more efficient than nonresonant excitation in dissociating NH_3 molecules and enhancing the GaN deposition rate and quality. The OES results showed the resonant excitation of the NH-wagging modes modifies the synthesis process in a way that increases the supplies of NH, NH_2, N, N^+, and H. This leads to the enhancement in GaN deposition rates and improvement in crystalline quality. The extremely high GaN growth rate of ~ 84 μm/h with an improved crystalline quality was achieved under the resonant excitation at 9.219 μm. The red-shift in the position of E_{2H} of Raman spectra indicated that the GaN films grown on Si suffered from tensile stress and the films grown at laser wavelengths of 9.219 μm exhibited the lowest stress. The FWHM value of the XRD rocking curves of GaN (0002) and GaN (10-12) diffraction peaks decreased at resonant depositions and reached its minimum values at 9.219 μm, indicating reduced TDs density.

The LMOCVD technique was developed for low-temperature growth of GaN films on sapphire substrates through laser resonant vibrational excitation of NH_3 molecules. With a parallel incidence related to the substrate surface, lasers permit gas-phase excitations and precursor disassociations, leaving the substrate temperature very low. The highly c-oriented GaN films were successfully grown at temperatures as low as 250 ^oC. Low-temperature growth of GaN films is ascribed to the enhanced decomposition efficiency of NH_3 with resonant excitation of rotational-vibrational transition (1084.71 cm^{-1}) of the NH-wagging mode at the laser wavelength of 9.219 μm. The FWHM of (0002) diffraction peaks obtained from XRD for GaN films grown at 600 ^oC decreased from 0.20^o (MOCVD) to 0.18^o (LMOCVD), indicating an improvement in crystalline quality by LMOCVD. SEM images showed that the laser resonant vibrational excitation

of NH_3 helped to grow GaN films with smooth and uniform surface morphology. A high GaN growth rate of up to 12 μm/h was achieved at 600 ^oC by LMOCVD, which is ~4.6 times faster than that of conventional MOCVD with 2.6 μm/h.

We have demonstrated the fast growth of high-quality GaN epilayers with an extremely high growth rate of ~ 25.8 μm/h using the CO_2 laser LMOCVD method in a perpendicular irradiation geometry. It is found that the substrate temperature plays an important role in different aspects of GaN film growth, including morphology, structural evolution, electrical and optical properties. The surface morphology of LMOCVD GaN films demonstrates no degradation of the growth mode, maintaining a dislocation-mediated step-flow growth with RMS roughness of ~ 1.9 nm. For the GaN samples grown at 990 °C with high growth rates, the FWHM in rocking curve ω-scan for the GaN (0002) line and (10-12) lines are 313 and 390 arcsec, respectively, suggesting the high purity and high crystalline quality. Raman measurement shows the presence of biaxial compressive stress in the as-grown GaN layers. We have also fabricated UV photodetectors based on the as-grown GaN layers, which exhibit a high responsivity of 0.12 AW^{-1} and a fast response time of 125 ns, indicating the excellent optical properties of GaN layers. These results demonstrate that LMOCVD technique can produce high-quality GaN epilayers with fast growth rates, opening a new pathway for nitride related material fabrication used for next-generation electronics and optoelectronics.

9.2 Future directions

9.2.1 Investigation of the unexplored photocatalytic mechanism in 2D/3D graphene-MoS_2 ($MoSe_2$)-GaN heterostructure photocatalysts for stable water splitting and hydrogen (H_2) generation

H_2 is a major energy carrier in future, which can provide high combustion heat. The industrial production of H_2 is achieved by steam reforming of methane and water, in which the byproduct is carbon dioxide as greenhouse gas.[1-4] Since, sunlight and water as clean and renewable are most abundant energy source and natural resource, respectively, the production of H_2 via photocatalytic water splitting has been considered as one of the key sustainable energy technologies to enable storable and affordable energy for future generations and an ideal solution to counter the depletion and environmental problems of fossil fuels.[1-4]

Photocatalytic water splitting and H_2 production system involves three fundamental processes: photon absorption of photocatalytic semiconductor with bandgap higher than 1.23 eV to generate electron-hole pairs, charge separation and migration of photogenerated carriers to surface, and surface reduction and oxidization of water by photoelectrons and holes, respectively. Considering the requirements for efficient light absorption and photogenerated carrier separation and transfer, photocatalytic semiconductors preferably should have high surface area, good crystallinity and stability, and a suitable band structure.[5,6]

Currently, photocatalytic semiconductors are metal oxides, nitrides, or sulfides, such as titanium oxide (TiO_2), carbon nitride (C_3N_4) and cadmium sulfide (CdS).[7-9] Most of photocatalysts require the loading of a high-cost co-catalyst such as Pt, Rh, and RuO_2 to

obtain a good activity.[10] On the other hand, various photocatalysts including inorganic sulfide same as CdS and (oxy) nitride-based photocatalysts are less stable and more susceptible to oxidation than water and show poor stability.[11] Wide band-gap materials including TiO_2 is the most commonly used photocatalyst due to its exceptional stability to exposure to sunlight and electrolyte. However, indirect and large band gap of 3.2 eV severely limit absorption of most solar spectrum and generation of electron-hole pairs and catalysts suffer from low quantum efficiency (QE) in the visible range with low solar to hydrogen (STH) efficiencies. Moreover, despite progress in the past decade, photocatalytic semiconductors that can harvest visible light typically do not exhibit good activity.[12,13] The STH efficiency of photocatalytic water-splitting devices is still low around 1% and far from 10% STH, which allows achievement of the DOE price target for H_2 production.[14,15]

Recently, the emerging two-dimensional (2D) nanosheets and layered materials hold a high potential to address the existing challenges in the potocatalysts. Due to their unique physicochemical properties, 2D material as photocatalysts and co-catalysts are expected to offer fascinating features such as high specific surface areas, high stability, better charge carrier separation, and abundant surface active sites. Moreover, graphene is an excellent sunlight absorber, achieving 2.3% visible light absorbance in just 3.3 Å thickness and TMD monolayers including MoS_2 and $MoSe_2$ can absorb up to 10% incident sunlight in a thickness of less than 1 nm.[16,17] Graphene could function as an efficient and cost-effective cocatalyst to promote electron separation and transfer from semiconductor catalysts and catalyze the proton reduction on its surface. Molybdenum disulfide (MoS_2) with a layered structure and band gap of 1.9 eV has been investigated as

a promising potocatalyst for H_2 evolution under visible light irradiation. Moreover, the significant enhancement of the photocatalytic H_2 production activity of CdS and TiO_2 by loading MoS_2 layers as cocatalyst were recently reported opening new insights into high-performance cost-effective photocatalyst based on 2D materials.

On the other hand, Gallium nitride (GaN) has received much interest for use in the photocatalyst as it offers several advantages.[18,19] It is resistive to chemical corrosion during an electrochemical process and its direct band structure straddles with water redox potentials. The photocatalytic activity of p-type GaN photocatalyst has been reported and can reach to 1525.0 μmol h^{-1} H_2 evolution rate, with a 1.8% STH efficiency under light incident in the UV wavelength range which is much higher than that of previously reported photocatalyst materials even in visible light range. However, with a large band gap of 3.4 eV, GaN only absorbs UV light which is about 4% of the solar spectrum. The integration of GaN and 2D semiconductors including MoS_2 and (molybdenum selenide) $MoSe_2$ is anticipated to extend the light absorption in visible range and significantly enhance charge separation, photocatalytic efficiency and long-term stability. Thus, it is strategically important to explore the water splitting mechanism in unexplored MoS_2 ($MoSe_2$)/GaN heterostructures and develop 2D/3D photocatalysts suitable for stable H_2 production.

9.2.1.1 Growth of large-scale MoS_2 ($MoSe_2$)/GaN heterostructures

The growth of 2D materials on semiconductor substrates and formation of large-scale MoS_2 ($MoSe_2$)/GaN heterostructures is still limited. In this task, a scalable, cost-effective synthesis method will be investigated to grow MoS_2 ($MoSe_2$)/GaN 2D/3D heterostructures through RTP process. Our previous studies demonstrated fast growth of

high-quality c-plane GaN films on various substrates by LMOCVD, as discussed in chapter 8. In this subtask, the objective is to form 2D/3D heterostructures based on the epitaxially grown MoS_2 ($MoSe_2$) on GaN films. The MoS_2 ($MoSe_2$)/GaN heterostructures are a lattice matched system, unlike most reported epitaxial 2D/2D and 2D/3D heterostructures to date. The Mo film of particular thickness will be deposited on cleaned GaN films for the controlled MoS_2 ($MoSe_2$) synthesis in a single-step RTP process. Then, Mo films will be directly sulfurized (selenidized) in the RTP furnace in an Ar/S atmosphere. The critical parameters, including heating time, temperature, heating rate, and cooling rate, will be systemically studied to achieve large-scale MoS_2 ($MoSe_2$) synthesis with controlled layer numbers. Compared with the mechanical transferring method, the direct synthesis of 2D MoS_2 ($MoSe_2$) on GaN via the RTP method will be much more cost-effective. Moreover, by tuning the deposition thickness of Mo films prior to the RTP step, the final layer numbers of MoS_2 ($MoSe_2$) films will be precisely controlled. Due to a very small lattice mismatch of 0.8% (3%) the lattice parameter of GaN and layer MoS_2 ($MoSe_2$), an intimate contact will be formed between MoS_2 ($MoSe_2$) and GaN.

9.2.1.2 Investigation of photocatalytic water-splitting and H_2 production mechanism in 2D/3D heterostructures

In this task, heterostructure interfaces between the GaN films and layers MoS_2 ($MoSe_2$) are studied using ab-initio calculations. By comparing the lattice mismatch along crystallographic orientations, it is found that the mismatch is quite small between layer MoS_2 ($MoSe_2$) and GaN and an intimate contact with excellent charge transport in vertical direction is predicted. The effects of junction on the charge separation properties

of MoS_2 ($MoSe_2$)/GaN semiconductor heterostructures will be theoretically determined. Several physical mechanisms that need to be modelled in order to understand and predict the behaviour of such heterostructures for photocatalysis;[14] the relative positions of the band edges of materials, which determine the band offsets; the electronic structure of materials (density of states), which provide information on the charge separation properties of photocatalysts such as electron and hole mobility and information on the alignment of bands and the magnitude and effects of any interface dipoles.

To accurately determine the band offsets of semiconductor heterojunctions, the calculations will be directly done by modelling of periodic heterojunctions and construction of a supercell MoS_2 ($MoSe_2$)/GaN heterostructure. The ab-initio calculations will be performed based on the density functional theory (DFT) with the generalized gradient approximation (GGA, in the PBE version[20]) in the plane-wave basis code Quantum ESPRESSO Simulation Package.[21]

Additionally, a systematic experimental investigation will be conducted to unveil the photocatalytic mechanism in a MoS_2 ($MoSe_2$)/GaN heterostructures. Similar to the proposed mechanism for photocatalytic H_2 production from conventional photocatalysts, under the excitation of light, photo-induced electrons and holes were produced in the conduction band and valance band of both GaN, and MoS_2 ($MoSe_2$) semiconductors. GaN absorbs only UV light because of its wide band gap. Due to its direct band gap, photo electron-hole pairs generate easily. There are three ways to consume photo-induced electrons: (a) recombine with holes inside the material (b) recombine with spices on particle surface (surface recombination); (c) react with protons to produce H_2. The

recombination of the photo-induced electrons and holes resulted in low photocatalytic water-splitting and H_2 production activity.

When MoS_2 ($MoSe_2$) layers are synthesized on the surface of GaN with RTP process, vertical heterojunction with an intimate contact with high charge transfer properties between MoS_2 ($MoSe_2$) and GaN semiconductors are formed.[22] The band positions of the p-type GaN and MoS_2 ($MoSe_2$) are appropriate as shown in Fig. 9.3, photo-induced electrons produced in GaN conduction band transferred to MoS_2 conduction band. Therefore, recombination possibility of electron-hole pairs will decrease and more electrons can be used to produce H_2. Moreover, single layer MoS_2 serves as an ideal candidate for an efficient photocatalyst powering the visible sunlight-driven photocatalytic water splitting reaction. While, the absorption edge of GaN falls in the UV region, with small band gap of MoS_2 ($MoSe_2$) ($E_{g(MoS2)} \sim 1.89$ eV, $E_{g(MoSe2)} \sim 1.4$ eV), the MoS_2($MoSe_2$) can absorb more than 10% of solar light and MoS_2 ($MoSe_2$)/GaN heterostuctures can absorb most of solar light including UV and visible lights. A broader absorption of the solar energy spectrum will highly improve photocatalytic activity.

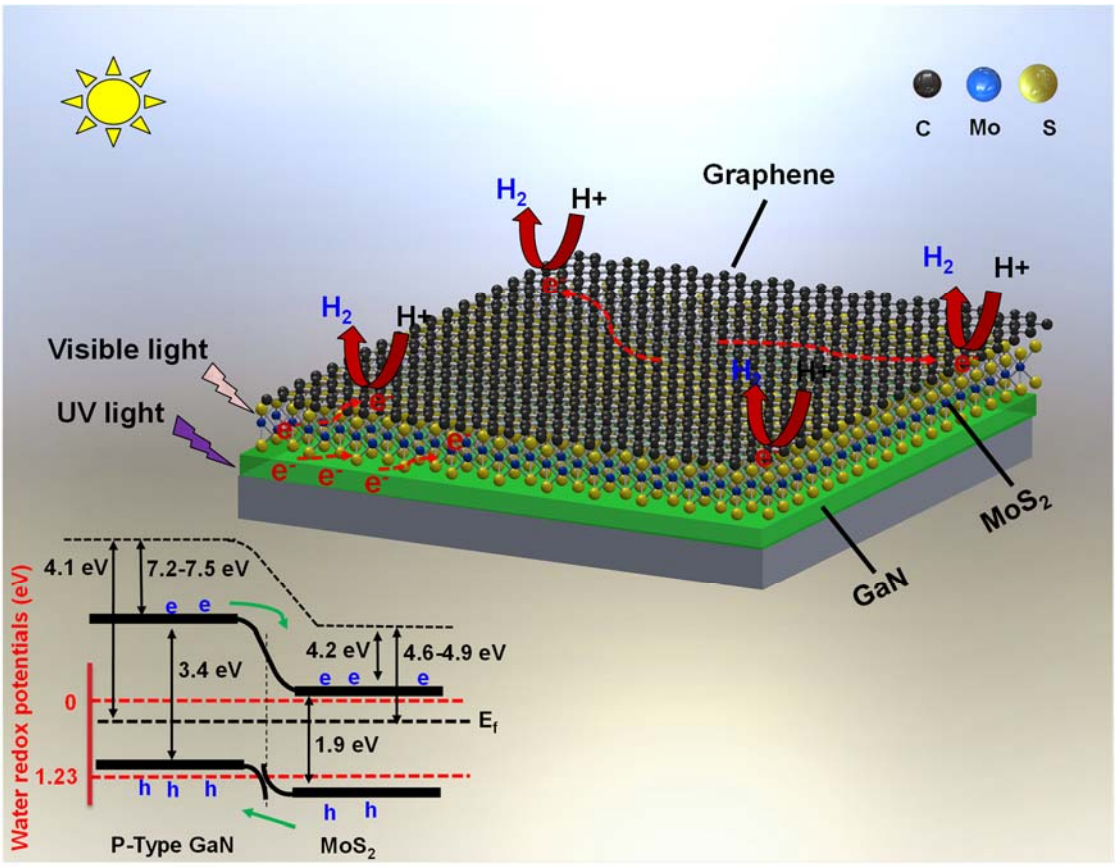

Figure 9.1. Proposed mechanism for photocatalytic water splitting in MoS_2 ($MoSe_2$)/GaN 2D/3D heterostructures with graphene layers as cocatalyst.

Previous computational and experimental results confirmed the high activity of adsorbed H+ ions of unsaturated active S atoms on exposed edge of MoS_2 ($MoSe_2$). Therefore, the photogenerated electrons could directly react with H+ ions to form H_2. However, active catalytic sites of layered MoS_2 ($MoSe_2$) crystals are located at the sulfur edge (Fig. 9.1), while basal planes are catalytically inert. The electrical conductivity and activity for photocatalytic H_2 production can be improved through decreasing the MoS_2 ($MoSe_2$) layers and adding other conducting materials.

The advantageous material properties of graphene, including large exposed area (2630 m^2 g^{-1}, calculated value), high charge mobility (200,000 cm^2 V^{-1} s^{-1}), and high mechanical

and chemical strength, make graphene a promising candidate not only to replace traditional co-catalysts but also to improve the stability of catalyst underlayers. It is a widely held belief that graphene can quickly separate and transfer photo-generated electrons from the conduction band of photocatalysts. Under UV-visible light, the photogenerated electrons of GaN are excited and transferred to the MoS_2 surface. Some of the electrons approaching the edge of MoS_2 ($MoSe_2$) are directly reacted with adsorbed H+ in H_2O to produce H_2 under the catalytic activities of unsaturated active S atoms, which can accept electrons and act as active sites for H_2 production. Other electrons on the MoS_2 ($MoSe_2$) basal planes, which have no catalytic activity, can be transferred to the edge of MoS_2 ($MoSe_2$) through the graphene sheets and then react with adsorbed H+ at the edges or graphene surface to form H_2 (see Fig. 9.1). Therefore, in this task, graphene will be chosen as co-catalyst to further enhance the catalytic efficiency and stability of MoS_2 ($MoSe_2$) /GaN for H_2 reduction.

9.2.1.3 Characterization of the performance of photocatalytic water splitting and H_2 production of proposed heterostructures

Micro Raman spectroscopy in aqueous environment will be applied to microscopically investigate the stability of MoS_2 ($MoSe_2$)/GaN under photocatalytic conditions, respectively. The photodegradation process can be monitored in situ by real-time Raman (Renishaw InVia Reflection) utilizing the irradiation laser. The diffuse reflectance spectra of the GaN and MoS_2 ($MoSe_2$)/GaN samples will be recorded on a UV-visible spectrophotometer (UV-2500PC; Shimadzu Corp., Japan) and the absorption spectra will be obtained from the reflectance spectra. The range of light absorption plays a very important role in photocatalysis. To understand the interaction between GaN and MoS_2

($MoSe_2$), X-ray photoelectron spectroscopy (XPS) measurement (XPS, Thermo Scientific, ESCALAB 250Xi) will be also carried out to investigate the surface composition and the electronic states of the catalysts (GaN, MoS_2 ($MoSe_2$), MoS_2 ($MoSe_2$) /GaN, and Graphene/MoS_2/GaN). Photoelectrochemical activity measurements including cyclic voltammetry and stability will be carried out using a three electrodes configuration on a CHI 760D (Shanghai Chenhua, China) electrochemical workstation. Therefore, both high-resolution AFM (Bruker Dimension ICON SPM) and cross-sectional TEM (Hitachi H7500 transmission electron microscope) will be used to observe the morphological and interfacial contact of the photcatalyst structures under photocatalytic conditions, with an aim to verify the proposed interfacial photocatalytic water splitting mechanism.

The H_2 evolution of photocatalytic heterostructure devices will be separately carried out with samples suspended in an appropriate amount of different aqueous solutions in a Pyrex glass reaction cell and the reaction cell will be connected to a gas-closed system with a gas-circulated pump. A 300 W xenon (Xe) lamp is used as light source to generate visible ($\lambda > 420$ nm) and UV lights with different long-pass filters. The evolved H_2 was analyzed using an online gas chromatograph (GC-8A, Shimadzu Co., Japan) equipped with a thermal conductivity detector. The apparent quantum yield (AQY) and STH conversion efficiency i.e ECE (energy conversion efficiency) will be measured by applying a Xe lamp (300 W). The number of incident photons was measured using a radiant power energy meter (Ushio spectroradiometer, USR-40). The AQY and STH will be calculated using the following equations:

$$AQY\ (\%) = \frac{4 \times Number\ of\ evolved\ H2\ molecules}{\text{Number of incident photons}} \times 100, \quad (1)$$

$$STH\ (\%) = \frac{\mathrm{R(H2)} \times \Delta\mathrm{Gr}}{\mathrm{P} \times \mathrm{S}} \times 10, \quad (2)$$

Where $R(H_2)$, ΔGr, P and S denote the rate of H_2 evolution during the water splitting reaction, the reaction Gibbs energy of the water splitting reaction, the energy intensity of the AM1.5G solar irradiation and the irradiated sample area, respectively.

9.3 References

1. Luo, B.; Liu, G.; Wang, L. Recent advances in 2D materials for photocatalysis. Nanoscale 2016, 8,6904-20.

2. Chen. X.; Shen, S.; Guo, L.; Mao, SS. Semiconductor-based photocatalytic hydrogen generation. Chemical reviews 2010, 110, 6503-70.

3. Kärkäs, MD.; Verho, O.; Johnston, EV.; Åkermark, B. Artificial photosynthesis: molecular systems for catalytic water oxidation. Chemical Reviews 2014, 114,11863-2001.

4. Rahman. MZ, Kwong CW, Davey K, Qiao SZ. Correction: 2D phosphorene as a water splitting photocatalyst: fundamentals to applications. Energy & Environmental Science 2016, 9, 1513-4.

5. Walter, MG.; Warren, EL.; McKone, JR.; Boettcher, SW.; Mi, Q.; Santori, EA.; Lewis, NS. Solar water splitting cells. Chemical reviews 2010, 110, 6446-73.

6. Zhao, Z.; Sun, Y.; Dong, F. Graphitic carbon nitride based nanocomposites: a review. Nanoscale 2015,7, 15-37.

7. Chen, X.; Liu, L.; Peter, YY.; Mao, SS. Increasing solar absorption for photocatalysis with black hydrogenated titanium dioxide nanocrystals. Science 2011, 331,746-50.

8. Li, Q; Guo, B.; Yu, J.; Ran, J.; Zhang, B.; Yan, H.; Gong, JR. Highly efficient visible-light-driven photocatalytic hydrogen production of CdS-cluster-decorated

graphene nanosheets. Journal of the American Chemical Society 2011, 133, 10878-84.

9. Zou, X.; Zhang, Y. Noble metal-free hydrogen evolution catalysts for water splitting. Chemical Society Reviews 2015, 44, 5148-80.

10. Maeda, K. Z-scheme water splitting using two different semiconductor photocatalysts. ACS Catalysis 2013, 3, 1486-503.

11. Zou, Z.; Ye, J.; Sayama, K.; Arakawa, H. Direct splitting of water under visible light irradiation with an oxide semiconductor photocatalyst. Nature. 2001, 414, 625-7.

12. Wang, X.; Maeda, K.; Thomas, A.; Takanabe, K.; Xin, G.; Carlsson, JM.; Domen, K.; Antonietti M. A metal-free polymeric photocatalyst for hydrogen production from water under visible light. Nature materials 2009, 8, 76-80.

13. Moniz. SJ.; Shevlin, SA.; Martin, DJ.; Guo, ZX.; Tang, J. Visible-light driven heterojunction photocatalysts for water splitting–a critical review. Energy & Environmental Science 2015, 8,731-59.

14. Muradov, NZ.; Veziroğlu, TN. “Green” path from fossil-based to hydrogen economy: an overview of carbon-neutral technologies. International Journal of Hydrogen Energy 2008, 33, 6804-39.

15. Bernardi, M.; Palummo, M.; Grossman, J.C. Extraordinary sunlight absorption and one nanometer thick photovoltaics using two-dimensional monolayer materials. Nano letters 2013, 13(8), 3664-3670.

16. Chen, Z.; Liu, H.; Chen, X.;Chu, G.; Chu, S.; Zhang, H. Wafer-size and single-

crystal MoSe2 atomically thin films grown on GaN substrate for light emission and harvesting. ACS Applied Materials & Interfaces 2016, 8(31), 20267-20273.

17. Kibria, MG.; Chowdhury, FA.; Zhao, S.; AlOtaibi, B.; Trudeau, ML.; Guo, H.; Mi, Z. Visible light-driven efficient overall water splitting using p-type metal-nitride nanowire arrays. Nature communications 2015, 9, 6.

18. Wang, D.; Pierre, A.; Kibria, MG.; Cui, K.; Han, X.; Bevan, KH.; Guo, H.; Paradis, S.; Hakima, AR.; Mi, Z. Wafer-level photocatalytic water splitting on GaN nanowire arrays grown by molecular beam epitaxy. Nano letters 2011,11, 2353-7.

19. Perdew, J.P.; Burke, K.; Ernzerhof, M. Generalized gradient approximation made simple. Physical review letters 1996, 77, 3865.

20. Giannozzi, P.; Baroni, S.; Bonini, N.; Calandra, M.; Car, R.; Cavazzoni, C.; Ceresoli, D.; Chiarotti, G.L.; Cococcioni, M.; Dabo, I.; Dal Corso, A. QUANTUM ESPRESSO: a modular and open-source software project for quantum simulations of materials. Journal of Physics: Condensed Matter 2009,21, 395502.

21. Chen, Z.; Liu, H.;Chen, X.; Chu, G.; Chu, S.;Zhang, H.; Wafer-size and single-crystal MoSe2 atomically thin films grown on GaN substrate for light emission and harvesting. ACS Applied Materials & Interfaces 2016, 8(31), 20267-20273.

LIST OF PUBLICATIONS

1. Patent and patent applications (1)

Y. Lu, **H. Rabiee Golgir**, and Y. Zhou, “Growth of nitride films” US Patent App. 15/158,305, 2016.

2. Journal papers (10)

H. Rabiee Golgir, Keramatnejad, K., Li, D.W., Silvain, J.F. and Lu, Y.F. “Fast growth of GaN epitaxial layers via laser-assisted MOCVD for high-performance ultraviolet photodetectors”. ACS applied materials & interfaces (2017).

H. Rabiee Golgir, Keramatnejad, K., Zhou, Y.S., Wang, M., Jiang, L., Silvain, J.F. and Lu, Y.F. “Resonant and nonresonant vibrational excitation of ammonia molecules in the growth of gallium nitride using laser-assisted metal organic chemical vapour deposition”. Journal of Applied Physics 120.10 (2016) 105303.

H. Rabiee Golgir, et al. "Low-Temperature Growth of Crystalline Gallium Nitride Films Using Vibrational Excitation of Ammonia Molecules in Laser-Assisted Metalorganic Chemical Vapor Deposition." Crystal Growth & Design 12, 6248-6253 (2014).

Qiming Zou; Leimin Deng; Dawei Li; Yunshen Zhou; **Hossein Rabiee Golgir**; Kamran Keramatnejad; Lan Jiang; Jean-Francois Silvain, "Thermally stable and electrically conductive, vertically aligned carbon nanotube/silicon infiltrated composite structures for high-temperature electrodes. “ Carbon, (2017).

Li, Dawei, Lijia Jiang, Zhiyong Xiao, **H. Rabiee Golgir,** Xi Huang et al. " Large-Area 2D/3D MoS2-MoO2 Heterostructures with Thermally Stable Exciton and Intriguing Electrical Transport Behaviors." Advanced Electronic Materials, (2017).

Li, Dawei, Qiming Zou, **H. Rabiee Golgir,** Kamran Keramatnejad, Xi Huang et al. "Controlled defect creation and removal in graphene and MoS_2 monolayers." Nanoscale, (2017).

Keramatnejad, K, Li, Dawei, **H. Rabiee Golgir**, Xi Huang et al. " Laser-assisted Nanowelding of Graphene to Metals: An Optical Approach towards Ultralow Contact Resistance" Advanced Materials Interfaces, (2017).

Li, Dawei, Wei Xiong, Lijia Jiang, Zhiyong Xiao, **H. Rabiee Golgir,** Mengmeng Wang, Xi Huang et al. "Multimodal Nonlinear Optical Imaging of MoS2 and MoS2-Based van der Waals Heterostructures." ACS nano, 10 (3), pp 3766–3775 (2016).

Keramatnejad, K., Zhou, Y.S., Gao, Y., **Rabiee Golgir, H.,** Wang, M., Jiang, L., Silvain, J.F. and Lu, Y.F. “Skin effect mitigation in laser processed multi-walled carbon nanotube/copper conductors”. Journal of Applied Physics. 118 p.154311 (2015).

Y. Gao, Y. S. Zhou, W. Xiong, M. Wang, L. Fan, **H. Rabiee Golgir**, L. Jiang, W. Hou, X. Huang, L. Jiang and Y. F. Lu, "Highly efficient and recyclable onion-like carbon soot sponge for oil cleanup" ACS applied materials & interfaces (2014): 5924-5929.

3. Conference papers (5)

Keramatnejad, K., Y. S. Zhou, D. W. Li, **H. Rabiee Golgir**, X. Huang, J. F. Song, S. Ducharme, and Y. F. Lu. "Reducing Graphene-Metal Contact Resistance via Laser Nano-welding." In Proc. of SPIE Vol, vol. 10092, pp. 100921X-1. 2017.

H. Rabiee Golgir, Y. S. Zhou, K. Keramatnejad, and Y. F. Lu, "On- and Off-Resonant Vibrational Excitation of Ammonia Molecules in Gallium Nitride Synthesis", ICALEO, October 18-22, 2015, Atlanta, GA, USA.

K. Keramatnejad, **H. Rabiee Golgir**, Y. S. Zhou, and Y. F. Lu, "The suppression of skin effect in infrared-laser irradiated planer multiwalled carbon nanotube/Cu conductors", ICALEO, October 18-22, 2015, Atlanta, GA, USA.

H. Rabiee Golgir, Y.Gao, Y. S. Zhou, L.Fan, K. Keramatnejad, and Y. F. Lu, "Effect of Laser-Assisted Resonant Excitation on the Growth of GaN Films at low temperatures" ICALEO, October 19-23, 2014, San Diego, CA, USA.

P. Thirugnanam, **H. Rabiee. Golgir,** Y. S. Zhou, Y. Gao, and Y. F. Lu, "Synthesis of m-plane gallium nitride nanoplates using laser-assisted metal organic chemical vapour deposition" ICALEO, 2013, Miami, FL, USA.

4. Presentation (2)

H. Rabiee Golgir, "On- and Off- Resonant Vibrational Excitation of Ammonia Molecules in Gallium Nitride Synthesis", ICALEO, October 18-22, 2015, Atlanta, GA, USA.

H. Rabiee. Golgir “Synthesis of m-plane gallium nitride nanoplates using laser-assisted metal organic chemical vapour deposition” ICALEO, 2013, Miami, FL, USA.

Note: The content of this dissertation has been gathered from my below publications.

REFERENCES

[1] Rabiee Golgir, H.; Gao, Y.; Zhou, Y. S.; Fan, L.; Thirugnanam, P.; Keramatnejad, K.; Jiang, L.; Silvain, J.-F. o.; Lu, Y. F., Low-Temperature Growth of Crystalline Gallium Nitride Films Using Vibrational Excitation of Ammonia Molecules in Laser-Assisted Metalorganic Chemical Vapor Deposition. *Crystal Growth & Design* **2014,** *14* (12), 6248-6253.

[2] Golgir, H. R.; Zhou, Y. S.; Li, D.; Keramatnejad, K.; Xiong, W.; Wang, M.; Jiang, L. J.; Huang, X.; Jiang, L.; Silvain, J. F., Resonant and nonresonant vibrational excitation of ammonia molecules in the growth of gallium nitride using laser-assisted metal organic chemical vapour deposition. *Journal of Applied Physics* **2016,** *120* (10), 105303.

[3] Lu, Y.; Golgir, H. R.; Zhou, Y., GROWTH OF NITRIDE FILMS. US Patent 20,160,340,783: **2016**.

[4] Golgir, H. R.; Gao, Y.; Zhou, Y.; Fan, L.; Keramatnejad, K.; Lu, Y. In *Effect of laser-assisted resonant excitation on the growth of GaN films*, Proceedings of the 33nd International Congress on Applications of Lasers and Electro-Optics (ICALEO), **2014**.

[5] Golgir, H. R.; Zhou, Y.; Keramatnejad, K.; Lu, Y. In *On- and Off of Resonant Vibrational Excitation of Ammonia Molecules in Gallium Nitride Synthesis*, Proceedings of the 34nd International Congress on Applications of Lasers and Electro-Optics (ICALEO), **2015**.

[6] Thirugnanam, P.; Zhou, Y.; Golgir, H.; Gao, Y.; Lu, Y. In *Synthesis of gallium nitride nanoplates using laser-assisted metal organic chemical vapor deposition*, Proceedings of the 32nd International Congress on Applications of Lasers and Electro-Optics (ICALEO), **2013**.

[7] Rabiee Golgir, H., Li, D.W., Keramatnejad, K., Zou, Q.M., Xiao, J., Wang, F., Jiang, L., Silvain, J.F. and Lu, Y.F., 2017. Fast Growth of GaN Epilayers via Laser-Assisted Metal–Organic Chemical Vapor Deposition for Ultraviolet Photodetector Applications. *ACS Applied Materials & Interfaces*, *9*(25), pp.21539-21547.